Determination of alpha-sheet secondary structure as an early biomarker in the pathogenesis of Alzheimer's disease

Dylan Charles Shea

A dissertation

submitted in partial fulfillment of the

requirements for the degree of

Doctor of Philosophy

University of Washington

2020

Reading Committee:

Valerie Daggett, Chair

Andre Berndt

Michael Regnier

Gabriele Varani

Program Authorized to Offer Degree:

Bioengineering

University of Washington

Abstract

Determination of alpha-sheet secondary structure as an early biomarker in pathogenesis of Alzheimer's disease

Dylan Charles Shea

Chair of the Supervisory Committee:
Dr. Valerie Daggett
Bioengineering

Alzheimer's disease (AD) is one of over 50 amyloid diseases discovered to-date and is now the sixth leading cause of death in the United States, affecting over 5.8 million Americans and projected to cost upwards of $1.1 trillion in paid and unpaid care by 2050. It is characterized by the deposition of β-sheet-rich, insoluble amyloid β-peptide (Aβ) plaques; however, the presence of toxic soluble oligomers – not plaque burden – is correlated with cognitive impairment in AD patients. Additionally, plaque deposition is a late-stage indicator of disease, while the early-stage oligomers mediate toxicity 10-20 years before symptoms present. Most existing treatments for AD target and alleviate symptoms of the disease, rather than the early stages of pathogenesis. Additionally, current diagnostics either detect late-stage indicators of disease progression or utilize biomarker levels that are not directly correlated with toxicity in AD pathogenesis. Here, we show

that Aβ oligomers adopt a nonstandard secondary structure, termed α-sheet, in the early stages of aggregation that is strongly correlated with toxicity. *De novo* designed α-sheet peptides specifically and tightly bind the toxic oligomers over monomeric and fibrillar forms of Aβ. α-sheet peptides inhibit aggregation *in vitro*, neurotoxicity in cell culture, and remove toxic oligomers from the brains *in vivo* in transgenic (Tg) mice. We further developed and characterized a novel diagnostic agent, termed the soluble oligomer binding assay (SOBA), that specifically detects α-sheet containing Aβ oligomers in solution. SOBA detected toxic Aβ oligomers in the brains of Tg mice long before plaques deposited or symptoms presented, and correctly identified all mild cognitive impairment (MCI) and AD patients in a cohort using plasma samples. SOBA also correctly identified all control (CO) patients (including some with non-AD-related MCI) with an overall sensitivity of 100% and specificity of 100%. Additionally, 8 pre-symptomatic CO patients that converted to MCI within 1-5 years were correctly identified by SOBA before clinical assessments or biomarker characterizations could. The α-sheet hypothesis proposes the earliest mechanism through which AD pathology initiates and propagates, presenting the possibility for novel therapeutic agents for efficacious treatment of AD.

TABLE OF CONTENTS

LIST OF FIGURES

LIST OF TABLES

ACKNOWLEDGEMENTS

I am immensely grateful for the outstanding mentorship that I received from Valerie Daggett. I appreciate her accessibility, understanding, and guidance on the issues of scientific approach, professional development, and personal growth. Valerie consistently treated me as a scientific peer, providing guidance as much as engaging in meaningful discussions about our shared research endeavors together. Authoring and assisting in writing manuscripts and paper reviews has been a valuable experience that will benefit me in many ways in my future. I anticipate that the work that Valerie and I continue to pursue together will prove to be immensely impactful for the scientific and medical world, and I truly look forward to it.

I acknowledge the members of the Daggett lab who have provided me with immense patience, understanding, advice, technical support, insight, camaraderie, kindness, and friendship. This list includes Matthew Childers, Alissa Bleem, Tatum Proswimmer, Natasha Paranjapye, Timothy Bi, Steven Hsu, Andee Ott, Delaney Wilde, Jin Li, and Lucas Masjoan. Outside of the Daggett lab, I have had countless collaborators that I owe so much. This list includes Professors Suzie Pun, Gabriele Varani, Mike Regnier, James Bryers, and Xiaohu Gao, fellow cohort members Daniel Lee and Tyler Jorgenson, as well as Mike Mullan of the Roskamp Institute, Christopher Link at UC Boulder, and Jeffrey Zonderman from RedShiftBio.

I especially thank my fellow graduate students in the Daggett lab, who undoubtedly spent more time answering questions or listening to my stream-of-consciousness than they thought they could ever withstand. Thanks for always being there with me.

I was privileged to be funded by several sources during my time in the Daggett lab. In addition to funding provided to Valerie Daggett, I was supported by the Bioengineering Cardiovascular Training Grant overseen by Mike Regnier.

Finally, I thank my parents, sister, and my partner Maura for a lifetime of love and support.

DEDICATION

I would like to dedicate this dissertation to my parents, Daniel and Susan Shea. For 26 years I have been gifted with the love, support, and encouragement that I cannot even begin to describe the impacts of. At every step in life you have been there supporting me with sage advice and a camaraderie that I hold near to my heart. Thank you for everything.

I would also like to dedicate this to my partner, Maura. Nearly every day that was spent working toward what I have written on this paper was also spent together. Your endless love and support for me throughout it all has been my guiding light.

Finally, to my Aunt Donna.

Chapter 1. ALZHEIMER'S DISEASE INTRODUCTION, CHALLENGES, & POTENTIAL

1.1 AMYLOID BETA OLIGOMERS: A MOVING TARGET

Alzheimer's Disease (AD) is a fatal neurodegenerative disorder clinically characterized by the progressive deterioration of memory and cognitive functions. It is the sixth leading cause of death in the US and the leading cause of dementia worldwide, affecting more than 50 million people[1-3]. The primary pathological indicators of AD are extracellular β-amyloid (Aβ) plaques and intraneuronal neurofibrillary tangles of the tau protein[2]. The cascade of plaque deposition and tangle formation follows a pattern: starting in the entorhinal/perirhinal cortex, spreading through limbic structures and the hippocampus, and eventually reaching the frontal, temporal, and parietal cortex[4]. The process begins with the misfolding of the Aβ peptide, which is clipped from the amyloid precursor protein (APP) by α–, β–, and γ–secretase enzymes. In its monomeric form, Aβ is associated with a variety of biological functions,[5-10] but it can misfold into an aggregation competent state, leading to a heterogeneous distribution of low- to high-molecular-weight oligomers that eventually form the characteristic amyloid plaques[11]. Importantly, disease progression is not correlated with amyloid plaque burden nor tau tangle formation, but rather with the presence of soluble oligomers of the Aβ peptide that act as the primary toxic agents[12-23]. In fact, in the absence of fibrils, the low molecular weight (LMW) soluble oligomers induce toxicity and neuronal death, as demonstrated in mouse models of AD[21,24] and familial cases of AD that do not produce plaques[25]. Additionally, tau-mediated neuronal injury is a downstream component of AD progression preceded by Aβ accumulation and synaptic dysfunction (**Figure 1.1**). Over the

past few decades, researchers have pursued various avenues to gain a molecular level understanding of Aβ misfolding and its relation to toxicity as the primary agent in AD pathogenesis[24-31].

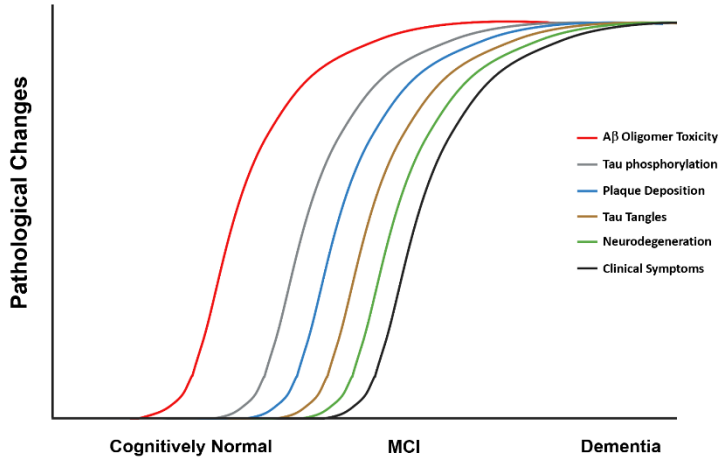

Figure 1.1. Biomarker and clinical manifestations of AD over time.

Many labs have shown that Aβ oligomers are more cytotoxic than protofibrillar and fibrillar structures and that they inhibit critical neuronal activities, including long-term potentiation (LTP), a classic model for synaptic plasticity and memory loss in vivo and in culture[21,28,32-33]. Isolated soluble oligomer aggregates from *in vitro* and/or *in vivo* sources are reported to range in size from dimers to 24-mers, to even higher-ordered assemblies moving through the aggregation process[34-37]. However, some techniques may bias the oligomer profile, thereby making it difficult to correlate what is observed in the lab with what is present in the brain[38]. In this review we present studies on the oligomerization process – as characterized by a range of methods – to delve into the role that Aβ oligomers play in toxicity, the techniques that help to characterize different oligomer assemblies, and how the field might use this information to better interpret the broad spectrum of Aβ-related data and propel AD research toward a potential treatment.

1.2 AGGREGATION & CHARACTERIZATION

Monomeric Aβ (4.5 kDa) is produced by the sequential proteolytic cleavage of APP (120 kDa) by β-secretase and γ-secretase in endosomes and at the plasma membrane[39]. α-Secretase also presents a pathway for formation of shorter Aβ fragments that are thought to be nonamyloidogenic[40]. Despite their common origin, the variants each possess different solubilities, stabilities, and biological and toxic properties. Clipping at the C-terminus by the γ-secretase results in variants ranging from Aβ43, Aβ42, Aβ40, Aβ38, and Aβ37 (where the number indicates the length of the fragment, ex. Aβ43 is residues 1-43), which are detected in cell culture and body fluids[3,12,15-17]. Further heterogeneity is exacted by diverse enzymatic processes by aminopeptidases, glutaminylcyclase, isomerases, and phosphorylation reactions, which all contribute to the sprawling list of 20 Aβ peptides that contribute distinctly to the intrinsic Aβ functions in the normal brain as well as aggregation and toxicity in the AD brain[40-41]. Of this list, Aβ40 is the most abundantly and constitutively produced fragment in both healthy and AD patients, while the other Aβ peptides are continuously produced, but at lower levels.

Despite Aβ40 being the most abundant form, it is not the most pathologically relevant. Rather Aβ42 – with two additional hydrophobic residues Ile41 and Ala42 at the C-terminus – comprises the majority of plaque deposits, can seed fibril formation, and more robustly induces toxicity than its counterparts[42-44]. Additionally, there are distinct kinetic characteristics for the aggregation of Aβ40 and Aβ42, as well as different toxicity profiles and altered behavior when the two are co-incubated[45-46]. A common biomarker to confirm clinical AD diagnoses includes the ratio of the concentrations of Aβ42:Aβ40, which in the early stages of the disease is relatively high but then decreases as the disease progresses and more Aβ42 is deposited into the plaques in the

brain. In addition to the complex interplay between Aβ variants, oligomer formation can occur through both primary or secondary nucleation, involving a pool of Aβ monomers assembling, or monomers that interact with Aβ aggregates to produce higher-order aggregates, respectively[47]. Worthy of Heraclitus's Law of Change, this results in a wildly heterogeneous and dynamic distribution of oligomer species in a state of constant change.

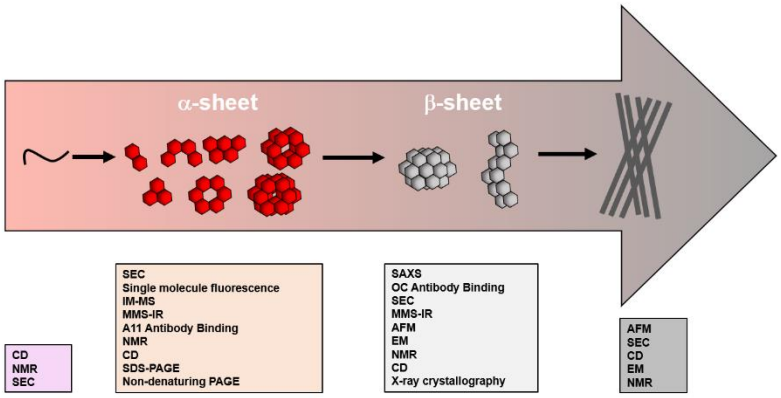

Figure 1.2. Techniques used to isolate and characterize Aβ species at various stages in the aggregation process.

Over the years, AD researchers have ventured to understand the paths by which these various intermediates play a role in the pathogenesis. However, it is difficult to isolate homogeneous species for analysis and even more so to verify that what has been generated synthetically recapitulates what is found in the body. Much like how the static structure of a protein does not fully represent its dynamic nature nor functional state(s), Aβ aggregates isolated under denaturing conditions or by using methods that necessarily break apart structured oligomers cannot accurately represent their state in the brain. Furthermore, the oligomers isolated from brain tissue may not be representative of those physiologically present, but rather a product of the isolation technique. It is likely that several of the identified species (from different techniques) may have

similar characteristics, but different labs do not always share or corroborate their oligomer samples with others in the field.

Table 1.1. Aβ species and isolation technique reference table.

Species	Size & Characterizations	Isolation Technique (source, i.e. *in vitro* or *in vivo*)
Aβ*56[28]	Dodecamer, ~56 kDa, globular, A11 positive	SEC and PAGE (Human brain isolates)
ADDLs[21]	Trimer-24mer, 17 kDa tetramer major, globular, 2-5 nm height, A11-positive	Nondenaturing electrophoresis (synthetic *in vitro*)
AβO[58-60]	15-20mer, spherical vesicles 2-5 nm diameter, A11 positive	SEC (synthetic *in vitro*)
SDS-stable dimers/trimers[32]	Dimer/trimer, 6-12 kDa, Aβ40/Aβ42 with Arg5 N-term truncated species	SDS-PAGE (transfected CHO cell culture medium)
SDS-stable dimers and synthetic dimers[30]	Dimers, 8-12 kDa, 3-4 nm height, no detected secondary structure	SDS-PAGE (brain derived or synthetic Aβ40Ser26Cys mutant)
ASPD (amylospheroids)[76]	32-150mers, spheroids, 10-15 nm diameter assemblies, A11 negative	SDS-PAGE (brain derived and synthetic)
Hexamer/dodecamer*[50]	Hexamer-dodecamer, 27-56 kDa, α-sheet secondary structure, A11 positive	SEC (synthetic *in vitro*)
Trimers from mutant human APPV717F[29]	Trimers, 12 kDa, unstructured	SEC and PAGE (7PA2 cells)
Aβ42 Ellipsoids[31]	High molecular weight, ellipsoidal and annular	SAXS (Cu(II)-guided Aβ42 oligomerization *in vitro*)
Aβ40 Protofibrils[45]	High molecular weight, protofibrillar	SAXS (Cu(II)-guided Aβ40 oligomerization *in vitro*)
Tetramers (Aβ42 and Aβ40)[46]	Tetramer, 18 kDa, ring-shaped (Aβ40) or bent (Aβ42), non-aggregation prone (Aβ40) or aggregation prone (Aβ42)	IM-MS (synthetic *in vitro*)
HMW soluble oligomers[31]	Large, circular, 8-12 nm, form membrane-permeable pore at lipid bilayers	AFM (synthetic *in vitro*)
Pentamer[22]	Pentamer, compact pentagonal shape with C-termini buried	ssNMR (synthetic kinetically trapped)

A wide range of Aβ sizes and structures have been isolated and characterized using a variety of techniques, as depicted in **Table 1.1** and **Figure 1.2**. Characterization techniques can be separated into a few categories: (i) those that can be utilized throughout the aggregation process – nuclear magnetic resonance spectroscopy (NMR), circular dichroism spectroscopy (CD), and size

exclusion chromatography (SEC); (ii) those used in the early stages of aggregation where LMW, toxic oligomers dominate – single molecule fluorescence microscopy, ion-mobility separation–mass spectrometry (IM-MS), A11 oligomer antibody binding, and polyacrylamide gel electrophoresis (PAGE); (iii) those used in the late stages of aggregation where HMW β-sheet rich oligomers dominate – small-angle X-ray scattering (SAXS) and OC oligomer antibody binding; (iv) those used throughout aggregation for both LMW and HMW oligomers – microfluidic modulation spectroscopy (MMS-IR); (v) and those used to characterize the HMW, β-sheet-rich aggregates – atomic force microscopy (AFM) and electron microscopy (EM). Thus, it is important to utilize a variety of techniques to characterize data and to test hypotheses gathered from those experiments in various biological models to confirm their physiological relevance. An interesting example of isolation discrepancy is the use of SDS-PAGE for analysis of Aβ oligomerization. Bitan et al.[48] have shown that SDS artificially alters the aggregation state of Aβ by dissociating the aggregates. This finding was independently corroborated by Hepler et al.[49], who obtained the same low molecular weight (dimer-trimer) bands for oligomer and fibril preparations of Aβ. Thus, the use of SDS-PAGE alone is not sufficient for assessing the aggregation states of Aβ. Alternative methods for analysis include: native gels, SEC, and single molecule fluorescence spectroscopy for isolation and size estimation; IM-MS (combined with molecular dynamics simulations) for insights into the assembly mechanism; AFM and EM for visualization of bulk morphological features; SAXS and cryo-EM for low resolution three-dimensional arrangements; NMR spectroscopy and x-ray crystallography for atomic-level details; and the use of conformation-specific probes for oligomer-specific recognition. **Figure 1.3** illustrates the size ranges probed for each technique, ranging from monomeric to fibrillar assemblies.

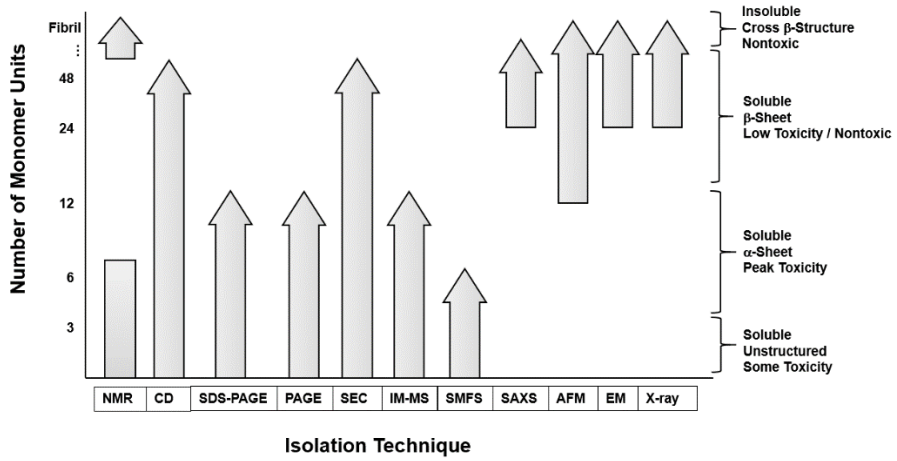

Figure 1.3. Isolation techniques and the associated size ranges of aggregates.

1.2.1 *Aggregate size characterization*

The dynamic nature of the aggregation process makes it difficult to elucidate a structure-based toxicity mechanism. Thus, the isolation and characterization of the species comprising the oligomeric distributions is paramount. Much effort has been focused on purification of samples from AD brain tissue or cultured AD-derived cells, mainly using non-denaturing PAGE and SEC[28-30]. Both techniques require minimal sample preparation and are non-denaturing, so that complex and heterogeneous samples can be isolated based on their molecular weight with relatively little bias. SEC is more useful for synthetic preparations of samples or in conjunction with PAGE, which with the use of antibodies allows characterization of biological fluids for specific peptides or proteins.

SEC alone can be a useful technique for characterizing distinct oligomer sizes in synthetic preparations of Aβ, as there are no other confounding proteins that will interfere in the resulting traces. Recently, our lab reported[50] distinct oligomerization states of synthetic Aβ42, particularly hexamer and dodecamer species by SEC. These assemblies directly correlated with early

aggregation events when toxicity was highest, preceding β-sheet formation, and eventually proceeded to HMW species rich in β-sheet. As described below, dodecamers (and to a lesser extent hexamers) have been implicated by a variety of different studies as the primary toxic agent(s) found in patient-derived samples, and our studies have corroborated this potential role. Importantly, we were able to show that oligomers were stabilized for extended periods of time with storage on ice at various points in the aggregation process and that isolated peaks maintained the same MW upon subsequent analyses with SEC[50]. This was a critical component of our *in vitro* studies, ensuring that the oligomers were stable and could be studied reliably from the same preparations at various times using a variety of instruments and methods.

The dodecameric Aβ oligomer that we characterized *in vitro* is consistent with those previously isolated and characterized from the brains of 6-month old transgenic mice that had begun to show symptoms of AD by Ashe and coworkers using both SEC and nondenaturing PAGE, which they refer to as Aβ*56[28]. Adding the purified Aβ*56 directly into the brains of healthy, non-transgenic rats induced memory decline. A commonly used metric for cognitive decline is the Morris water maze, which tests spatial learning and memory based on the ability of the animal to find a platform and escape the water. This was one of the first studies that isolated and characterized a specific oligomeric species from animal brain and demonstrated a direct link between that species and toxicity *in vivo*. Implicit in the results of this study is another critical component of AD research, where it is possible to isolate oligomers from a patient's brain[28-30,51-52]. This again is contrary to the belief of many that these oligomers are transient and unstable, an idea likely from *in vitro* studies at much higher Aβ concentrations that drive plaque formation. Instead, the toxic oligomers are stable and can withstand processing while maintaining their structural and pathological features[20].

Another example demonstrating the ability to isolate the stable oligomers for biophysical characterization is described by Selkoe and coworkers, who used non-denaturing PAGE to isolate trimers from 7PA2 cells expressing mutant human APP_{V717F} and showed that they affected LTP more strongly than other high MW aggregates[29]. Additionally, LTP was decreased when dimers directly isolated from the brains of AD patients were added to the brains of healthy wild type rats[30]. This, however, poses the question of whether these low MW species are directly responsible for toxicity, or if they rapidly aggregate and form the putative species to induce toxicity. Nonetheless, Selkoe and coworkers present the argument that soluble, low MW oligomers are the on-pathway aggregates that directly affect cell death and LTP[30].

To combat the difficulty of determining exact size distributions of Aβ40 oligomers, single molecule fluorescence spectroscopy was recently employed[53]. This method quantitatively infers the number of monomer subunits in an assembly by counting individual fluorophore-labeled Aβ peptides. This technique works at more physiologically relevant Aβ concentrations and is performed at the single molecule level so that it can give insights as to population heterogeneity rather than just bulk characteristics. Single molecule fluorescence spectroscopy determines the actual heterogeneity implicit in a given sample instead of heterogeneity induced by preparation protocols, and it has the potential to flesh out individual assemblies responsible for toxicity. However, the question remains as to the influence of sample preparation, particularly for the more 'sticky' Aβ42 peptide, and the effect of fluorescent probes on which species are formed during aggregation and whether these protocols recapitulate what is present *in vivo*.

SAXS is another technique employed to monitor Aβ oligomerization[54]. SAXS has much lower spatial resolution, however, its temporal resolution is much better when combined with in-line rapid mixing. This combination can give critical information as to the early events in

aggregation, and the results can give insights into the diameter, molecular weight, and polydispersity of oligomeric species[54]. Ryan and coworkers used SAXS to investigate the influence of Cu(II) on Aβ oligomerization, as Cu(II) is proposed to play a role in AD pathogenesis. Interestingly, they found that Aβ42 aggregates formed ellipsoids in the presence of Cu(II), which recapitulates other widely reported annular structures, whereas Aβ40 quickly formed protofibrillar structures in the presence of Cu(II)[31,45,54-55]. SAXS presents a unique opportunity to monitor the early events in the aggregation of Aβ that spur the eventual fibrillization.

1.2.2 *Conformation and topology*

Purification and characterization of Aβ oligomers are essential in determining the specific assemblies in the heterogeneous distribution responsible for toxicity. The next step, then, is to ask how these discrete assemblies induce toxicity, and the structural basis for the mechanism. Previously, it has been stated that unstructured oligomers are regarded as nontoxic[34,56-57] whereas structured oligomers are much more likely to be toxic[26,31,45-46,50]. Interestingly, Kayed and coworkers developed a polyclonal antibody (A11) that cross-reacts with a wide range of amyloid peptides and proteins in the oligomer state, independent of sequence and native starting structure[28,58-60]. This implicates a common structural motif during oligomerization that is likely associated with toxicity, as this antibody was able to mitigate toxicity of the oligomeric species. It is necessary, then, to study the structural characteristics of Aβ oligomers throughout aggregation to better understand the process and which features contribute to the toxicity mechanism. Several labs have undertaken this biophysical approach to studying AD, in a variety of different ways, as discussed below.

Our lab has recently presented evidence for the α-sheet hypothesis in Aβ42 aggregation and the structure of the toxic oligomers[50]. The α-sheet structure is a unique, nonstandard secondary structure with distinct hydrogen bonding patterns and spectroscopic characteristics separate from those of α-helix, β-sheet, or random coil[50,61-68]. The α-sheet structure was discovered in molecular dynamics simulations (MD) of amyloidogenic proteins as they unfolded and misfolded under amyloidogenic conditions. This unique conformation was predicted to be a key component of the toxic soluble oligomers. Nontoxic, synthetic peptides designed using alternating L- and D-amino acids form this structure stably without aggregating and are recognized by the A11 antibody, suggesting that the α-sheet structure is present *in vivo*[50,64-68]. Furthermore, these *de novo* α-sheet peptides mitigate toxicity in cell culture, and specifically bind and neutralize soluble toxic oligomeric aggregates in both an *ex vivo* and *in vivo* transgenic AD mouse model, and an *in vivo* AD *C. elegans* model[50]. The α-sheet hypothesis poses a new avenue for the conformation-specific detection of toxic aggregates in AD, and the use of sophisticated techniques to determine the conformation of aggregates may help shed light on this and other proposed mechanisms[68].

In this regard, IM-MS is a promising technique for interrogating the structure of oligomeric assemblies, and it has been used to suggest that Aβ40 and Aβ42 form unique conformations[45-46]. For example, Aβ40 tetramers formed a compact ring-shaped structure, making it more difficult to form further contacts. Alternatively, Aβ42 tetramers preferred a bent structure with subunits at either end that easily facilitated the addition of subsequent species. This technique showed that Aβ40 remained smaller, while the Aβ42 tetramers further assembled into large donut-shaped dodecamers, which could seed and accelerate protofibril formation and elongation[45-46]. As the dodecamers (Aβ*56) have been shown to specifically cause memory deficits[28], these IM-MS

studies shed light on the higher order structure behind the biologically relevant Aβ42 toxic isoform.

AFM and EM are also useful techniques to gain insights as to the structural topology of specific aggregates. These two techniques have been used to understand the morphologies of oligomers and fibrils that form on the micrometer or nanometer scale[26,31]. AFM in particular has been used to probe the morphology of oligomers at lipid bilayers. One study demonstrated that Aβ42 oligomers assembled into circular aggregates on the order of 8-12 nm that interacted with the lipid bilayers to form a membrane-permeable pore[31]. This mechanism of toxicity is specifically implicated to trigger flow through the cell membrane leading to cell death and provides an explanation for the toxic nature of the more structured Aβ oligomers over the amorphous aggregates[31,69].

1.2.3 *Atomic details of oligomer conformations*

The intrinsic heterogeneity and dynamic nature of Aβ oligomers has made high-resolution structural analysis of Aβ oligomers very difficult. Despite this, 2D NMR spectroscopy[22,70] and X-ray crystallography[71] have been used to probe the atomic details of kinetically trapped oligomers. Ishii and coworkers[70] proposed that despite the size heterogeneity of prefibrillar Aβ40 oligomers, they maintain parallel β-strand structure similar to amyloid fibrils. Incubating the solution at 4 ºC and flash freezing them in liquid nitrogen allowed them to quickly collect 2D solid state NMR spectra at 15 ºC[70]. Though the oligomers produced less overall Nuclear Overhauser Effect cross peaks (NOEs) and formed less contacts than the fibrils, they claimed that the similar spectral characteristics and connectivities shown at key amino acids throughout the peptide indicated that the underlying structures must be related despite major morphological differences. Importantly,

the species they focused on were 650 kDa spherical aggregates, formed just prior to fibril deposition, and were non-reactive with the A11 antibody, indicating that they were likely the late stage protofibrils rich in β-sheet that seed fibril formation and are not directly associated with the physiological toxicity mechanism, providing a likely explanation for the spectral similarities noted in the study.

Some labs have turned to the use of peptides that contain specific subsets of the Aβ sequence to explore potential aggregation mechanisms mediated by these core regions. Pham and coworkers utilized X-ray crystallography to isolate a crystal structure of oligomers that were formed by a core Aβ segment (containing residues 15-23) and demonstrated how this region generated a wide array of oligomer assemblies, possibly due in part to the missing residues[71]. Once the discovery of self-propagating molecular-level polymorphism in Aβ fibrils was established, protocols for preparing relatively homogenous samples were developed[72-73] and structural models for Aβ40 polymorphs were produced from solid state NMR data. Smith and coworkers[22] also used solution-based NMR to develop pentamer and fibril models at an atomic resolution using low temperature and low salt conditions. The atomic-level details of full-length Aβ oligomers under physiological conditions are still yet to be elucidated, but techniques are improving and may pave the way for important discoveries in the near future. It must be noted, however, that these higher resolution approaches are heavily reliant on model building and inference to known oligomer structures. This is due to the relative lack of experimental observables such that other, unrelated (or lesser characterized) structures are also consistent with experiment but not easily assignable with existing tools and structural biases.

1.2.4 *Brain-derived oligomer characterization*

Several labs have shown that brain-derived soluble Aβ species can be extracted from AD brain tissue using saline buffers and without detergents[16,74]. The extracted samples can then be fractionated with nondenaturing SEC to isolate individual assemblies for discrete characterizations[16,74]. Using such methods, O'Nuallain and coworkers demonstrated that synaptotoxicity is correlated with soluble Aβ oligomers ranging from dimers-hexamers[16,74]. Shankar and coworkers used SDS-PAGE to isolate dimeric Aβ and suggested that the dimer is the minimal toxic component *in vivo*, but due to recognized artifacts with SDS-PAGE, questions remain as to whether the toxicity was directly caused by the dimers seen in SDS-PAGE[30]. Dissociation into low MW species by using SDS-PAGE and rapid aggregation of the putative dimers into larger aggregates might provide an alternate explanation. In a later study, these authors found that synthetically prepared dimers – used as a model for the brain-derived species – rapidly aggregate into metastable protofibrils, which suggests a much more complex process is likely at play[75]. Larger Aβ oligomers, >100 kDa and A11-negative, with specifically identified spherical bulk structure of roughly 10 nm have also been isolated from AD-affected brain tissue and been proposed as the likely toxic agents, further confounding the study of brain-derived oligomers[76-77]. These assertions are in opposition to Ashe and coworkers who have reproducibly isolated the Aβ*56 oligomer from AD brains, indicating that the LMW oligomers responsible for synaptotoxicity are largely present, despite not being a primary component in the pathological characterizations (which rely on plaque burden)[28]. Furthermore, Ashe and coworkers have found that the larger MW oligomers are OC-positive (OC is an antibody that specifically binds the fibril plaques) and are not toxic. Nonetheless, that this range of soluble oligomers are stable enough to be isolated from diseased human brains is again critical to the study of AD, indicating that

oligomers are persistent in both the beginning and late stages of disease where the primary pathology is plaque burden.

1.3 Mechanisms of Toxicity by Oligomers

In recent years, the view that the low molecular weight, soluble oligomers are the primary toxic agents has been more widely accepted. Furthermore, neuronal damage begins to occur 10-20 years before presentation of the symptoms in AD patients, and amyloid plaques are late-stage pathological indicators of the disease. Due to the heterogeneous and dynamic nature of the Aβ oligomers, the mechanisms by which these aggregates carry out their toxic effects and initiate neuronal death is difficult to determine. Despite the difficulties, increasing information about the mechanism of action of these oligomers is becoming available **Figure 1.4**.

1.3.1 *Membrane interactions*

It has been proposed that Aβ oligomers can affect neuronal membranes by a number of different mechanisms. Synapse loss is an indication of AD and greatly contributes to the cognitive deterioration of patients, which is often preceded by attenuation of LTP, lowered synaptic plasticity, and decline of spine density[78]. These neurological features have been known for years, but recent studies have shed light on the mechanistic details.

Several studies have shown that Aβ oligomers bound to receptors on the neuronal membrane, which induced endocytosis of oligomers into the intracellular space and initiated damage from aberrant neuronal signaling[79-81]. Treatment of astrocytes with oligomeric aggregates of Aβ specifically increased glutamate release, as detected with a FRET-based glutamate sensor; however, this effect was not observed following treatment with Aβ monomers[79]. This glutamate

response was calcium-dependent and was initiated by the binding of Aβ trimers (isolated by SEC) to the α7 nicotinic acetylcholine receptors of astrocytes, which is a calcium permeable ion channel[79]. The effect on synapse signaling was due largely to the overactivation of extrasynaptic N-methyl-D-aspartate receptors (eNMDAR) on hippocampal neurons following the glutamate increase.

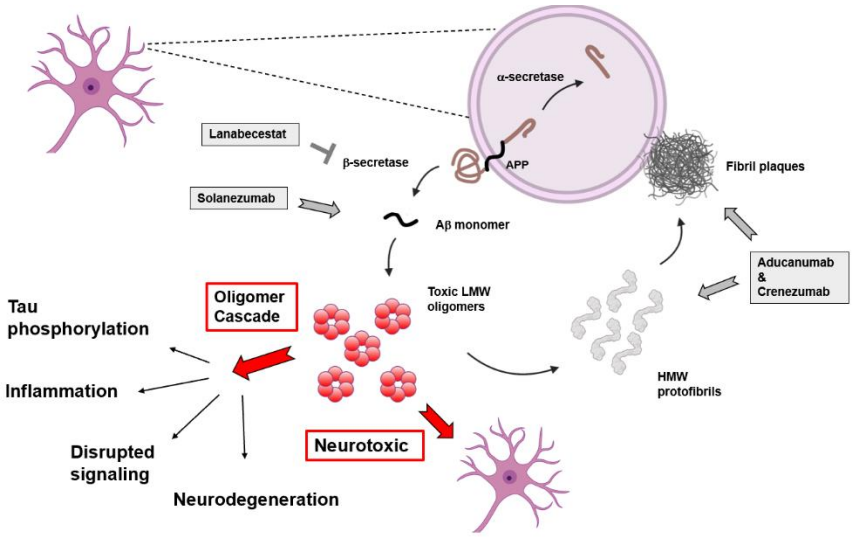

Figure 1.4. Proposed development of pathogenesis in AD and intervention strategies by commercial therapeutics.

Additionally, other studies have shown that Aβ oligomers formed complexes with receptors on membranes to promote their internalization through endocytosis, triggering damage to the intracellular compartments[81]. This complexation also affected cellular signaling; for example, the activation of eNMDARs by SEC-isolated trimers increased calcium flux, which initiated the nitric oxide synthase to increase NO concentration, which then led to apoptosis[79]. Increased NO levels also affected synaptic spine density, where a loss often results in degeneration of neuronal synapses and thus connectivity. These complexes activated specific kinases that decreased NMDAR density and caused dendritic spine loss. In this case, Aβ oligomer toxicity was

augmented by both receptor- and spine density-mediated mechanisms, purportedly due to the misfolded prion-like activity of the oligomer species.

Aβ oligomers have also been shown to merely bind to the membrane, causing local perturbations that damage membrane integrity[69,82-83]. Specifically, SDS-PAGE isolated Aβ dimers were shown to accumulate at lipid rafts in the brains of transgenic Tg2576 mice, which overexpress the Swedish mutation (KM670/671NL) in human APP[82]. Importantly, the dense localization of Aβ oligomers at lipid rafts increases the local concentration of Aβ and might help to seed aggregation and plaque formation, which is not found in most cases at physiologically relevant concentrations. This may help to explain why the Aβ monomers show little inclination to aggregate into the toxic oligomers at such low concentrations in healthy brains, but under certain circumstances that promote localization they misfold, aggregate, and form the toxic species. Furthermore, Selkoe and coworkers confirmed the observation that SDS-dimers interact with lipid membranes much more rapidly than their monomeric counterparts[83]. Upon immunoprecipitation, the dimers associate with GM1-gangliosides in the lipid rafts. These sites are hubs for signal transduction, and the density of oligomers in these regions necessitates the oligomer effect on signal propagation, thus aiding in memory decline. This result is further supported by the correlation of Aβ dimer localization at lipid rafts in 6-month-old Tg2576 mice with memory impairment symptoms[82]. Disregarding the assertion of dimer-specific influence here due to the issues associated with SDS-isolation, the fact that the misfolded and aggregated forms of Aβ – and not the monomeric form – localize at neuronal membranes indicates that misfolding and localization play important roles in the pathogenesis in AD.

The formation of annular structures ranging from 40-170 kDa (from SDS-PAGE and AFM combination studies) that insert themselves at the neuronal membrane has been shown to initiate

dysregulation of efflux/influx through the creation of membrane pores[69,84]. The perforation of neuronal membranes has been attributed to the antiparallel β-sheet conformation of late-stage oligomers and fibrils, which can disrupt cellular systems by penetrating into membranes[84]. This penetration leaves large channels where passive diffusion of small molecules can take place, thus dysregulating the intracellular and extracellular environment. Additionally, some researchers have proposed that the pore formation is instead due to the formation of α-helical structures due to the repeat motif GxxxG throughout the Aβ peptide[85-86]. It is proposed that this motif may facilitate the formation of α-helical structures that can form pores at the membrane and disrupt molecular flux. Along these lines, as support for the possibility that the pores may contain α-sheet, we note that the potassium channel contains four α-strands with the aligned main chain carbonyl oxygens pointing toward the center of the channel to facilitate ion flow[63,87].

In line with the belief that pore formation and membrane leakage are key to the toxicity mechanism in AD, recent research has indicated that Aβ oligomers may induce toxicity by interacting directly with the membrane or its receptors, which then initiates a series of downstream signaling pathways eventually leading to neuronal death. It has been shown that more ordered oligomers are specifically able to damage the membrane, which may lead to the further effects of signaling and chemical flux dysregulation. Additionally, the structure of these more ordered oligomers is likely important in determining the mechanism of action for membrane disruption and pore formation. The α-sheet hypothesis presents a compelling case for the role of a specific, early nonstandard secondary structure associated with aggregation and toxicity in a variety of models. It is imperative to explore the mechanisms of toxicity further at the structural level to intervene at early stages to prevent the propagation of disease pathology.

1.3.2 *Intracellular oligomer effects*

Extracellular Aβ can interact with membranes and receptors, but it can also be internalized into neurons by endocytosis. Additionally, Aβ may also accumulate intracellularly where a portion of APP is localized[88-90]. The mitochondria, endoplasmic reticulum (ER), trans-Golgi network, endosomes, autophagosomes, and lysosomes are all implicated as potential sites for Aβ generation and aggregation. Intracellular Aβ oligomers can enact cellular damage and initiate cell death through elevated ER stress, mitochondrial damage, calcium ion dysregulation, and apoptosis[88-90].

Umeda and coworkers used an $APP_{E693\Delta}$ (Aβ E22Δ) transgenic mouse line to express mutant Aβ (termed the Osaka mutant) that forms soluble oligomers but does not form fibrils[25,88]. Umeda and coworkers demonstrated that aggregates (of an undetermined size) colocalized at cellular organelles in neurons, and these mice had elevated levels of markers indicative of heightened ER stress[88]. This stress was specifically due to the intracellular accumulation of Aβ oligomers and was determined to be activated by phospholipase C signaling, which initiates release of calcium from the ER into the cytosol[89]. Cell viability specifically decreased and caspase 3 (an apoptotic initiator) was activated in response to this dysregulation[88,90]. The Osaka mutant is a very unique case of AD, but importantly portrays the essential role that soluble oligomers play in the toxicity mechanism, even in the absence of amyloid fibrils.

This brief summary of the vast number of alternative pathways of Aβ oligomer-induced toxicity demonstrates that no single mechanism explains all aspects of toxicity in AD. The process is multifaceted and may involve a myriad of interconnected processes and signaling pathways to initiate the neurodegenerative decline characteristic of AD. Importantly, however, there is recent evidence from several groups for a more generic type of toxicity. Wogulis et al. have shown that

the ongoing self-assembly of Aβ42 into fibrils from soluble monomers and oligomers was, by itself, sufficient to cause cell impairment and death[91]. Additionally, synthetic α-sheet peptides designed to specifically target the toxic species neutralize the toxicity and prevent further aggregation[50]. Thus, the dynamic aggregation-based model of toxicity is compatible with most observations in the literature, however, an exact mechanism has yet to be proved.

1.4 Potential Alzheimer's Treatments in Clinical Trials

There have been a wide range of small molecules and antibodies that have entered clinical trials in recent decades for the treatment of Alzheimer's disease, with varying degrees of outcomes. Trials include drugs from large companies such as Biogen, Roche, Genentech, and many more, and despite the abundance of funding and manpower dedicated to drug development, there has been little clinical success[92]. Early clinical trials took three main approaches to AD treatment, including: (1) disrupting the fibrillar form by binding to and breaking up plaques; (2) sequestering the monomeric form of Aβ through sequence-specific binding; or (3) halting the production of Aβ by inhibiting the β-secretase enzyme that clips APP to give rise to Aβ (BACE inhibitors)[92]. While there has been much discussion of enrolling patients earlier to obtain better outcomes, it would be inherently difficult to obtain significant clinical efficacy with any of these approaches. Targeting fibrils is not only an intervention that takes place too late in the disease, but it also might increase the level of soluble oligomers in the brain, thereby increasing toxicity rather than halting disease progression[47,92]. Similarly, targeting the monomer directly through sequence recognition or with BACE inhibitors would remove the physiologically necessary form of Aβ from the brain, thereby disrupting processes that promote normal function, not to mention affecting the processing of other peptides[5-10,92]. Recent proposals by many companies have claimed that their compounds target the

soluble oligomers formed in the early stages of disease, but further analysis of the antibodies and small molecules used indicates that they are targeting late-stage β-sheet rich protofibrils, fibril plaque deposits, or they indiscriminately bind different forms of Aβ. We outline a few of these examples below.

Aducanumab™ is a monoclonal antibody that preferentially binds to the protofibrils and plaques formed in the late stages of disease (**Figure 1.4**)[92-94]. Aducanumab™ was developed using an immunotherapeutic approach wherein human B-cell clones were exposed to aggregated Aβ and screened for reactivity[93]. The resultant library went through molecular cloning, sequencing, and recombinant expression and eventually resulted in the monoclonal antibody Aducanumab™ which selectively reacts with both soluble oligomers and insoluble fibrils[93]. The cross-reactivity of the monoclonal antibody for soluble and insoluble forms of aggregated Aβ indicates that the recognition motif is likely the β-sheet structure shared by late-stage protofibrillar HMW aggregates and the fibril plaque deposits. Due to the binding preference of this antibody, measures of efficacy were necessarily contingent upon initial plaque presence in a variety of animal and human cohorts and was verified using amyloid PET imaging (which uses a plaque-specific radiotracer to measure amyloid burden). Thus, enrolled patients were likely in the mid-to-late stages of the disease when they were undergoing treatment. Despite claims that Aducanumab™ can be an effective intervention in the early stages of the disease[94], it is preferentially a late-stage indicator of disease progression[92-93].

Solanezumab™ is a monomer-specific monoclonal antibody probe that has been discussed as a potential early-stage therapeutic option for AD patients in the mild cognitive impairment (MCI) stage (**Figure 1.4**)[92,95-96]. The parent monoclonal antibody for Solanezumab™ (m266) was generated in A/J mice using a synthetic $A\beta_{13-28}$ peptide (HHQKLVFFAEDVGSNGGC) where

several positive clones were identified that all selectively bound to $A\beta_{1-28}$, but not $A\beta_{1-16}$ nor $A\beta_{17-28}$, indicating the specificity for the central domain of Aβ[95]. Early characterizations showed that this antibody was unable to bind to Aβ aggregates, but completely prevented $A\beta_{1-42}$ fibrillization *in vitro* by binding and sequestering the monomer peptide[95]. Thus, Solanezumab™ is considered the AD paradigm of a 'capture antibody' which selectively binds the free, but not the aggregated, form of Aβ. Based on past clinical trials and the scientific literature surrounding Aβ functions and toxicity mechanisms, sequence-based interventions for AD will not halt nor prevent disease progression[92]. In fact, monomer-specific compounds have been associated with various side effects, likely due to removing the physiologically active form of the peptide from the brain[92]. This may produce positive results in the short-term, which is generally measured in animal models and early trials, however, the long-term rehabilitative effects will likely be minimal. Regardless, Solanezumab™ is still being proposed for interventions in ongoing clinical trials (ex. LEARN).

Crenezumab™ is a monoclonal antibody that has been used in several AD clinical trials, promoted as a truly oligomer-specific marker that binds to the LMW, soluble oligomers formed in the early stages of AD (**Figure 1.4**)[92,97-99]. Crenezumab™ was generated by immunizing mice with an Aβ1-15 peptide antigen and screening for antibodies that bound several different species of Aβ (including monomer) and inhibited Aβ1-42 assembly into small cytotoxic aggregates[99]. Early clinical studies indicated that Crenezumab™ specifically reduced Aβ oligomers present in CSF after treatment in humans and a variety of different animals[97-99]. Interestingly, however, the antibody specifically binds to protofibrillar Aβ and mature amyloid plaques, indicating that the conformational specificity was for the β-sheet structure formed in the late stages of disease[99]. Thus, Crenezumab™ was likely binding to the late-stage, β-sheet rich aggregates.

Finally, Lanabecestat™ is one of many examples of BACE inhibitor therapeutics tested for AD treatment (**Figure 1.4**)[92,100]. Lanabecestat™ works by inhibiting the β-secretase enzyme from clipping at the β-site of APP, thus mitigating the production of Aβ monomers in the brain. Many labs have shown the efficacy of this approach in lab, animal, and early clinical models[92,100]. Removal of Aβ prevents formation of the toxic oligomers, protofibrils, and plaques. Lanabecestat™ was eventually stopped under futility analysis, unlike similar BACE inhibitors Verubecestat™ and Atabecestat™ which were halted due to side effects[92]. Even though Lanabecestat™ was well tolerated, neither of the two doses tested were effective at shifting the primary or secondary outcomes from placebo[92]. Targeting BACE is an enticing strategy for treating AD, as mitigating the production of more Aβ monomers can halt further oligomer/fibril formation; however, as most patients will be treated only after showing symptoms, oligomers and fibrils are largely already present so that intervening in the Aβ production process cannot lessen the effect. Also, there are concerns about removal of Aβ monomers given their many biological functions, as well as other peptides processed by the inhibitor secretases.

The unfortunate failures of past AD clinical trials, along with the information presented here regarding the importance of the early-stage oligomer species, indicates the dire need for a shift in AD diagnosis and treatment toward an oligomer-based approach. The studies above have outlined the latency for AD symptoms years after neuronal damage has taken place. An associated component in the refinement of therapeutic efforts is that AD diagnostics must detect in a more prognostic capacity prior to the development of late stage disease markers. In this case, new therapeutics could then be tested for their ability to mitigate disease progression, rather than reverse neuronal damage that has taken place over 10-20 years.

1.5 CONCLUSIONS & OUTLOOKS

AD is an amyloid disease characterized by the aggregation of the Aβ peptide monomer into a heterogeneous distribution of soluble, toxic oligomers, followed by relatively nontoxic protofibrils, and eventually results in the characteristic nontoxic cross-β pleated sheet fibrils. The toxic intermediates are dynamic in nature, making the study of their size, structure, and the detailed mechanism of toxicity difficult to characterize. The fibrils are nontoxic, but they can act as a reservoir of soluble oligomers by fragmentation and secondary nucleation. Recent advances in biophysical and biochemical methods have revealed a moderate number of structural characteristics of the intermediate oligomers. Isolation and size estimation using PAGE and SEC have led to informed studies of the effects that different size aggregates have on neuronal function. Assembly pathways have been investigated with the aid of IM-MS experiments and MD simulations. Bulk features of morphology and topology have been directly visualized with techniques like AFM and EM, while atomic detail can complement those studies using NMR or X-ray crystallography. Importantly, conformation-specific probes have been developed to investigate and interfere in specifically assembled structures that are associated with the most toxic states.

Along with advances in oligomer characterization, many toxicity mechanisms governed by structured Aβ oligomers have been proposed and investigated. These mechanisms range from extracellular interactions with membranes or receptors, intracellular accumulation disrupting normal function, and cell-to-cell transmission of toxic aggregates. Researchers are shifting their focus now to the relationship between oligomer conformations and toxicity and using this information to design probes that can intervene in the early stages of disease progression for diagnosis and treatment. In this regard, it is critical for researchers to carefully report their oligomer

preparation protocols and experimental conditions to compare what is done in different labs to help facilitate progress in the field. Further development and refinement of techniques based on these approaches should aid in the design of efficacious therapeutics to combat and halt the progression of AD.

Chapter 2. ALPHA-SHEET CHARACTERIZATION *IN VITRO* AND EARLY APPLICABILITY *IN VIVO*

2.1 INTRODUCTION

A mechanistic explanation for the role of the β-amyloid peptide (Aβ) in Alzheimer's disease (AD) has eluded scientists for over 50 years, with advancing technologies and discoveries seemingly further confounding the understanding of the disease—a modern iteration of Zeno's Paradox. Monomeric Aβ has been associated with a variety of biological functions, including memory, learning, and neuroprotection[5-10]. The modified amyloid cascade hypothesis, the prevailing theory of pathogenesis, adds additional complexity to the study of the disease by implicating a dynamic and heterogeneous distribution of soluble Aβ oligomers as the primary toxic agents and asserting that the resultant amyloid fibrils are relatively benign[12-22]. Furthermore, the toxic soluble oligomers are correlated with disease progression while amyloid burden is not[17-18,51,54-55]. The ability of the A11 oligomer-specific antibody to recognize and block toxicity in a variety of amyloid systems illustrates the importance of these oligomers[56]. The cross-reactivity of the A11 antibody suggests that soluble oligomers share a conformational, rather than sequence-based, epitope that promotes structural uniformity upon deposition, as determined for the fibrillar state by a variety of spectroscopic methods[57-60]. A similar conclusion was reached based on atomistic molecular dynamics simulations in which we discovered a secondary structure—α-sheet—that is adopted by unrelated proteins under amyloidogenic conditions[61]. We proposed that it is linked to aggregation and toxicity of the soluble oligomers and is the common structure targeted by the A11 antibody[61-63]. Outwardly, α-sheets resemble β-sheets except that the carbonyl oxygens are aligned on one face of a strand and the NH groups on the other instead of alternating,

which gives rise to different physical properties[63,66] (**Figure 2.1**). Here, we investigate the implications of the α-sheet hypothesis using a variety of experimental techniques. Aggregation of Aβ (1–42)— hereafter referred to as Aβ—was monitored over time by several biophysical methods. Aβ has a high propensity to form soluble oligomers containing α-sheet structure, and the extent of α-sheet is correlated with toxicity. Novel synthetic α-sheet peptides designed to bind to the predicted α-sheet structure from simulations specifically bind toxic Aβ oligomers, inhibit aggregation *in vitro*, and protect against toxicity in cell-based assays and in two animal models: *Caenorhabditis elegans* and transgenic APPsw mice.

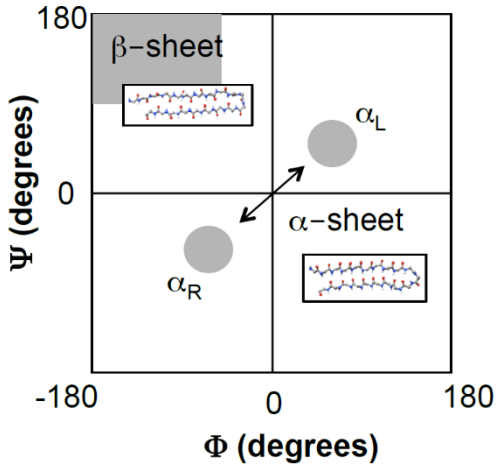

Figure 2.1. Schematic comparison of α-sheet and β-sheet structures.

2.2 METHODS

2.2.1 *Aβ (1-42) sample preparation*

Aβ(1-42) hereafter referred to as Aβ, was obtained from the ERI Amyloid Laboratory, LLC (Oxford, CT). Aβ was aliquoted using hexafluoroisopropanol (HFIP, Sigma-Aldrich, St. Louis, MO, USA) for use when needed. Aβ was sonicated at 1 mg/ml in HFIP in a bath sonicator

for 5 min, followed by 25 min on ice, twice. The resulting solution was then blown under a gentle stream of N_2 gas and concentrated using a SpeedVac concentrator (Savant ISS110, Thermo Fisher Scientific) for 30 min on low setting, thus creating a monomerized Aβ film that was stored at -20 °C and could be thawed and prepared as necessary. Aβ stocks were prepared by removing a film aliquot from -20 °C, and letting it equilibrate to RT (5 min). The film was dissolved to 0.75 mg/mL in filtered 6mM NaOH (pH 11.6, Sigma-Aldrich), flicked to ensure the film was in solution, and sonicated for 5 min. This solution was transferred using a glass pipette to a 0.22 μm Costar Spin-X cellulose acetate centrifuge filter (Sigma- Aldrich), and centrifuged at 7,000 rpm for 2 min. This solution was then transferred using a glass pipette to an Eppendorf LoBind microcentrifuge tube (Sigma-Aldrich) and concentration was measured using a NanoDrop 2000 Spectrometer (Thermo Fisher Scientific) at 280 nm using an extinction coefficient of 1490 M^{-1} cm^{-1}. The resulting stock solution rested at 25 °C for four hours, after which it was either used immediately or stored at 4 °C until needed (no longer than 1 week).

2.2.2 *Peptide Synthesis*

The α-sheet and other control peptides were produced manually using standard solid phase peptide synthesis on Rink amide resin with Fmoc chemistry and HBTU activation. The resin-bound peptides were cleaved and side chains deprotected with (trifluoroacetic acid) TFA/TIPS/H2O (95:2.5:2.5) and precipitated with cold ether. Crude peptides were purified by Reverse phase-HPLC to ~98% purity (Phenomenex 5 μm C12 100 Å semiprep column). Purified peptides were confirmed by mass spectrometry (MS) on a Bruker Esquire Ion Trap electrospray mass spectrometer, and peptide stocks were lyophilized for storage at −20 °C.

2.2.3 *Thioflavin-T (ThT) aggregation assay*

Stock Aβ was diluted using phosphate buffered saline (PBS) buffer (10 mM phosphate, 130 mM NaCl, and 2.7 mM KCl; Sigma-Aldrich) to the relevant working concentration for each experiment, as described previously (1, 2, 3). Briefly, a portion of the stock Aβ was added first to a separate LoBind tube. Concentrated stock ThT (Thermo Fisher Scientific) was prepared monthly, by dissolving ThT powder to 5 mg/ml in H_2O; concentration was measured of 1:10 dilutions of the stock using a NanoDrop 2000 Spectrometer at 412 nm using an extinction coefficient of 36,000 M^{-1} cm^{-1}. In another separate tube, the concentrated stock ThT in H2O was first added, with the calculated volume corresponding to a final concentration of 24 μM ThT for aggregation studies. PBS buffer was added to this tube and mixed by pipette. A portion of this solution was then added gently – along the side of the tube – to the Aβ-containing LoBind tube and mixed once by pipette. In the case of inhibition studies, the ThT-PBS solution was first added to a tube containing concentrated inhibitor peptide and this final solution was used to dilute Aβ and 60 μL of the resulting solution was added to a single well in a black 384-well plate and read on a multimode plate reader (PerkinElmer, Waltham, MA). Relevant parameters include: λ_{ex} 438 nm, λ_{em} 495 nm, measurement height 7.5 mm, 8 flashes, with readings taken either every 90 min or once per time point.

2.2.4 *MTT Cell Viability Assay*

Cell viability was determined using a 3-(4,5-dimethylthiazol-2-yl)-2,5-diphenyltetrazolium bromide (MTT) assay. The SH-SY5Y cells (American Type Culture Collection, Manassas, VA, USA), neuroblastoma from human, were cultured in 1:1 DMEM:F12 (Invitrogen, Waltham, MA, USA) supplemented with 10% FBS (Invitrogen), 100 units/ml

penicillin (Invitrogen), and 100 μg/ml streptomycin (Invitrogen). The cells were seeded in 96-well plate at 4 x 10^4 cells per well and cultured in CO_2 water-jacketed incubator (37 ºC, 5% CO_2; Forma Scientific) for 24 hours. The cell culture medium was removed and replaced with 100 μL preincubated Aβ in medium, either with or without designed peptides. The Aβ (either 75 μM or 25 μM, in NaOH/PBS) was incubated at 25 ºC for the desired duration and diluted to 30 μM or 10 μM with cell culture media before application. The cells were cultured with experimental solution for 24 h at 37 ºC before addition of 25 μL MTT (5 mg/mL in PBS; Sigma-Aldrich) and incubated for 4 h at 37 ºC. 100 μL lysis buffer (20% SDS, 50% DMF, 1% glacial acetic acid, and 0.2% HCl) was added to each well and incubated overnight at 25 ºC covered in foil. The optical density was read at 570 nm with a multimode plate reader (PerkinElmer). The cell passage numbers for the experiments were 6 to 8.

2.2.5 *Size Exclusion Chromatography (SEC)*

Stock Aβ was diluted and preincubated in PBS to the relevant working concentration for each experiment. First, 2 column volumes (CVs) of PBS buffer was equilibrated through a Superdex 75 10/300 GL column (GE Healthcare, Buckinghamshire, UK) at a flow rate of 0.6 mL/min, using an AKTAprime Plus unit (GE Healthcare). After equilibration, 150 μL of Aβ was injected into a 100 μL sample loop and introduced to the column flow for several minutes. Species were eluted under a constant elution profile of PBS and fractions were collected and immediately stored on ice.

2.2.6 *Circular Dichroism*

Stock Aβ, pre-incubated Aβ at 75μM, or α-sheet peptide was diluted in PBS to a concentration of 25μM. A portion of the peptide solution was added, first, to a LoBind tube. The corresponding volume of buffer was then added gently – along the side of the tube – to the peptide-containing LoBind tube and mixed once by pipette to ensure adequate mixing. 300 μL of the resulting solution was added to a 1 mm pathlength quartz cuvette (Starna Cells, Atascadero, CA, USA) and scans collected using a Jasco J-720 CD machine. All experiments aggregated 8 scans and used a Savitzky-Golay smoothing protocol, followed by reduction of noise by an FFT filter. The mean residual ellipticity (MRE) was calculated by first subtracting the peptide signal from the blank signal, and the curve zeroed against the value at 270 nm.

2.2.7 *Microfluidic Modulation Spectroscopy*

Microfluidic Modulation Spectroscopy (MMS) is a novel protein characterization and spectroscopic technique that combines a microfluidic cell and a tunable mid-IR quantum cascade laser to analyze the higher order structure of proteins and peptides. A RedShiftBio (RSB, Burlington, MA, USA) AQS3pro preproduction unit was used to analyze samples at ambient temperature. A microfluidic transmission cell of approximately 23.8 μm path length was used. The sample and the buffer fluids were introduced into the flow cell by modulating at a frequency of 1 Hz and a pressure of 5 psi. 31 discrete wavenumbers across the amide-I band from 1714 cm^{-1} to 1590 cm^{-1} were scanned and the differential absorbance spectra were collected. The data were analyzed using AQS3delta, RSB's proprietary data analysis software, to produce the final spectral plots and results. AP5, AP90, AP407, AP421 and P411 samples were measured at 0.8-1 mg/mL

in PBS buffer; PSMα1 was measured at 0.8 mg/mL in 5% DMSO:PBS solution; while Aβ 24h and Aβ 120h were measured at 0.38 mg/mL in 1:1 6 mM NaOH:PBS solution.

2.2.8 *NMR Spectroscopy*

AP407 samples were dissolved in 1000 µL of 50 mM KPO_4 and 10 mM KCl at pH 5.8 and split into two 800 µM AP407 samples. One sample was flash frozen, lyophilized, and reconstituted in 99% D2O solution (Cambridge Isotope Laboratories). Both samples were subjected to 1H-1H Homonuclear Overhauser Spectroscopy and Total Correlation Spectroscopy at 25 °C with an 800 MHz Ascend series magnet, AVANCE III console, equipped with a cryoprobe (Bruker, Billerica, MA, USA). In addition, natural abundance 1H-13C and 1H-15N Heteronuclear single quantum coherence experiments were performed on both samples. Proton chemical shifts and NOE cross-peaks were assigned based on NOE connectivities, chemical shift location, and the associated nitrogen and carbon chemical shifts. A total of 455 NOEs were assigned. Of these, 432 were short-range (i → i+1, i+2); 17 were medium-range (i → i+3, 4, 5); and 6 were long-range between residues separated by more than 5 residues, with two of those falling near the ends of the strands. An ensemble of structures was constructed manually to satisfy the set of 455 inter-proton nuclear Overhauser-based distance restraints. Our designed conformation was used as the starting structure for 9 out of the 10 structures in the ensemble (one conformer was obtained from a MD simulation that used the designed conformer as starting coordinates) and atomic coordinates were examined to obtain an ensemble of 10 structures that collectively satisfied all NOE distance restraints. The models were then edited with in-house software and UCSF Chimera. First, short range NOEs between H atoms within a single residue were satisfied by modifying the side chain dihedral angles for each residue. Our rotamer libraries for L- and D- amino acids for residues within heterochiral

chains, derived from MD simulations of host- guest pentapeptides, were used for this purpose. Next, alternate backbone geometries were necessary to satisfy medium and long-range NOEs, which correspond to alternate conformations in the turn. Finally, the remaining medium- and long-range NOEs corresponding to alternate conformations of the strands were satisfied by making alterations to the backbone. This resulted in an ensemble of structures that had 100% NOE coverage and 100% agreement with the experimental NOEs. We used a method that deviates from standard NMR structure determination protocols for two reasons. First, standard protein structure programs typically rely on reference distributions obtained from the Protein Data Bank (PDB). Since there are no instances of α-sheet structures in the PDB, this kind of secondary structure was nearly impossible to generate with conventional programs and the structures generated were inconsistent with the experimental data. Instead, we specified the initial dihedral angles for the backbone conformation prior to manual refinement. The manual specification of backbone dihedral angles has been performed previously to determine the NMR structures of a de novo designed variant of gramicidin, which also contains L- and D-amino acids and adopts a nonstandard type of secondary structure, the double-stranded antiparallel α-helix. Second, the small number of examples of heterochiral peptides and examples of α-sheet structure in the PDB results in a bias against the predicted structures of our peptides. Finally, databases of heuristic structural information, frequently used in NMR programs, are biased against and, in some cases, explicitly exclude the geometries predicted for α-sheet secondary structure. Such approaches assign secondary structure based on known ‘normal’ proteins and cannot be used for novel structures that do not appear in the database of representative structures. Thus, we were forced to use other approaches, including utilizing our MD-derived libraries for the intrinsic conformational propensities of L-amino acids and L- and D-amino acids within heterochiral polypeptide chains to

determine the intrinsically preferred dihedral angles that best agree with the NOE data. The derived models were then compared with other NMR data acquired by us, for example the chemical shifts were compared with the results of SHIFTX2. Secondary chemical shifts for H_α (top) and H_N (middle) relative to random coil values were calculated to obtain chemical shift indices. The AP407 values (experiment and calculated from the NOE-derived models) were corrected by 'random coil' values obtained from MD simulations of the pentapeptide host-guest series, both homochiral and heterochiral. The chemical shift index plot for H_α was constructed using a threshold of |0.1| ppm: if the difference was greater (either positive or negative) the value was set to 1.0 or -1.0. If the value was $-0.1 \leq d \leq 0.1$ then it was set to 0. The 3J coupling constants obtained by NMR were compared to those calculated for the NOE-derived structural ensemble using the Karplus equation.

2.2.9 *Soluble Oligomer Binding Assay (SOBA)*

Stock Aβ was diluted and preincubated in PBS to the relevant working concentration for each experiment. We used one of our α-sheet designs, AP193, as the capture agent for all SOBA experiments. AP193 was first dissolved with DMSO (Sigma-Aldrich) to 36 mM and then diluted to 36 μM with CO_3^{2-} buffer (pH 9.6). 100 μL of AP193 was plated per well for all positive control wells – while CO_3^{2-} was plated as control blank wells – in a Nunc Immobilizer Amino 96-well plate (Corning, Corning, NY, USA). AP193 was coupled with shaking at RT for 2 h. The wells were then aspirated and washed with 300 μL PBS-T (0.01% Tween-20 by volume, Sigma-Aldrich) five times. 100 μL of 10 mM ethanolamine (Sigma-Aldrich) was then plated per well and used to quench unreacted sites on the surface by shaking at RT for 2 h. The wells were then aspirated and washed with 300 μL PBS-T five times. Pre-incubated Aβ was then diluted to 250 nM and 100 μL

per well incubated for 1 h at 25 °C without shaking. The wells were then aspirated and washed with 300 μL PBS three times. A 1:5,000 dilution of the primary 6E10 anti-Aβ antibody (BioLegend, San Diego, CA, USA) was prepared in 3% BSA in TBS-T (50 mM tris, 100 mM NaCl, 0.01% Tween-20 by volume, pH 7.6) and 100 μL of this solution was plated per well and incubated with shaking at RT for 1 h. The wells were then aspirated and washed with 300 μL PBS three times. 100 μL of a 1:10,000 dilution of the secondary goat anti-mouse HRP-conjugated antibody (Pierce Biotechnology, Waltham, MA, USA) in 3% BSA in TBS-T was plated per well and incubated with shaking at RT for 45 min while covered in foil to avoid bleaching of the HRP. The wells were then aspirated and washed with 300 μL PBS three times. 100 μL of room temperature tetramethylbenzidine (TMB, Thermo Fisher Scientific) was plated per well, and incubated with shaking at RT for 15 min while covered in foil. The reaction was quenched with 100 μL of 2 M H_2SO_4 (Sigma-Aldrich) and absorbance measured at 450 nm on a multimode plate reader (PerkinElmer).

2.2.10 *Biolayer Interferometry*

Aminopropylsilane (APS) biosensor tips (Pall ForteBio, Fremont, CA) were hydrated in PBS buffer for at least ten minutes. A ForteBio BioLayer Interferometry instrument (Blitz) was used to determine the kinetics of the binding of oligomer fractions from pre-incubated Aβ to AP5. The following parameters were used for the analysis: Initial baseline: 30 s; Loading: 180 s; Baseline: 30 s; Association: 180 s; and Dissociation: 180 s. The initial baseline was acquired by dipping the APS tip into the PBS buffer in an Eppendorf tube. 4 μL of AP5 was pipetted into the drop holder in the instrument and then it was loaded onto the APS tip with shaking for 180 s. The tip was then transferred back into the PBS tube and a secondary baseline was established for 30 s.

4 μL of Aβ sample was pipetted into a separate drop holder and allowed to interact with the peptide-coated APS tip with shaking for 180 s to gather association kinetics. The tip was transferred back to the PBS tube for dissociation kinetics. Analysis was performed using the ForteBio software provided and was carried out from the start of association to the end of dissociation and all parameters were calculated locally. Values presented here represent the average and standard deviation of at least 3 independent measurements.

2.2.11 *A11 Dot Blots*

Stock peptide was diluted in water to the relevant working concentration for each experiment and tested using the amyloid oligomer specific A11 primary antibody (Rabbit Anti Oligomer, Thermo Fisher Scientific), as described previously. Species were blotted in 2 μL, 1 μg portions on 0.2 μm pore-size nitrocellulose membranes (Whatman Protran, Thermo Fisher Scientific) dried at RT. The membrane was placed in a shallow dish and covered with 3% BSA in TBS-T (50 mM tris, 100 mM NaCl, 0.01% Tween-20 by volume, pH 7.6). The solution was shaken over the membrane for 1 h and then transferred into a 1:1,000 dilution of the A11 primary antibody in 3% BSA in TBS-T. The primary antibody was shaken over the membrane for 1 h and collected for future use. The membrane was washed three times with TBS-T for five minutes, then placed into a 1:10,000 dilution of the secondary goat anti- rabbit HRP-conjugated antibody (Santa Cruz Biotechnology, Santa Cruz, CA, USA) in 3% BSA in TBS-T. The secondary antibody was shaken over the membrane for 45 min while covered in foil, and the membrane then washed three times with TBS-T for five minutes. Room temperature Pierce ECL Western Blotting Substrate (Thermo Fisher Scientific) was added and then washed over the membrane for 1 min. The membrane was developed by chemiluminescence imaging on an Azure Biosystems c300 for 6 minutes and all

images were processed using ImageJ. The signals are presented as the integration of the sample dot relative to the A11 primary signal.

2.2.12 *Organotypic brain slices from the Tg APPsw mouse model*

Dissolution of the AP5 Peptide. The AP5 peptide was first dissolved with sterile PBS to a concentration of 20mM and further dissolved in complete DMEM/F12 medium to prepare 5 ml of culture medium containing either 50, 100 or 200 µM of AP5 peptide. Control culture medium contained the same volume of vehicle (50µl of PBS per 5 ml of complete culture medium) used to prepare the culture media with the different concentrations of AP5 peptide.

Preparation of organotypic brain slice cultures. Adult male (91-week-old) Tg APPsw mice (line 2576) were anesthetized with 3% isofluorane in oxygen and were rapidly euthanatized by exsanguination via cardiac puncture. Their brains were dissected in pre-cooled (4˚C) sterile HBSS containing 2 g/l of D-glucose. Coronal, 250 µm thick brain sections were cut at a speed of 0.3mm/s in pre-cooled (4˚C) HBSS using a Leica VT 1200S (Leica Inc., IL, USA) vibratome attached to a Julabo FL300 (Julabo Inc., PA, USA) recirculating cooler. Each brain section was immediately transferred into a well of a sterile 24-well cell culture plate containing 400µl of DMEM/F12 media containing 10% FBS (Thermo Fisher Scientific, MA, USA), 1% GlutaMax and 1% penicillin/streptomycin/fungizone. The sections were incubated at 37˚C in a humidified 5% CO_2 atmosphere. Organotypic coronal vibrosections were treated with 50, 100 and 200 µM of AP5 peptide (MW=2833.26g/mol) or control culture medium for 24 hours. After 24 hours, the supernatant was collected and stored at -80˚C for subsequent analysis of Lactate Dehydrogenase (LDH) released to assess cytotoxicity using a LDH assay (Roche Diagnostics, Germany) according

to the manufacturer's protocol. Ten organotypic vibrosections for each treatment condition were used.

Preparation of brain slice homogenates and quantification of Aβ. Each brain slice was sonicated in 150 µl of ice-cold MPER reagent containing 1x of a cocktail of proteases and phosphatases inhibitors (Thermo Fisher Scientific, MA, USA). Samples were centrifuged at 10,000g for 45 minutes at 4˚C and supernatants were collected. Protein concentrations were quantified in the supernatants using the BCA method (Thermo Fisher Scientific, MA, USA). Aβ38, Aβ40 and Aβ42 were quantified by electrochemiluminescence using an Aβ triplex ELISA kit (Meso Scale Discovery, MD, USA) following the manufacturer's recommendations. Samples were assayed in duplicate and results were standardized to the amount of total protein and expressed in pg of Aβ per mg of total protein. Brain slice homogenate pellets were resuspended with 20 µl 5M guanidine isothiocyanate (dissolved in Tris-HCl 50 mM pH=9) and incubated for 1 hour at room temperature. Samples were dissolved with 20 µl of Tris-Glycine-SDS and loaded (4 µl) onto a 0.45 µm pore-size nitrocellulose membrane (Biorad, CA, USA). The membrane was left to dry at room temperature for 1 hour and was blocked for 2 hours with 5% milk dissolved in TBS (Biorad, CA, USA) and hybridized for 24 hours at 4˚C with the antibody 6E10 (1/1000 dilution). Following washes for 30 minutes at room temperature, the membrane was hybridized with an anti-mouse-HRP conjugated antibody (1/2500 dilution) for 1 hour at room temperature. The 6E10 signal was revealed by chemiluminescence imaging using the SuperSignal West Femto Maximum Sensitivity Substrate (Thermo Fisher Scientific, MA, USA) on a ChemiDocTM XRS (Bio-Rad, Hercules, CA, USA).

Quantification of oligomers. Quantification of oligomers in brain slices homogenates was performed with 4 microliters of brain slices homogenates (approximately 8 µg of total protein)

loaded onto 0.45 µm pore-size nitrocellulose membranes (Biorad, CA, USA). Membranes were left to dry at room temperature for 1 hour and blocked for 2 hours with 5% milk dissolved in TBS (Biorad, CA, USA). One membrane was hybridized with a 1/1000 dilution of the A11 antibody (Thermo Fisher Scientific, MA, USA) at 4˚C for 48 hours. Another membrane was hybridized with an anti-actin antibody (1/1000 dilution, Cell Signaling Technology, CA, USA) as reference. Membranes were washed for 30 minutes with distilled water and hybridized with their respective secondary antibodies (mouse and anti-rabbit HRP conjugated antibodies at a 1/2000 dilution in 5% milk dissolved in TBS) for 2 hours at room temperature. Following washes for 1 hour at room temperature, A11 and actin signals were obtained by chemiluminescence imaging using the SuperSignal West Femto Maximum Sensitivity Substrate (Thermo Fisher Scientific, MA, USA) on a ChemiDocTM XRS (Bio-Rad, Hercules, CA, USA). A11 chemiluminescent signals were standardized to their respective actin chemiluminescence signals and expressed as % of A11/Actin signals detected in control Tg APPsw brain slices homogenates. For the analysis of Aβ oligomers by western-blot, the MPER soluble fractions of brain slice homogenates were resolved using 4-20% gradient PAGE under native conditions and electro-transferred onto PVDF membranes. PVDF membranes were hybridized for 24 hours at 4˚C with the Aβ antibody 6E10 (1/1000 dilution, BioLegend, CA, USA). Following washes for 30 minutes at room temperature, the membranes were hybridized with an anti-mouse-HRP conjugated antibody (1/2500 dilution) for 1 hour at room temperature. The 6E10 signal was revealed by chemiluminescence imaging using the SuperSignal West Femto Maximum Sensitivity Substrate (Thermo Fisher Scientific, MA, USA) on a ChemiDocTM XRS (Bio-Rad, Hercules, CA, USA). PVDF membranes were also probed with an anti-actin antibody (1/1000 dilution, MilliporeSigma, MA, USA) used as a reference

protein. 6E10 Aβ oligomer signals were standardized to actin chemiluminescent signals and expressed as a percentage of the signals observed in control brain slices homogenates.

Statistical Analyses. Data were examined for assumption of normality using the Shapiro-Wilk statistic and for homogeneity of variance using the Levene's test. Statistical significance was determined by univariate or repeated measures analysis of variance (ANOVA) where appropriate followed by post- hoc comparisons with Sidak corrections. For data not satisfying assumptions of normality and homogeneity of variance, a nonparametric Mann-Whitney test was used instead. A p-value below 0.05 was assumed to indicate a statistically significant difference. Statistical analyses were performed with IBM SPSS statistics.

2.2.13 *Intracranial Injections of AP5 Peptide in Tg APPsw mice*

Stereotaxic intracranial injections of AP5. Mice were maintained under pathogen-free conditions in ventilated racks in the Association for Assessment and Accreditation of Laboratory Animal Care International (AAALAC) accredited vivarium of the Roskamp Institute. All work involving mice for this study was conducted in compliance with the National Institutes of Health Guidelines for the Care and Use of Laboratory Animals and received approval by the Roskamp Institute Institutional Animal Care and Use Committee (IACUC) prior to initiation. The AP5 peptide was dissolved to 20 mM concentration in sterile PBS. The intracranial injections (IC) of AP5 were performed in ten Tg APPsw mice with an average age of 103.7 ± 0.3 weeks. Mice were anesthetized with 3% isofluorane in oxygen. The depth of anesthesia was verified by the absence of reflex after toe-pinch and tail-pinch. An auto-regulated warming blanket was used to maintain the body temperature of the mice at 37°C during anesthesia. The heads of the mice were secured in a mouse stereotaxic apparatus and anesthesia was maintained with a gas mask. The AP5 solution

was loaded into a 10 microliter Hamilton syringe connected to a 27G needle. The 27G needle was slowly inserted into the hippocampus of the right brain hemisphere using the following coordinates: Bregma, -2.7 mm; lateral -2.5 mm; depth, -3.0 mm. The preparation of AP5 was injected (3 μl) over a period of 2 min and the needle left in place for 5 minutes after the injection. The needle was then moved vertically to a depth of -1.0 mm to allow the injection of an additional 3 μl of AP5 solution in the cortex. Mice were then removed from the stereotaxic apparatus and placed in their home cage stationed on a heating pad until complete recovery from the anesthesia. 24 hours following the IC injections, mice were humanely euthanatized (deep anesthesia with isofluorane (5% in O_2 until complete cessation of reflexes) and then exsanguinated by cardiac puncture while under anesthesia) before harvesting tissues.

Preparation of brain homogenates. Right and left hemispheres (without cerebellum) were separated and immediately frozen in liquid nitrogen. 800 μl of ice-cold MPER reagent containing 1x cocktail of protease and phosphatase inhibitors (Thermo Fisher Scientific, MA, USA) was added to each brain hemisphere. Samples were homogenized by sonication and centrifuged at 10,000g for 45 minutes at 4˚C. The supernatant (MPER soluble fraction) was collected while the pellet was resuspended by vortexing with 200 μl of ice-cold MPER reagent containing 1x cocktail of RI-18-02 protease and phosphatase inhibitors (MPER insoluble fraction). 100 μl of the MPER insoluble fraction was denatured with 100 μl of 5M guanidine isothiocyanate (dissolved in Tris-HCl 50 mM pH 9) and incubated for 1 hour at room temperature to solubilize fibrillar Aβ material. Protein concentrations were quantified in the MPER soluble fractions and in the guanidine denatured MPER insoluble fractions using the BCA method (Thermo Fisher Scientific, MA, USA). Aβ38, Aβ40 and Aβ42 were quantified by electrochemiluminescence using an Aβ triplex ELISA kit (Meso Scale Discovery, MD, USA) following the manufacturer's

recommendations. Samples were assayed in duplicate and results were standardized to the amount of total protein and expressed in pg of Aβ per mg of total protein.

Quantification of A11 oligomers in brain homogenates. Three microliters of brain homogenates (MPER soluble fraction and non-denatured MPER insoluble fraction) were loaded onto 0.45 μm pore-size nitrocellulose membranes (Biorad, CA, USA). Membranes were left to dry at room temperature for 1 hour and were blocked for 2 hours with 5% milk dissolved in TBS (Biorad, CA, USA). Membranes were hybridized with a 1/2000 dilution of the A11 antibody (Thermo Fisher Scientific, MA, USA), with an anti-actin antibody (1/1000 dilution, Cell Signaling Technology, CA, USA) and β-tubulin (1/1000 dilution) as references at 4˚C for 24 hours. Membranes were washed for 30 minutes with distilled water and hybridized with their respective secondary antibodies (mouse and anti-rabbit HRP conjugated antibodies at a 1/2000 dilution in 5% milk dissolved in TBS) for 2 hours at room temperature. Following washes for 1 hour at room temperature, A11, actin, and β-tubulin signals were revealed by chemiluminescence imaging using the SuperSignal West Femto Maximum Sensitivity Substrate (Thermo Fisher Scientific, MA, USA) on a ChemiDocTM XRS (Bio-Rad, Hercules, CA, USA). The A11 chemiluminescent signals were standardized to their respective actin and β-tubulin chemiluminescence signals and expressed as % of A11 detected in control left hemisphere.

2.2.14 *C. elegans experiments*

Paralysis assays. Synchronous populations of CL 4176 (transgenic C. elegans with temperature inducible expression of human Aβ (1-42)) were cultivated at 16 ºC from hatching. When animals reached the third larval stage they were incubated at 16 ºC for 10 hr in 20 μl drops containing 16 μL HEPES buffer, 4 μL of PULsin protein delivery reagent (VWR Scientific), and 4 μL of

peptide at 2 mg/mL. Worms were then transferred to standard NGM plates and upshifted to 25 ºC. Worms were scored for paralysis every 2-4 h 24 hr after temperature upshift. We chose a transgenic C. elegans model that has been used extensively to assay the ability of exogenous compounds to reduce Aβ toxicity.

Endosome induction assays. Intestinal endosomes were induced by feeding worms E. coli expressing Aβ (1-42). Briefly, *E. coli* engineered to inducibly secrete Aβ [strain LMG194 transformed with a plasmid (pCL241) consisting of Aβ cloned into the pBAD gIII arabinose-inducible vector, Invitrogen] was grown to logarithmic phase in 5 ml Luria Broth + 100 mg/ml ampicillin, then induced by addition of 50 μl 20% arabinose. α-sheet peptides were added simultaneously to the arabinose-induced cultures to a final concentration of 100 μM; after 1 hr growth at 37 ºC induced cultures were used to seed NGM plates containing 0.2% arabinose and 100 mg/ml ampicillin. Seeded plates were allowed to dry overnight, then 4th larval stage worms of reporter strain GK280 [unc-119(ed3); dkIs166 (Popt-2::GFP::pgp-1; unc-119 rescuing DNA)] were added and allowed to feed for 4-6 hr. Treated worms were mounted on slides and imaged using a 40X objective on a Zeiss Axiphot microscope. GFP- tagged intestinal endosomes were counted in the first 50 microns of the intestine.

2.3 RESULTS

2.3.1 *Aβ forms toxic oligomers during the lag phase of aggregation*

To assess the oligomeric behavior of Aβ, a standard thioflavin T (ThT) fluorescence binding assay was employed to monitor its aggregation at pH 7.6 in PBS. ThT binding is generally assumed to reflect formation of β-sheet fibrils. Sigmoidal kinetics were observed, indicative of a nucleation polymerization pathway[91] (**Figure 2.2A**). There was a pronounced lag phase before a

sharp increase in ThT binding and fibril formation with modulations of the onset of aggregation dependent on concentration as well as the fluorescence measurement frequency due to robotic action of the plate reader (**Figure 2.3A**). To align the various experiments, we used the kinetics for the "undisturbed" method (**Figure 2.2A**, 36 h lag; **Figure 2.3A**) as the frame of reference for most experiments, from which aliquots were removed at various times during aggregation to investigate the structure and toxicity of the samples. As we are interested in characterizing species populated during aggregation using different methods, the kinetic stability of the aliquots was assessed by storing pre-incubated Aβ on ice at 4 °C for up to 300 h and taking periodic ThT measurements. Storing samples on ice stalled aggregation, which recommenced when the samples were brought back to 25 °C (**Figure 2.3B,C**).

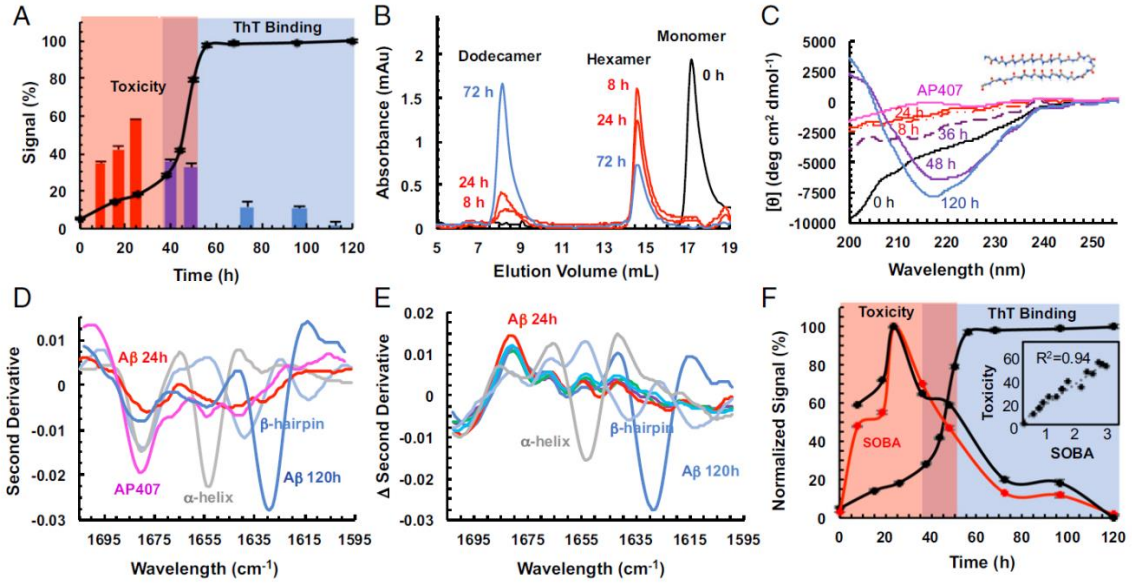

Figure 2.2. Determination of Aβ aggregation kinetics, toxicity, and structure. (A) ThT binding assay overlaid with MTT cell toxicity for pre-incubated 75 μM Aβ at 25 C in PBS. Cell toxicity peaks in the lag phase at 24h and recovers as β-sheet content exponentially increases. (B) SEC traces of Aβ aggregates over time. (C) CD spectra of 75 μM Aβ aggregation over time. NMR-derived structure of AP407 peptide displayed next to its CD spectrum. (D) MMS spectra for control peptides and aggregated Aβ at 75 μM. (E) Difference in second derivative spectra of MMS. (F) SOBA binding intensities plotted with ThT and cell toxicity gathered in (A), with SOBA-toxicity correlation depicted in the inset.

After establishing conditions for reproducible kinetics and stability of time-dependent samples for further analysis, we evaluated the effect of Aβ on cell viability, which was indirectly measured by mitochondrial function as a surrogate for toxicity in SH-SY5Y neuroblastoma cells. Samples matched with those of the ThT assay showed increasing toxicity during the lag phase, which peaked at 24 h (**Figure 2.2A**). The toxicity trend indicated that Aβ was most toxic during the lag phase and did not appear to involve β-sheet structure, as reflected in the lack of ThT binding. In contrast, the β-sheet–rich fibrils were relatively nontoxic. Similar results were obtained by Luo *et al.*[44] for Aβ (1–40). In addition, Giuffrida *et al.*[5] established that high-molecular- weight aggregates contain predominantly β-structure, whereas the low-molecular-weight aggregates are much more heterogeneous and dynamic in both size and structure. Consequently, we characterized the size and structure distributions of the Aβ aggregates over time, particularly those associated with toxicity in the lag phase.

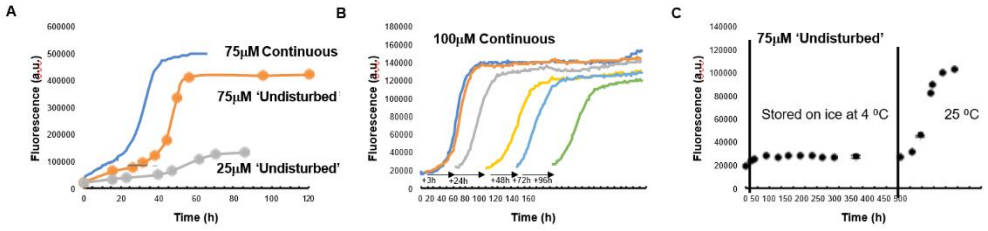

Figure 2.3. Aggregation kinetics and oligomer stability.

To characterize the size distribution of the Aβ aggregates over time, we employed size exclusion chromatography (SEC) (**Figure 2.2B**; standard curve **Figure 2.4**). Early in aggregation, the Aβ monomers converted to small oligomers, with hexamers being the dominant species; however, it should be noted that these SEC measurements are not precise enough to rule out pentamers, for example. Over time, the hexamer peak decreased, and a broad, higher-molecular-

weight peak appeared, corresponding to dodecamers and larger species (further referred to as dodecamer). Primarily higher order species were obtained during the plateau phase of the ThT curve. Interestingly, we did not observe a multitude of oligomers but instead only two main populations: hexamers and dodecamers in equilibrium, shifting over time both during the lag phase and beyond (**Figure 2.2B**).

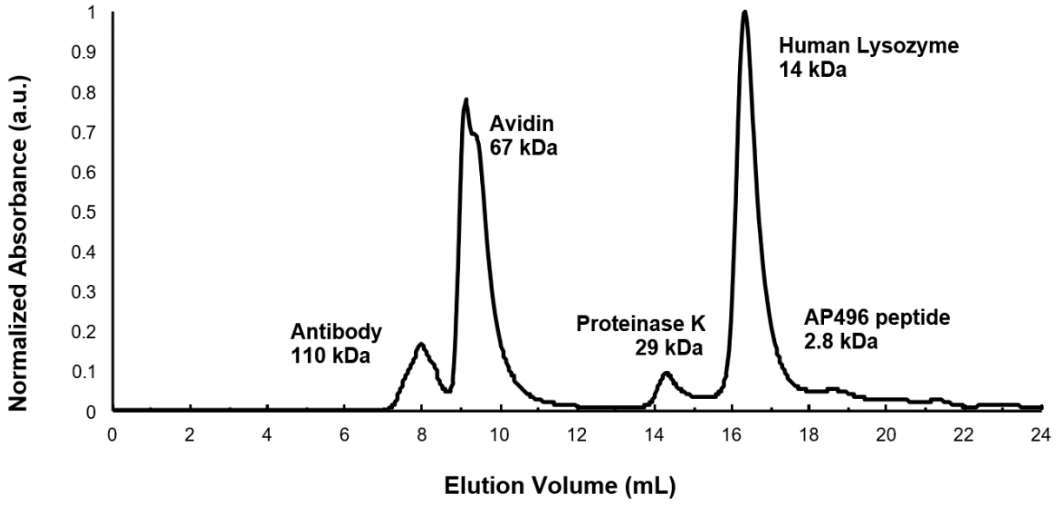

Figure 2.4. Standard SEC curve with associated MW values.

Oligomers derived from human brains have molecular weight distributions corresponding to a mix of dimers to dodecamers, and the dodecamer in particular has been linked to disease[55,27-29]. For example, dodecamers derived from transgenic (Tg) APP-overexpressing mice impair memory when injected into brains of young rats[27]. Dissociation of dodecamers into trimers and tetramers leads to cognitive recovery in mouse models[30], while hexamers are in dynamic equilibrium with the dodecamers [also referred to as Aβ*56 in the literature based on molecular weight[55]]. We did not observe the smaller oligomers that have been observed by SDS/PAGE and SDS purification from brain, such as dimers, trimers, and tetramers, which some have suggested

may be the result of the dissolution of larger aggregates[48-49]. Thus, the lack of small oligomers and the existence of the dodecamers obtained here at neutral pH in PBS suggest that we are likely probing physiologically relevant oligomeric species.

2.3.2 *Toxic oligomers contain α-sheet structure, not β-sheet structure*

The secondary structure of Aβ was then evaluated as a function of time by circular dichroism (CD) (**Figure 2.2C**). Consistent with the ThT profile, aggregation initiated from an unstructured random coil conformation (0 h) and proceeded to β-sheet structure in the course of aggregation (48 h and beyond). Interestingly, the curve lifted and flattened in the lag phase before β-sheet formation (shown for 8–36 h). Thus, the hexamer and dodecamer oligomers populated during the lag phase do not contain measurable conventional secondary structure, while the higher-molecular-weight late species (48 h and beyond) contain β-structure consistent with the inference from the ThT-binding assay. The featureless CD spectra of the intermediate oligomers (in both size and time) are similar to what we proposed and confirmed experimentally for α-sheet structure[64-67]. Designed α-sheet peptides (denoted as AP#, for alternating peptide) produce a "null signal" due to their unique structural characteristics that lead to cancellation of the CD signal, as shown in **Figure 2.2C** for the α-sheet design AP407, which is distinct from random coil, α-helical, and β-sheet CD spectra[64-67]. Contrary to our results, many assume that Aβ soluble oligomers adopt β-sheet structure in the lag phase, but a number of other studies report CD spectra very similar to the α-sheet spectra provided here[22,44,101-102]. While similar spectra were obtained, they were not recognized to be α-sheet due to its novelty, as model compounds are critical to the assignment of spectra. Here we used our synthetic α-sheet designs, such as AP407, for that purpose, but to do so, further characterization of the structure was necessary.

To obtain more detailed structural information for our α-sheet designs, 2D NMR experiments of AP407 were performed, which resulted in 455 distinct nuclear Overhauser effect interactions (NOEs) between protons for this 23-residue peptide (**Appendix A**), allowing for the calculation and testing of structural models of AP407 (**Appendix A**, **Figure 2.5A**). The chemical shifts from NMR and the NMR-derived structural ensemble are in excellent agreement (**Appendix A**, **Figure 2.5B**). The secondary chemical shifts, which are often used to determine regions of secondary structure, are consistent with α-helical structure while the coupling constants reflecting the Φ dihedral angles are not (**Appendix A**, **Figure 2.5C**). Instead, the coupling constants are indicative of β-sheet or extended structure. Thus, the NMR results point to both α-helix and extended sheet structure, as we would expect for an α-sheet comprised of local helical (Φ,Ψ) values of alternating chirality (**Appendix A**, **Figure 2.1**) forming a hairpin sheet structure. The NOEs provide further support for this conclusion. Sequential H_N-H_N NOEs expected for α-sheet structure were observed, while the standard main-chain NOE patterns expected for α-helical and β-sheet structures were not present (**Appendix A**, **Figure 2.5D,E**), which is consistent with the flat CD spectrum for AP407 (**Figure 2.2C**, with one of the NMR structures provided in the Inset). In an earlier study, we obtained NOEs for two other α-sheet designs, but not a sufficient number to calculate a structure[64]. Here, however, we obtained a greater number of NOEs —including side-chain NOEs—by using a more con- strained design with a disulfide bond linking the α-strands. One hundred percent of the 455 NOEs are satisfied by the ensemble presented in **Appendix A**, as shown in **Figure 2.5**. As is generally the case with small peptides, however, AP407 retains conformational flexibility, as is particularly evident in the turn region due to alternative side- chain packing (**Appendix A**, **Figure 2.5A**).

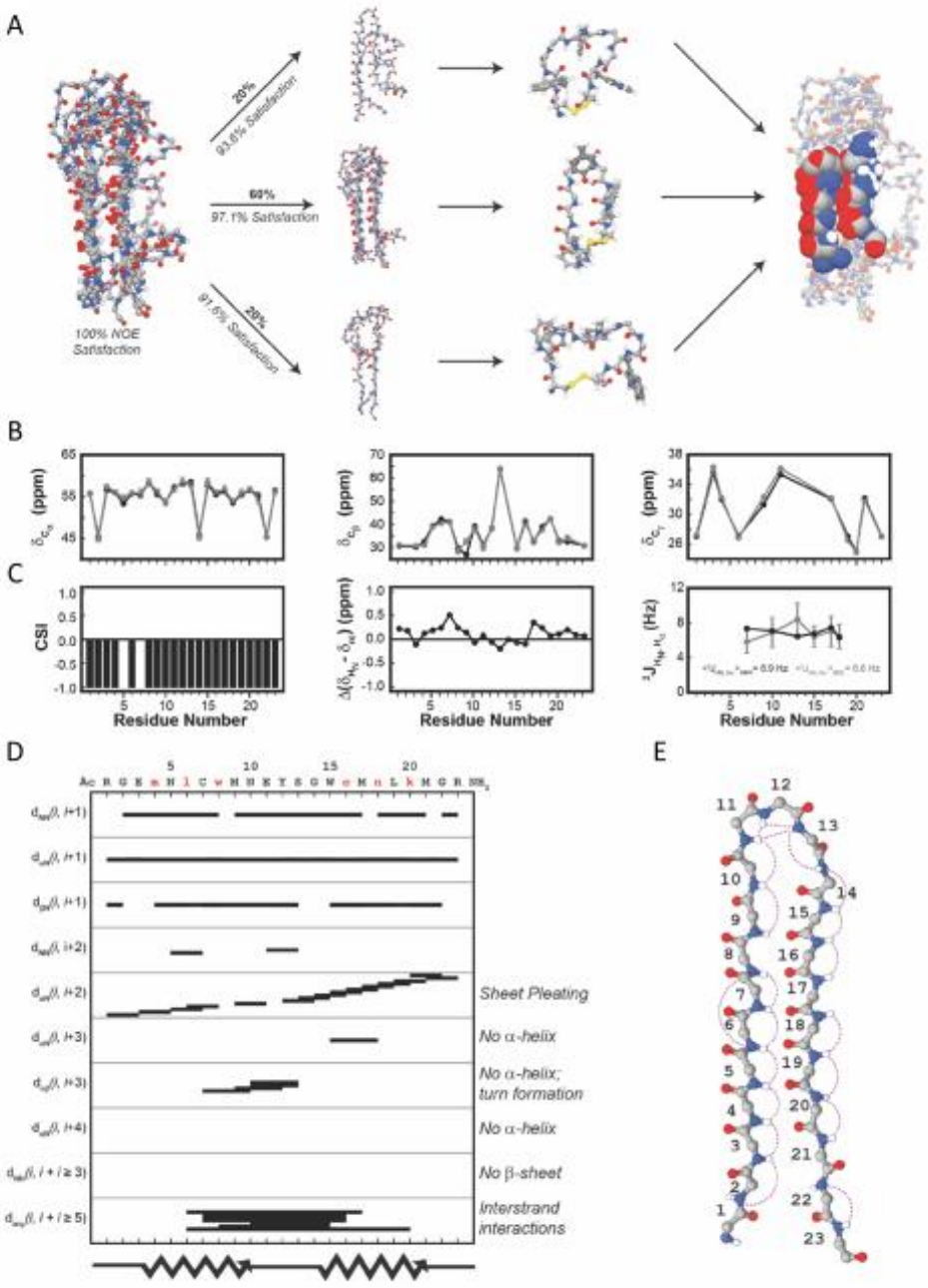

Figure 2.5. Structural and NMR data highlighting the presence of α-sheet secondary structure in AP407. (A) Backbone atoms of the 10 NMR structures for AP407 (left). The 10 conformers clustered into 3 groups (center left). The dominant cluster contained 6 structures with well defined structure, while the other clusters were more disordered near the turn. (B) Comparison of the chemical shifts between the NMR data (black) and the model (grey). (C) Secondary chemical shifts calculated as the difference between the AP407 values and 'random coil' values obtained from MD simulations. (D) Summary of short- and long-range NOEs. (E) Observed H_N-H_N NOEs are mapped onto the peptide structure and represented as magenta lines.

Microfluidic modulation spectroscopy (MMS) was used to further characterize the structural characteristics of Aβ during aggregation. MMS measures peptide absorption spectra by optically scanning across the amide I band, which reflects a combination of patterns of hydrogen bonding, dipole–dipole interactions, and the geometric orientations throughout the peptide. As this is a new technique and α-sheet is a nonstandard structure, we used synthetic designed α-sheet hairpins as model compounds to help interpret the spectra, along with controls for other conventional secondary structures: designed α-sheet hairpins (AP5, AP90, AP407, and AP421), β-sheet (P411), and α-helical (PSMα1) peptides. Each class of peptide produced distinctive spectral features, as shown in the second derivative plots of the amide I region (**Figure 2.2D**). This is further illustrated by subtracting the AP407 α-sheet peptide spectrum from the other samples, highlighting the similarities between the different α-sheet peptides with the largest difference at 1,680 cm^{-1}, which we surmise is due to the improved dipole alignment from stabilization of the α-sheet structure in the hairpin due to the disulfide cross-link (**Figure 2.2E**). Moreover, this band was predicted to be dominant for non-solvated α-sheet structure[103] and confirmed experimentally by conventional Fourier-transform infrared spectroscopy (FTIR) of dry films[64-66].

After establishing the spectral features of the model compounds, we analyzed the most toxic Aβ sample (24 h) and found its spectrum to be consistent with α-sheet and distinct from β-sheet and α-helix (**Figure 2.2D,E**). In fact, the Aβ oligomer spectrum nicely overlays the other α-sheet spectra. With increasing aggregation time, the Aβ spectrum shifted and was most similar to our β-sheet control (P411) rather than any of our α-sheet designs (120 h, **Figure 2.2D,E**), but note the shift in the 120-h Aβ sample relative to the monomeric β-hairpin P411. Such shifts are routinely seen between conventional β-structure and fibrils by FTIR[104]. Consistent with the ThT and CD results, the α-sheet structure preceded β-sheet formation. In addition, it was recently found that

fibrils of a fragment of a variant of the amyloidogenic protein transthyretin contain spectroscopic signals of both α-sheet and β-sheet structures by FTIR, providing further support for the presence of α-sheet in amyloid systems and the possibility of coexistence of an α- and β-sheet[62,105].

2.3.3 *De novo α-sheet peptides specifically bind toxic oligomers*

The CD, FTIR, and NMR results all support the presence of α-sheet secondary structure in our designed peptides, and the toxic oligomeric Aβ samples are essentially indistinguishable from the peptides. As another probe of α-sheet content during aggregation, we developed the soluble oligomer-binding assay (SOBA), which is an ELISA-like assay that utilizes an α-sheet peptide (AP193) instead of an antibody as the capture agent. Under the conditions used here, SOBA detects α-sheet content in toxic Aβ solutions at concentrations below 2.5 nM, corresponding to ~1.1 ng (**Figure 2.6**). In effect, SOBA is an indirect reporter of α-sheet structure owing to the binding via complementary α-sheet structure in the designed peptide and the amyloid species. Consistent with the ThT, CD, and MMS experiments, SOBA-detected α-sheet structure was highest in the lag phase and preceded the formation of β-structure (**Figure 2.2F**). The progression of α-sheet corresponded with cell toxicity and revealed that both peaked at 24 h and decreased drastically as β-sheet content increased exponentially. Importantly, there was a strong correlation between α-sheet formation by SOBA and cell toxicity (R^2 = 0.94, **Figure 2.2F** Inset), supporting our hypothesis that oligomeric α-sheet structure is associated with toxicity.

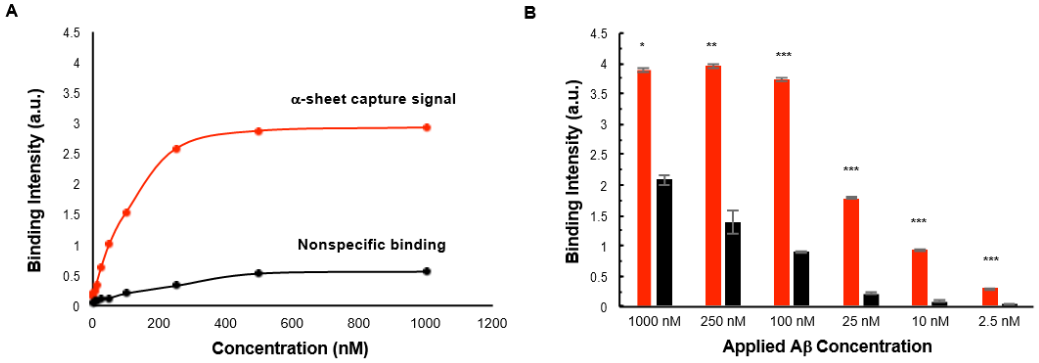

Figure 2.6. Calibration curves to determine best signal / noise ratio for SOBA. (A) Optimization of signal / noise using pre-incubated Aβ with serial dilutions. (B) Effect of new, fresh antibodies on SOBA signal.

SEC was then used to assess the affinity of α-sheet designs for soluble, toxic Aβ oligomers of different sizes. First, excess AP407 was added to monomeric Aβ (4:1 by concentration), and there was no effect on the elution curve (**Figure 2.7A**). However, addition of AP407 to Aβ preincubated for 24 h at 25 °C resulted in a shift in both the hexamer and dodecamer peaks toward higher molecular weights consistent with specific binding of the peptide to these assemblies (**Figure 2.7A**). Additionally, biolayer interferometry was employed to quantify the binding kinetics of individual SEC fractions to the AP5 α-sheet peptide design. The hexamer peak from an 8-h incubation and the dodecamer peak from a 24-h incubation had nanomolar binding affinities (0.48 and 8.1 nM, respectively).

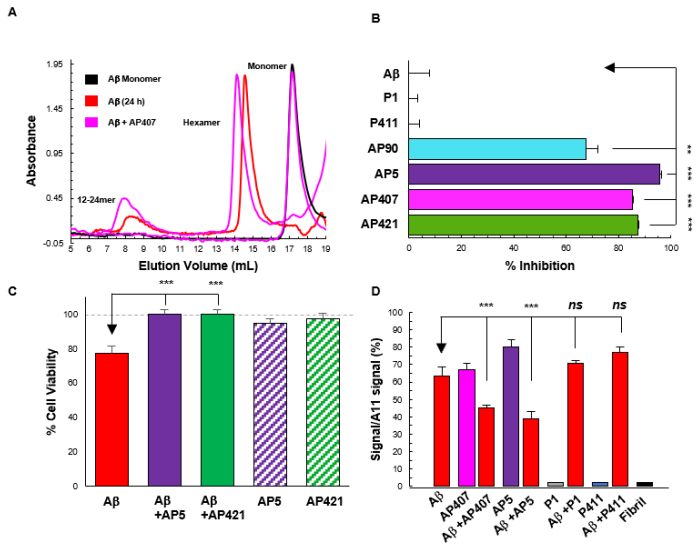

Figure 2.7. α-sheet specificity for oligomer Aβ. (A) SEC traces of Aβ at different points in the aggregation process with and without α-sheet peptide added. (B) Effect of α-sheet, β-sheet, and random coil peptides on Aβ aggregation obtained by ThT fluorescence. (C) Neutralization of toxicity by α-sheet peptides. (D) Dot blot with A11 oligomer-specific antibody used as the primary, showing specificity for Aβ oligomer over fibril, α-sheet peptide over β-sheet or random coil controls, and effect of co-incubation of α-sheet peptide with α-sheet-containing Aβ oligomer.

2.3.4 *α-sheet peptides inhibit Aβ aggregation and cytotoxicity*

Having shown that designed α-sheet peptides bind to toxic oligomeric aggregates of Aβ specifically and tightly, we assessed their ability to inhibit aggregation using the ThT assay. Overall, incubation of Aβ with α-sheet designs in excess (4:1) reduced aggregation by up to 96% while the random coil (P1) and β-sheet (P411) controls had no significant effect (**Figure 2.7B**). The α-sheet peptides inhibited aggregation by binding the complementary structure in the toxic soluble oligomers in the lag phase (**Figure 2.7A**), which are on-pathway to aggregation. We then tested whether inhibition also led to neutralization of toxicity using a preincubated 24-h Aβ sample with AP5 or AP421 (**Figure 2.7C**). Cell viability was recovered upon addition of the α-sheet designs, confirming that the inhibitory effect targeted the toxic oligomers. Notably, the peptides

alone (hashed bars in **Figure 2.7C**) were not toxic although they too contain α-sheet structure, but by design they remain monomeric to avoid toxicity. To investigate the hypothesis that the A11 antibody recognizes toxic oligomers with different sequences through α-sheet structure, we performed dot-blot experiments with the A11 antibody and our α-sheet peptides[56]. As expected, A11 bound toxic Aβ oligomers (red bars, preincubated 24 h) while binding to fibril samples was negligible (**Figure 2.7D**). Interestingly, A11 bound designed α-sheet peptides with high intensity comparable to Aβ oligomers (67% and 80% of A11 positive control for AP407 and AP5, respectively, compared with 63% for Aβ), while values for the random coil (P1) and β-sheet (P411) controls were negligible. Recognition of the α-sheet motif by an oligomer-specific antibody supports the assertion that this structure is present in toxic Aβ oligomers. Furthermore, incubation of Aβ with α-sheet peptides (1:1 by mass) decreased A11 binding intensity, even if each bound with roughly equivalent intensity alone (**Figure 2.7D**, red bars). The reduction in intensity is shown relative to the A11 primary signal, but as both Aβ and the α-sheet peptides bind the A11 antibody, the effect is even greater when normalized by the sum of the observed Aβ and α-sheet peptide signals, leading to a drop of 35% and 27% for AP407 and AP5, respectively. This substantial drop in A11 binding suggests that the binding of the Aβ oligomers to the AP peptides alters their conformations, thereby changing the A11 epitopes, or that the antibody-binding sites are masked in the Aβ-AP407 complex. The CD spectra for the oligomer with and without AP407 are indistinguishable (**Figure 2.8**), supporting the latter interpretation that the epitopes are masked when AP407 binds Aβ. Thus, the A11 antibody and α-sheet peptides appear to share a common binding epitope on toxic Aβ oligomers. In contrast, incubation of Aβ with random coil and β-sheet peptides had no significant effect.

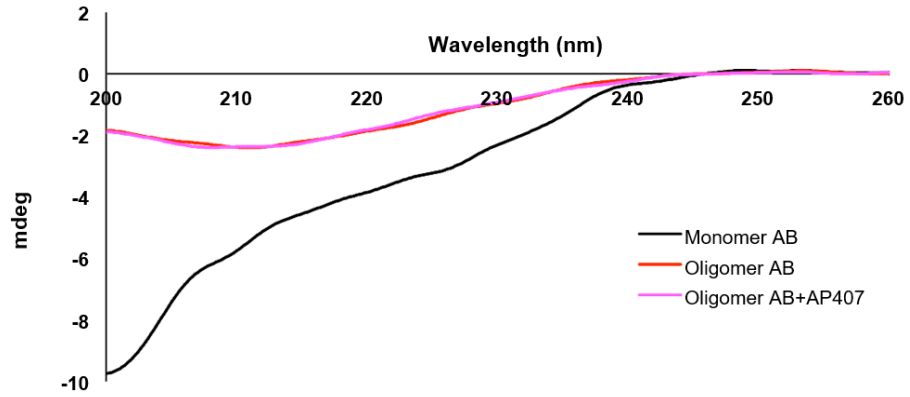

Figure 2.8. Circular dichroism spectra for Aβ monomer, and 24h pre-incubated toxic Aβ oligomers with and without AP407.

2.3.5 *α-sheet designs decrease toxic oligomers in AD mouse model*

Next, we investigated the effect of administering an α-sheet design (AP5) to transgenic (Tg) APPsw mice expressing human Aβ (1–42) both *ex vivo*[106] and *in vivo*[107]. The *ex vivo* system involved testing the effect of AP5 on 250-μm thick brain sections from 91-wk-old Tg APPsw mice. Coronal brain sections were excised and treated with either PBS (control vehicle to dissolve AP5) or AP5 and cultured for 24 h before quantification and analysis. AP5 had no significant effect on average protein concentrations or, as a more specific probe, lactate dehydrogenase released after 24 h in soluble fractions of brain slice homogenates (**Figure 2.9A,B**), indicating that AP5 did not induce toxicity in the organotypic brain slice cultures and that the brain tissue was still viable.

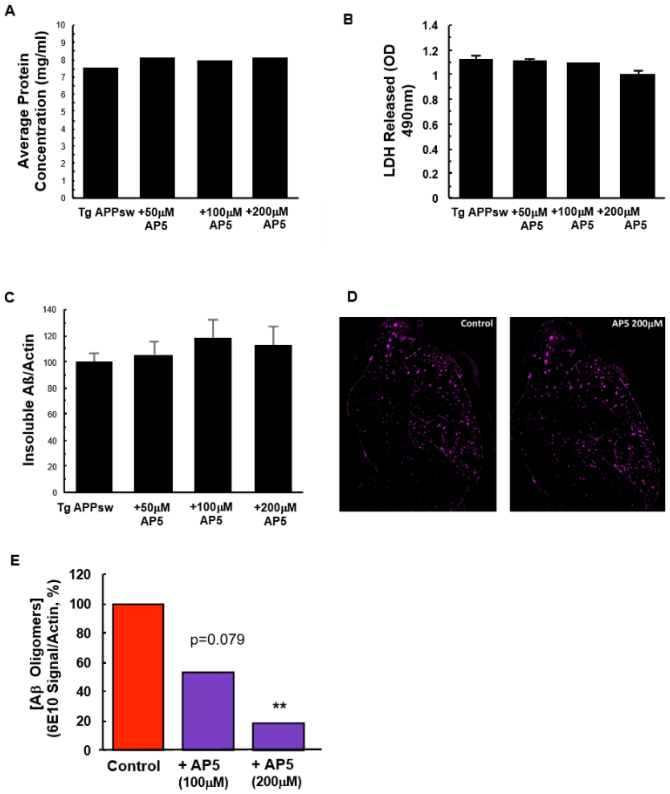

Figure 2.9. α-sheet peptides are nontoxic, do not target fibrils, and specifically target the toxic Aβ species in a transgenic mouse brain slice study. (A) Average protein concentrations in brain slice homogenates. (B) LDH released after 24h in Tg APPsw brain slice study. (C) Addition of AP5 reduced soluble oligomers of Aβ but did not affect insoluble levels of Aβ. (D) 6E10 immunostaining of 6 mm consecutive sections treated with control medium of medium containing 200 mM AP5. (E) Aβ oligomers were quantified through western blot in the detergent soluble fractions of control mice or mice treated with different amounts of AP5.

The A11 antibody was used to assess toxic oligomer levels in the detergent soluble fraction of the brain slice homogenates with and without AP5 treatment. AP5 had no effect on detergent insoluble levels of Aβ (amyloid fibrils and plaques) (**Figure 2.9C,D**), whereas the A11- detectable oligomers were reduced in a dose-dependent manner with a maximum drop of 79% (**Figure 2.10A**). To further evaluate the effects of AP5 on Aβ oligomers, the detergent-solubilized fractions of brain slice homogenates were analyzed by Western blots using the 6E10 Aβ antibody under nondenaturing conditions, which showed a maximum drop of 82%, confirming the A11 results

(**Figure 2.9E**). In contrast, the total Aβ dropped by 44% at the highest dose of AP5, with the largest decrease in the Aβ42 population (**Figure 2.10B**). These findings show that the preferential binding of the toxic oligomers presented above *in vitro* and in the cell-based assay were also operative *ex vivo* in the organotypic brain slices from Tg APPsw mice.

Following the encouraging results in brain sections, AP5 was administered via intracranial injection to the right hemisphere (hippocampus and cortex) of 103-wk-old Tg APPsw mice. A11-detectable oligomers were assessed 24 h later and were found to drop by up to 40% (compared with the left hemisphere control of the same animal, **Figure 2.10C**). It is noteworthy that these animals were in the late stages of cerebral amyloidosis, where anti-amyloid interventions typically have limited effects, and, as above, A11 binding to AP5 may be contributing to the signal, masking some of the effect. Recently, Luo et al.[108] reported a self-destructive nanosweeper that captures and clears Aβ by activating autophagy. However, this nanosweeper recognizes Aβ by a sequence-complementarity motif and thus indiscriminately captures and clears monomers as well as oligomers. In contrast, the α-sheet peptide AP5 was associated with clearance of toxic Aβ in a dose-dependent manner (**Figure 2.10A** and **Figure 2.9E**), suggesting a mechanism based on structure rather than sequence recognition, thereby selectively removing pathogenic forms of Aβ while leaving monomers and nontoxic fibrils intact.

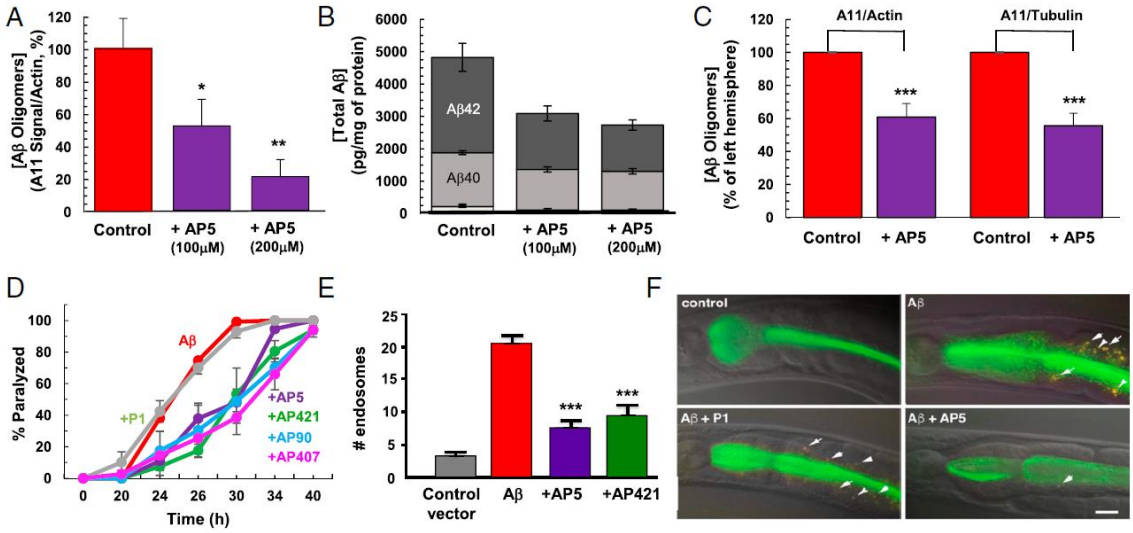

Figure 2.10. The effect of α-sheet peptides in transgenic mice and *C. elegans* expressing human Aβ. (A) A11 detectable oligomers were reduced with AP5 treatment in *ex vivo* Tg APPsw brain slices. (B) Detergent soluble Aβ38, Aβ40, and Aβ42 levels quantified for reduction with AP5 treatment using an Aβ ELISA test. (C) A11-detectable oligomers decreased by 40% in the right hemisphere injected with AP5 compared with the control left hemisphere. (D) Quantification of the effect of α-sheet peptides and controls on Aβ-induced paralysis in transgenic *C. elegans* expressing human Aβ. (E) Quantification of Aβ-induced membrane disruption tracked via extent of endosome formation, with and without α-sheet peptides. (F) Representative images of the anterior intestine of GFP reporter *C. elegans* fed engineered cultures of *E. coli* expressing human Aβ pretreated with either control or α-sheet peptide.

2.3.6 *α-sheet peptides inhibit Aβ-induced paralysis in AD C. elegans model*

Given the difficulty of long-term administration of compounds in transgenic mouse AD models, we sought an alternative model system to test the ability of α-sheet peptides to block Aβ toxicity *in vivo*. We chose a transgenic *C. elegans* model that has been used extensively to assay the ability of exogenous compounds to reduce Aβ toxicity[109]. Upon temperature upshift, the transgenic *C. elegans* strain CL4176 up-regulates Aβ expression in body-wall muscle, leading to a reproducible paralysis phenotype[109]. While in the past it has been difficult to treat *C. elegans* with large molecules such as peptides or proteins, Perni et al.[110] showed that treating *C. elegans* with a

novel cationic lipid vesicle transfection reagent allows ingested proteins to spread throughout the body. Using a FITC-labeled α-sheet peptide, we confirmed that co-exposure with the transfection reagent allowed whole-body exposure to the peptide (**Figure 2.11**). We then tested whether exposure to a set of α-sheet peptides would delay the onset of paralysis induced by Aβ up-regulation in strain CL4176. All α-sheet peptides tested (AP5, AP90, AP407, and AP421) significantly delayed Aβ-induced paralysis, while the control random coil peptide P1 had no effect (**Figure 2.10D**). These worms rarely form amyloid plaques, such that the paralysis is not associated with plaque burden[111], and instead, inducible Aβ expression leads to the formation of toxic soluble oligomers, which is consistent with the observed mechanism of inhibition by α-sheet compounds.

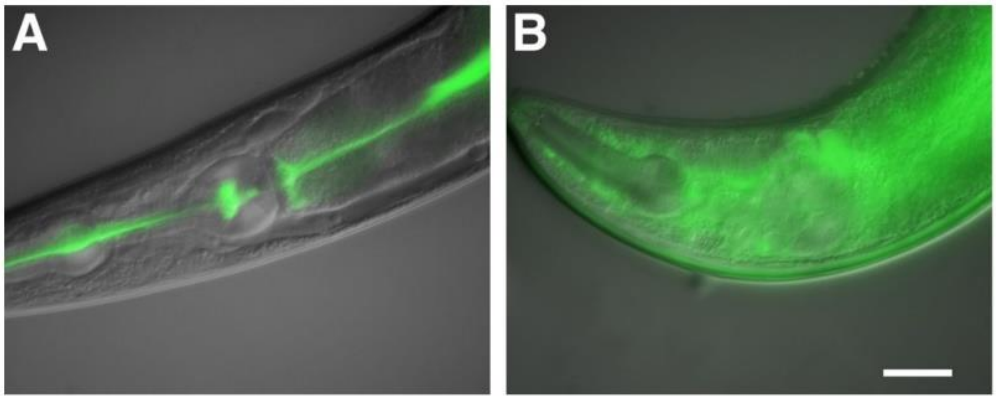

Figure 2.11. Co-incubation with transfection reagent allows α-sheet peptides to permeate worm tissue. (A) Anterior of *C. elegans* adult worm incubated with FITC-labeled AP5 in HEPES buffer, primarily restricted to the lumen of the intestine, versus (B) distributed throughout the body of the worm using PULSin reagent.

The transgenic *C. elegans* experiments described above cannot determine whether the protective effects of the α-sheet peptides result from their direct interaction with Aβ, as predicted by our proposed mechanism of action, or from an unknown interaction downstream in the toxic process. We therefore employed another *C. elegans* model in which transgenic GFP reporter worms were fed *Escherichia coli* engineered to secrete human Aβ (1–42)[112]. *C. elegans* ingestion

of Aβ-expressing *E. coli* leads to intestinal membrane damage, which can be measured by quantifying induced endosomes labeled with a GFP fusion protein that normally localizes to the intestinal lumen[112]. This model allowed us to pre-expose Aβ to the peptides (by treating the *E. coli* cultures rather than the worms) before assaying Aβ toxicity. As shown in **Figure 2.10E** and **Figure 2.10F**, treating the Aβ-expressing *E. coli* culture with α-sheet peptides significantly inhibited the induction of intestinal endosomes that normally occurs when these cultures are fed to the *C. elegans* reporter strain. We interpret this result to indicate that the α-sheet peptides are interacting with Aβ secreted by the *E. coli* strain and neutralizing the toxic oligomers.

2.4 CONCLUSIONS

AD is associated with a heterogeneous distribution of toxic oligomers, making it difficult to discern mechanisms of toxicity. Here, we isolated and characterized a unique secondary structure motif—α-sheet—in specific populations of Aβ oligomers associated with neurotoxicity. We showed that the α-sheet structure is recognized by the A11 amyloid-oligomer–specific antibody, that α-sheet peptides inhibited Aβ aggregation and blocked toxicity, and that α-sheet peptides bound specifically to oligomeric preparations of Aβ. Furthermore, α-sheet peptides specifically recognized and neutralized the toxic, soluble oligomers of Aβ in two very different animal models of AD. These findings open the possibility of novel therapeutic and diagnostic agents for AD and other amyloid diseases.

Chapter 3. ALPHA-SHEET AS AN EARLY BIOMARKER IN AD

3.1 INTRODUCTION

Alzheimer's disease (AD) is one of over 50 amyloid diseases and is now the sixth leading cause of death in the United States, affecting over 5.8 million Americans and projected to cost upwards of $1.1 trillion in paid and unpaid care by 2050[113]. AD is characterized by the aggregation of the amyloid beta-peptide (Aβ) into a heterogeneous and dynamic distribution of low molecular weight (LMW) oligomers that progress into high molecular weight (HMW), β-sheet rich protofibrils, and eventually results in the deposition of the characteristic cross-β pleated sheet fibril plaques that are the pathological hallmarks for clinical diagnosis of the disease[12-22] (**Figure 3.1A**). Recent studies suggest that the LMW soluble oligomers are the main toxic agents in AD and are strongly correlated with disease progression, while plaque burden is not[17,18,51,54-55]. Interestingly, disease symptoms do not surface until the late stages of Aβ aggregation when plaques have already deposited and the primary damage to the neurons has taken place. Furthermore, Aβ oligomerization is the first known biochemical change that occurs, preceding tau phosphorylation, plaque deposition, tau tangle formation, and neurodegeneration[114-116]. Current approaches diagnose AD in the later stages of disease when protofibrils and fibrils dominate, which is often decades too late to intervene and treat, and do not base diagnosis on factors directly correlated with toxicity and neurodegeneration (**Appendix B**)[117-147]. In fact, several drug candidates targeting late-stage Aβ aggregates have not been successful in large, multicenter clinical trials[92-100]. In the case of early diagnosis before the mild cognitive impairment (MCI) stage, upwards of $7.9 trillion could be saved in medical and long-term care alone[113].

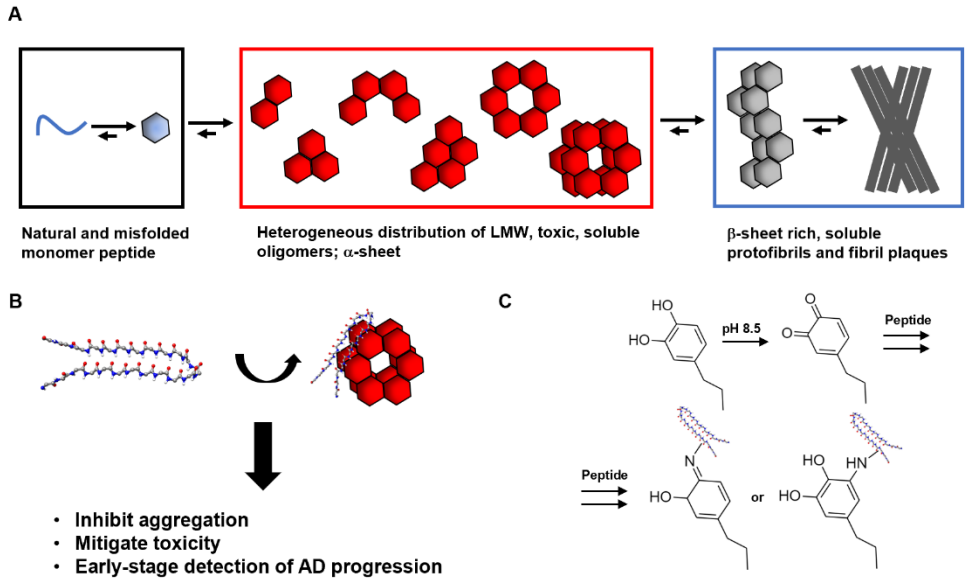

Figure 3.1. Schematic depiction of Aβ aggregation, α-sheet binding, and PDA polymerization. (A) Cartoon representation of initial Aβ misfolding and subsequent aggregation into toxic α-sheet LMW oligomers followed by HMW β-sheet oligomers and eventually fibril plaques. (B) Depiction of α-sheet binding to toxic oligomer and effects seen upon binding. (C) Schematic of dopamine hydrochloride polymerize to form PDA film with peptide linked.

Our lab has focused on characterizing the earliest structural changes that occur in a variety of amyloid systems using both computational and experimental techniques[50,61-68]. Through these studies we 'discovered' and characterized a novel secondary structure, termed α-sheet, which we proposed to be the main structure in the LMW toxic oligomers in the early stages of disease. α-sheet is a unique protein secondary structure that is distinct from α-helix, β-sheet, and random coil, characterized by the alternation of subsequent residues between the α_R and α_L regions of Ramachandran space and has been characterized by a variety of techniques, including: NMR, circular dichroism (CD), microfluidic modulation spectroscopy in the IR region (MMS-IR), and FTIR[50,64-68]. By focusing on the early misfolding that takes place at a molecular level, we have been able to measure α-sheet formation in Aβ oligomers in solution (using CD and MMS-IR) and design stable α-sheet peptides that: inhibit aggregation and mitigate toxicity *in vitro*[50,64-68], capture

toxic oligomers *in vivo*[50], and act as diagnostic agents that detect the α-sheet-containing toxic species pre-symptomatically in AD patients (**Figure 3.1B**). Our diagnostic test is termed the Soluble Oligomer Binding Assay (SOBA), which is an ELISA-like assay wherein an α-sheet peptide is covalently linked to the plate and used as the capture agent rather than an antibody. In this regard, SOBA reports on α-sheet structure in applied samples by binding to the toxic species through complementarity. We describe a novel technique using polydopamine (PDA) deposition to functionalize a 96-well polystyrene plate for peptide linkage. PDA surface coatings are well-studied for modifications of material surfaces and are extremely desirable due to their ability to self-polymerize on a wide variety of substrates and support facile linking of secondary molecules[148-153] (**Figure 3.1C**). Here, we exploit these characteristics to develop and describe the refinement and optimization of the SOBA assay for pre-symptomatic detection of toxic oligomers.

Early detection of AD, prior to symptom onset, could prove invaluable for improving therapeutic efficacy as well as quality of care for patients. Current biomarker standards diagnose disease far too late in the process, depending on a decrease in $A\beta_{42}$ concentration as it deposits into plaques, or changes in other biomarkers that occur downstream of $A\beta_{42}$ aggregation and cytotoxicity. Furthermore, these biomarker levels are subject to mixed results due to different techniques, lab protocols, or even kits used to measure concentrations. Many diagnostics also require painful and invasive cerebrospinal fluid (CSF) collection, as most techniques are not sensitive enough to detect in blood plasma (some plasma diagnostics are highlighted in **Appendix B**). PET scans have become more popular as an AD diagnostic, however, they rely heavily on Aβ plaque- or tau-based tracers that are only positive in the later stages of disease progression and are very expensive to administer. SOBA is an exciting diagnostic tool with prognostic capacity for AD that requires a minimally invasive plasma draw and is low cost. SOBA is a simple and

translatable assay that utilizes a biomarker specifically linked to cellular toxicity through our *de novo* peptides that have been shown to specifically inhibit aggregation and toxicity of Aβ oligomers both *in vitro* (**Figure 3.2**) and *in vivo*[50].

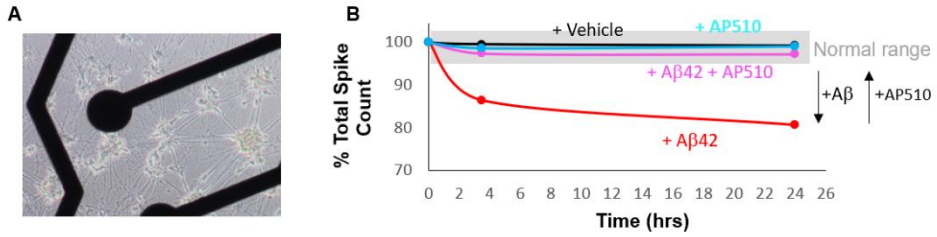

Figure 3.2. α-sheet peptide rescues neurons from Aβ-induced electrical activity effects. (A) SH-SY5Y neuroblastoma cells were differentiated into neuron-like cells, with representative image depicted on an Axion MEA electrode plate. (B) Aβ oligomers specifically reduced total spikes seen in neuronal culture, while addition of AP510 rescued this effect and AP510 alone had no effect.

3.2 METHODS

3.2.1 *Peptide Synthesis*

The α-sheet and other control peptides were produced either manually or using a Liberty Blue microwave peptide synthesizer (CEM) using standard solid phase peptide synthesis on Rink amide resin with Fmoc chemistry and HBTU activation (manual) and Oxyma activation (microwave). The resin-bound peptides were cleaved and side chains deprotected with (trifluoroacetic acid) TFA/DODT/TIPS/H2O (92.5:2.5:2.5:2.5) and precipitated with cold ether. Crude peptides were purified by Reverse phase-HPLC to ~98% purity (Phenomenex 5 µm C12 100 Å semiprep column). Purified peptides were confirmed by mass spectrometry (MS) on a Bruker Esquire Ion Trap electrospray mass spectrometer, and peptide stocks were lyophilized for storage at −20 °C.

3.2.2 *Synthetic Aβ aggregation*

Aβ(1-42) hereafter referred to as Aβ, was obtained from the ERI Amyloid Laboratory, LLC (Oxford, CT). Aβ was aliquoted using hexafluoroisopropanol (HFIP, Sigma-Aldrich, St. Louis, MO, USA) for use when needed. Aβ was sonicated at 1 mg/ml in HFIP in a bath sonicator for 5 min, followed by 25 min on ice, twice. The resulting solution was then blown under a gentle stream of N_2 gas and concentrated using a SpeedVac concentrator (Savant ISS110, Thermo Fisher Scientific) for 30 min on low setting, thus creating a monomerized Aβ film that was stored at -20 °C and could be thawed and prepared as necessary. Aβ stocks were prepared by removing a film aliquot from -20 °C, and letting it equilibrate to RT (5 min). The film was dissolved to 0.75 mg/mL in filtered 6mM NaOH (pH 11.6, Sigma-Aldrich), flicked to ensure the film was in solution, and sonicated for 5 min. This solution was transferred using a glass pipette to a 0.22 μm Costar Spin-X cellulose acetate centrifuge filter (Sigma- Aldrich), and centrifuged at 7,000 rpm for 2 min. This solution was then transferred using a glass pipette to an Eppendorf LoBind microcentrifuge tube (Sigma-Aldrich) and concentration was measured using a NanoDrop 2000 Spectrometer (Thermo Fisher Scientific) at 280 nm using an extinction coefficient of 1490 M^{-1} cm^{-1}. The resulting stock solution rested at 25 °C for four hours, after which it was either used immediately or stored at 4 °C until needed (no longer than 1 week). Stock Aβ was diluted using phosphate buffered saline (PBS) buffer (10 mM phosphate, 130 mM NaCl, and 2.7 mM KCl; Sigma-Aldrich) to the relevant working concentration for each experiment, as described previously. Briefly, a portion of the stock Aβ was added first to a separate LoBind tube. PBS buffer was added to Aβ-containing LoBind tube and gently mixed by pipette– along the side of the tube.

3.2.3 *Cell differentiation & electrical activity measurements*

SH-SY5Y neuroblastoma cells were differentiated using retinoic acid protocol, as described by Axion Biosystems. Briefly, DMEM media supplemented with 10% FBS and 10 μM retinoic acid was used to dilute SH-SY5Y cells to 1,600,000 cells/mL. A 5 mL droplet of the cell suspension was placed over the recording electrode of a MEA electrode plate and incubated in cell incubator for 4h. Media was added to the full 200 μL working volume and incubated in a cell culture incubator for 4 days with media replaced every day. DMEM with 1% Glutamax and 50 ng/mL BDNF was prepared as the Differentiation Media. After 4d of retinoic acid treatment, media was aspirated and cells rinsed with PBS. We added Differentiation Media and refreshed it every other day for 10 days, at which point MEA electrode measurements began. Electrical activity was measured per Axion Biosystems recommendations. Data reported is calculated from the total number of spikes measured in the culture plate for each well that received treatment (or control). Each measurement calculated the total number of spikes per well on the 16-electrode array over a 2 min measurement time, with minimum spike rate set at 5 spikes/min, pre-spike duration of 0.84 ms, post-spike duration of 2.16 ms, and a coincidence occurrence threshold of 4 electrodes for registering a spike event. Baseline data was acquired for neuron culture 5 days before applying oligomer or peptide samples. Baseline data was confirmed 1h prior to applying treatment, then measured at time of treatment (0h), post-treatment 3.5h, and post-treatment 24h. Data was reported as the change in total number of spikes (as % of baseline) as a function of time after treatment with oligomer, peptide, or control.

3.2.4 *Soluble oligomer binding assay (SOBA)*

We used one of our α-sheet designs, AP510, as the capture agent for all SOBA experiments. A standard 96-well white polystyrene plate was coated with a film of polydopamine (PDA), induced by polymerization of 5 mg/ml dopamine hydrochloride in Tris-HCl at pH 8.5. The PDA solution was incubated – 150 μL per well – with shaking (at a setting of 340 rpm) for 20h to form a sufficiently thick film. Wells were aspirated and washed aggressively with DI H_2O 5 times and allowed to dry at RT for 90 min. AP510 was then dissolved with DMSO (Sigma-Aldrich) to 36 mM and then diluted to 36 μM with CO_3^{2-} buffer (pH 9.6), and 100 μL of AP510 was plated per well. AP510 was coupled with shaking at RT for 2 h. The wells were then aspirated and washed with 300 μL PBS-T (0.01% Tween-20 by volume, Sigma-Aldrich) five times. 150 μL of 10 mM ethanolamine (Sigma-Aldrich) was then plated per well and used to quench unreacted sites on the surface by shaking at RT for 2 h. The wells were then aspirated and washed with 300 μL PBS-T five times. Aβ samples (either synthetic, mouse brain homogenates, or human plasma/CSF) were then applied at 100 μL per well and incubated for 1 h at 25 °C without shaking. The wells were then aspirated and washed with 300 μL PBS three times. For brain homogenates and human plasma a 0.1 μg/ml dilution of the primary 6E10 anti-Aβ antibody (BioLegend, San Diego, CA, USA) was prepared in 3% BSA in TBS-T (50 mM tris, 100 mM NaCl, 0.01% Tween-20 by volume, pH 7.6) and 100 μL of this solution was plated per well and incubated with shaking at RT for 1 h. For CSF, 6E10 antibody was applied at 0.05 μg/ml dilution. The wells were then aspirated and washed with 300 μL PBS three times. 100 μL of the secondary goat anti-mouse HRP-conjugated antibody (Pierce Biotechnology, Waltham, MA, USA) at half the concentration of the corresponding primary concentration in 3% BSA in TBS-T was plated per well and incubated with shaking at RT

for 45 min while covered in foil to avoid bleaching of the HRP. The wells were then aspirated and washed with 300 μL PBS six times. 150 μL of room temperature Super Signal ELISA Femto Maximum Sensitivity Substrate (Fisher Scientific) was plated per well, and luminescence measured at 450 nm on a multimode plate reader (PerkinElmer).

3.3 RESULTS

We have previously reported SOBA detection of α-sheet structure *in vitro*, which utilized a pre-functionalized Nunc immobilizer plate for lysine linkage of molecules and a TMB developing reagent for colorimetric readout[50]. This protocol has been refined in two major ways: (1) PDA functionalization of standard polystyrene plates is now used to coat wells of the microplate, which enables the facile linkage of lysine-containing peptides to the surface at high density, and (2) a chemiluminescent developing reagent is used in place of the colorimetric TMB reagent.

Using PDA as a surface coating molecule to covalently link the α-sheet peptide to the plate increased the uptake from 21 μg/ml to 196 μg/ml total peptide bound (**Figure 3.3**). Additionally, PDA functionalization increased signal for 4,500 μg/mL ($4.5x10^9$ pg/mL) applied Aβ from background levels to 10x background (**Figure 3.4**). Introduction of the chemiluminescent reagent on top of PDA functionalization decreased the limit of detection (LOD) to 45 ag/mL ($4.5x10^{-7}$ pg/mL) concentrations, greatly surpassing that of the 'original' TMB protocol of 45,000 μg/mL ($4.5x10^{10}$ pg/mL) (**Figure 3.4**). Importantly, the specificity was maintained throughout all protocols as monomeric Aβ applied at even a high concentration of 450 μg/mL ($4.5x10^8$ pg/mL) resulted in essentially a null signal on par with background (non-statistically significant differences).

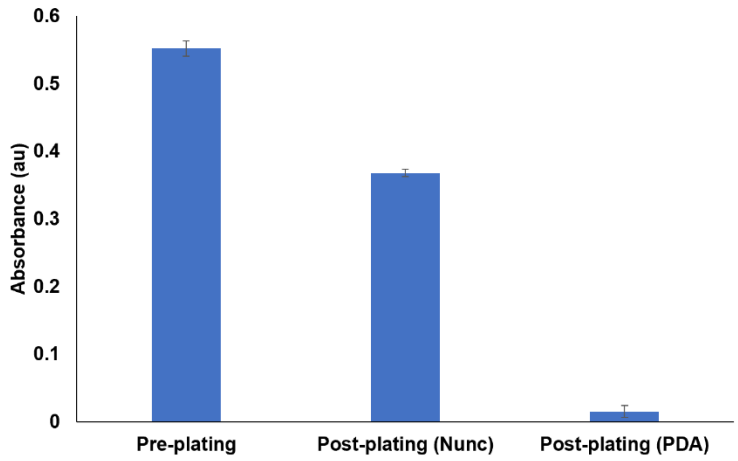

Figure 3.3. α-sheet uptake rate on conventional Nunc plate compared with our proprietary PDA coating.

The PDA+chemiluminescence protocol was first tested on samples from mice that were either wild type (WT), which do not make Aβ, transgenic (Tg) mice that carried the Swedish mutation (APP KM670/671NL, Tg APPsw) or double Tg mice that contain the Swedish mutation as well as a mutant presenilin (PSEN1) gene (APPsw,PSEN1dE9-85Dbo, Tg PSAPP) at various ages[13]. Utilizing Tg mice was particularly useful for gauging the prognostic capacity of SOBA, as we were able to test mice long before symptoms or pathology presented in the mice with the knowledge that they would progress to AD status. **Figure 3.5** shows the comparison of WT signals at various ages with those of Tg APPsw and PSAPP mice from 45 weeks to 108 weeks of age (45-51 weeks are defined as pre-MCI, 95-98 weeks as MCI, > 105 weeks as AD). At the pre-MCI stage, these mice did not have any pathological indicators nor plaque development and did not show any behavioral symptoms. However, at this stage the SOBA signals spiked to levels greater than WT and progressed even higher in the late stages of disease as the concentration of Aβ drastically increased (**Figure 3.5**). In the case of the Tg PSAPP mice that produced much more Aβ, there was some heterogeneity in their disease progression in the pre-MCI stage: pathological

features, memory and learning abilities, and varied magnitudes in SOBA signal that match the mixed populations of toxic oligomers present. These encouraging results in the pre-symptomatic detection of AD in Tg mice allowed us to refine our methods for use in human samples.

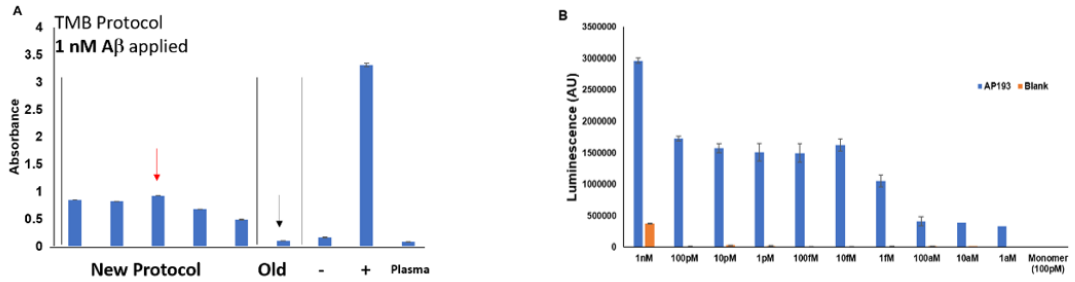

Figure 3.4. Improvements in the SOBA assay. (A) Original TMB protocol improved by an order of magnitude by introducing PDA coating to increase local peptide concentration. (B) Changing TMB developing reagent for a chemiluminescent one lowered LOD to fM range of applied Aβ.

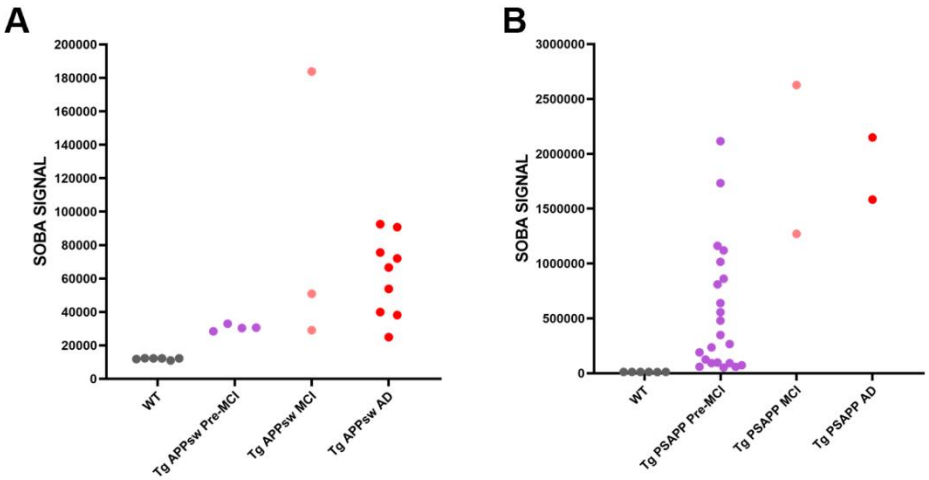

Figure 3.5. SOBA detection of oligomers pre-symptomatically in Tg mice. (A) SOBA analysis of brain homogenates from WT Tg APPsw mice at various stages in the disease process. (B) SOBA analysis of brain homogenates from WT or Tg PSAPP mice at various stages in the disease process.

We used SOBA to quantify the presence of toxic α-sheet-containing Aβ oligomers in banked human samples that were separated out by clinical diagnosis at the time of visit into either

control (CO, n=23), mild cognitive impairment (MCI, n=27), AD (n=17), or Other (non-AD MCI, n=3) status, as well as commercially purchased pooled human plasma (CO, n=1) and single-donor adolescent (17 yr) plasma (CO, n=1). A total of 72 samples were tested using our SOBA diagnostic, of which 8 had follow up visits 1-5 years later where their initial CO diagnosis progressed to MCI. Both plasma and cerebrospinal fluid (CSF) samples were tested with SOBA for all patients in the cohort, with relevant CSF biomarker values, cognitive assessment scores, and other pertinent information (including ApoE status) for each patient given in **Appendix C** with some shown in **Figure 3.6A-D**.

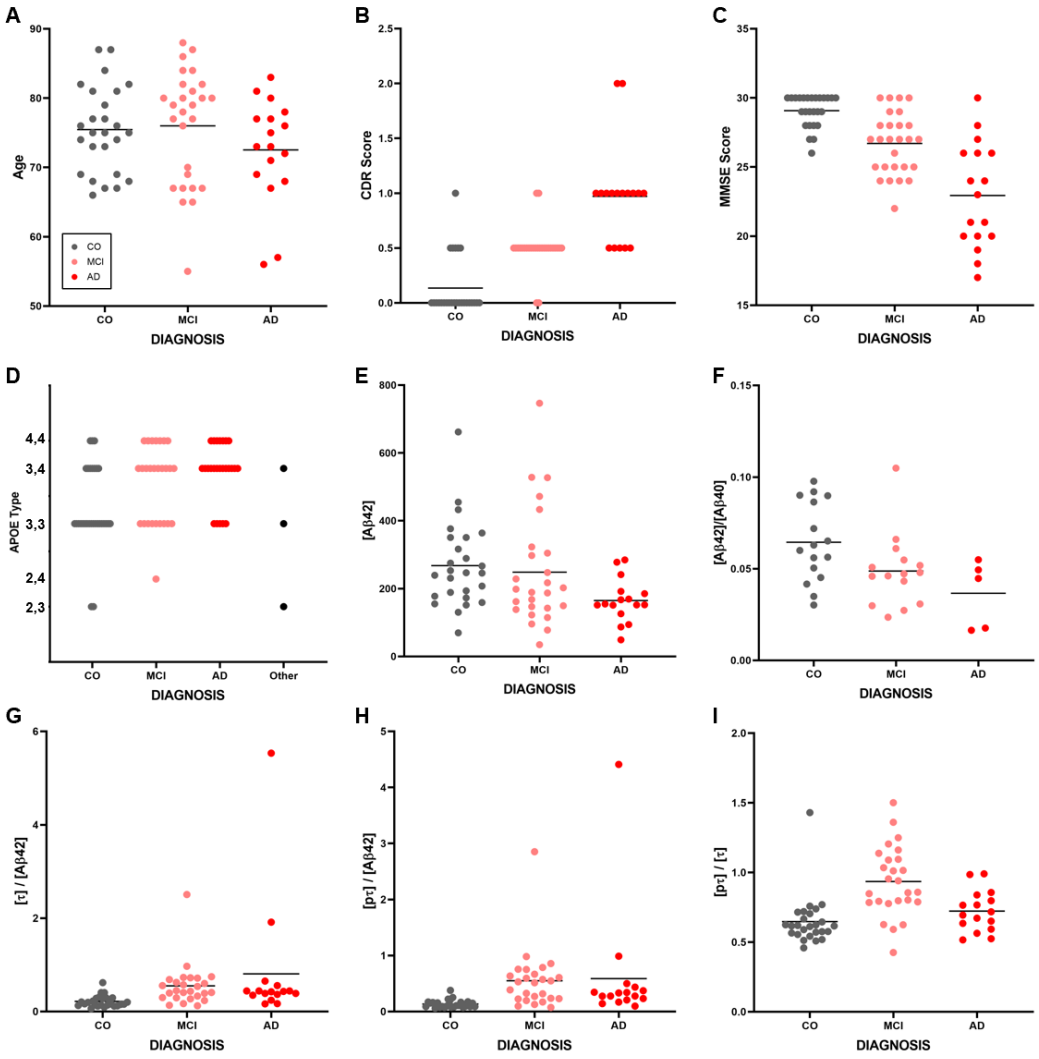

Figure 3.6. Risk and biomarker analysis of patient cohort. (A) Age, (B) CDR score, (C) MMSE score, and (D) ApoE genotype as risk factors/clinical assessments for AD. (E-I) Comparison of different biomarker levels and ratios commonly used in literature to diagnose AD. (E) [Aβ42], (F) [Aβ42]/[Aβ40], (G) [τ]/[Aβ42], (H) [pτ]/[Aβ42], and (I) [pτ]/[τ] cannot differentiate all CO from MCI/AD patients.

Though the average trends of cognitive tests proceeded as expected through clinical diagnosis (worse scores for AD over MCI and MCI over CO), there remained significant overlap between the groups (**Figure 3.6B,C**). Similarly, the current standards for AD diagnosis using CSF biomarkers ($A\beta_{42}$, $A\beta_{40}$, p-tau, t-tau, and combinations thereof) showed general trends

differentiating CO, MCI, and AD, however, there was significant overlap for a large portion of each group that precluded the ability to define objective cutoffs to separate patients into appropriate diagnoses (**Figure 3.6E-I**). Current diagnostics are dependent on either late stage plaque deposition, which results in a reduction of $A\beta_{42}$ concentration in blood and CSF, or tau alterations that occur downstream of Aβ oligomerization[15-17,23,115-124]. Additionally, by only measuring total concentrations of biomarkers in plasma or CSF, these measures are subject to natural variability as a function of lab techniques or based on what kit was purchased for quantification. These biomarkers also fail to differentiate patients in an objective way that is specifically tied to early-stage toxicity that mediates neurodegeneration downstream. By utilizing current standards of AD biomarker diagnostics, this small cohort of patients would largely be mis-diagnosed, due either to a lack of standardization of concentration determinations, or simply due to the fact that patient-to-patient variability of these biomarkers imposes enough difficulty to define objective, standardized levels for reliable AD diagnosis.

SOBA specifically measures the early transitions that take place at a molecular level, which confer the oligomer-mediated toxicity prior to symptom onset and plaque deposition. Thus, SOBA detects these early stages regardless of $A\beta_{42}$ concentration or $A\beta_{42}/A\beta_{40}$ ratio, prior to tau phosphorylation, and prior to clinical diagnosis via current biomarker characterizations and cognitive assessments (**Figure 3.7**). SOBA effectively separated 'true' CO patients from MCI and AD confirmed cases and resulted in an ROC curve with area under curve (AUC) = 1.00 (**Figure 3.7A,B**). Additionally, when we included the patients that were initially diagnosed as CO but converted to MCI within 1-5 years of follow-up, all 8 showed high SOBA signal during their CO stage which was maintained into MCI status (**Figure 3.7A**). Interestingly, a set of patients that had follow-up visits progressed from CO status to 'Other' (non-AD MCI), which we tested using

SOBA and found that these patients had low signals on par with CO and thus were not experiencing AD-related cognitive impairment.

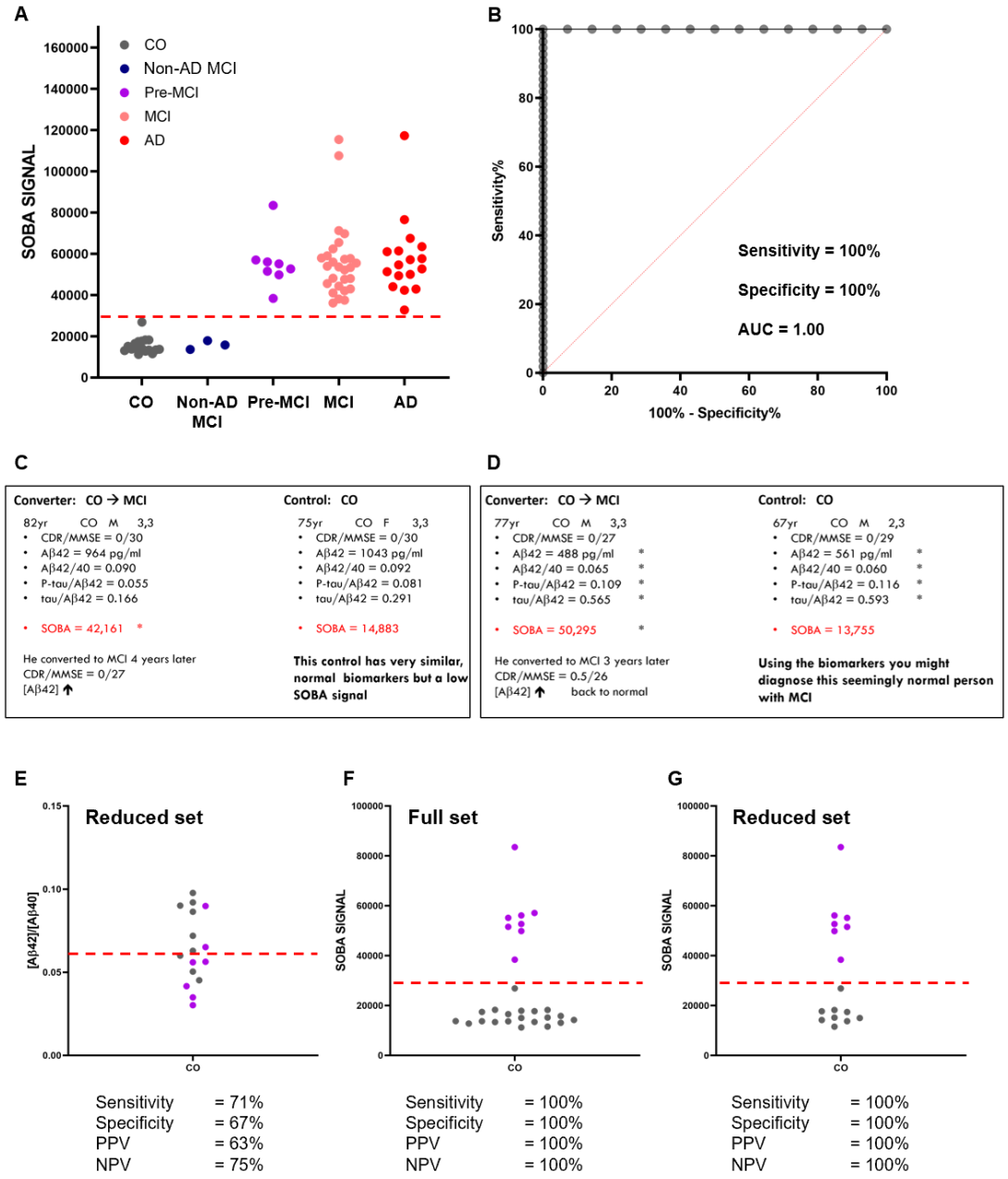

Figure 3.7. SOBA performance on patient cohort. (A) SOBA signals plotted by clinical diagnosis (pre-symptomatic converters in purple) and (B) resulting ROC curve. (C-D) 'Case studies' of CO converter cases diagnosed by SOBA but not by conventional methods. (E) Diagnostic efficacy of [Aβ42]/[Aβ40] ratio (reduced set), (F) SOBA (full set), (G) SOBA (reduced set).

To highlight the efficacy of SOBA for the pre-symptomatic detection of AD, we have included two 'case studies' comparing patients with similar biomarker levels and clinical evaluations that were diagnosed as CO, where one of the pair maintained CO status while the other progressed to MCI (**Figure 3.7C,D**). The first study compares a true CO patient – 75yr F, ApoE3,3, with normal CDR and MMSE scores as well as high CSF [$A\beta_{42}$] = 1043 pg/ml and 'normal' biomarker ratio levels – to a pre-symptomatic CO converter – 82yr M, ApoE3,3, with normal CDR and MMSE scores and [$A\beta_{42}$] = 964 pg/ml as well as similar biomarker ratio levels (**Figure 3.7C**). The pre-symptomatic CO converter had a SOBA signal of 42,161 and converted to MCI 4 years later, while the true CO had a low SOBA signal of 14,883. Similarly, the second case study compares a true CO – 67yr M with relatively low CSF [$A\beta_{42}$] = 561 pg/ml – to a pre-symptomatic CO converter – 77yr M with similarly low CSF [$A\beta_{42}$] = 488 pg/ml and roughly equivalent biomarker ratios. The CO converter had a SOBA signal of 50,295 while the true CO had a signal of 13,755 (**Figure 3.7D**). These two case studies show the unparalleled efficacy of SOBA as a pre-symptomatic diagnostic for AD that is independent of CSF or plasma biomarker concentrations, but rather directly correlated with the toxic forms of $A\beta_{42}$ formed in the early stages of disease that specifically mediate downstream neurodegeneration. When we analyzed all of the CO-diagnosed patients by [$A\beta_{42}$]/[$A\beta_{40}$] ratio (the current standard for CSF biomarker diagnosis) there was no separation between those that went on to MCI and those that remained CO (**Figure 3.7E**, notice this is a reduced set due to lack of $A\beta_{40}$ data for some patients). This approach also produced poor values for sensitivity (71%), specificity (67%), positive predictive value (PPV, 63%), and negative predictive value (NPV, 75%). Alternatively, SOBA analysis of the full set these same patients

nicely separated out true COs from pre-symptomatic CO converters with a cutoff of 27,000, with sensitivity of 100%, specificity 100%, PPV 100%, and NPV 100% (**Figure 3.7F,G**).

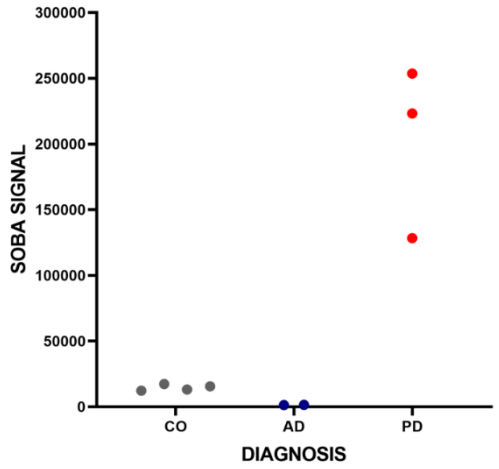

Figure 3.8. SOBA detection of oligomers in PD.

α-sheet is a unique biomarker for characterizing the early stages of AD pathogenesis, however, we have proposed that α-sheet is a conserved motif that mediates the aggregation and toxicity across a wide range of amyloid diseases. Thus, we used our SOBA diagnostic to test CSF from patients that had Parkinson's Disease (PD) by exchanging our antibody to be α-synuclein specific (clone 4B12, **Figure 3.8**). SOBA showed great differentiation between a small set of PD patients as compared to both CO and AD samples using the 4B12 antibody. This specificity reinforces the assertion that α-sheet is a conserved amyloid biomarker indicating the early stages of disease regardless of protein sequence or starting structure.

3.4 CONCLUSIONS

SOBA is a low-cost, minimally invasive, and specific biomarker diagnostic that, in this small patient cohort – based on clinical diagnosis and accounting for follow-up visits for 'converter' CO patients – resulted in an overall sensitivity of 100%, specificity of 100%, PPV of 100%, and NPV of 100%. Additionally, all 8 'converter' CO patients that progressed to MCI status within 1-5 years of initial diagnosis were positive for AD by SOBA, indicating that our SOBA diagnostic would have effectively diagnosed these patients prior to clinical or biomarker determination of their MCI status. Interestingly, only one 'true' CO patient had a relatively high SOBA signal of 27,000; unfortunately, there was not a follow-up visit for this patient. Current competitive diagnostics require progression into much later stages of the AD process and do not have the sensitivity nor specificity displayed here using SOBA, with max values in literature of 92% and 88%, respectively (**Appendix B**).

By exploring the nature of the early misfolding and aggregation process in AD, we characterized the α-sheet secondary structure that is specific to toxic oligomers formed in amyloid species. These oligomers mediate the earliest stages of disease progression, as well as neuronal toxicity that causes a wide range of downstream effects including tau phosphorylation, neurofibrillary tau tangle formation, amyloid plaque deposition, neurodegeneration, and eventually memory loss. By designing stable α-sheet peptides we were able to create a diagnostic test that specifically detected this structure in CSF and plasma prior to symptom presentation, as well as at the point of MCI and AD status. Furthermore, we showed that α-sheet detection of toxic oligomers for diagnosis is applicable to another amyloid system, PD. The α-sheet hypothesis presents an exciting and promising new avenue for the early and specific detection of AD prior to

neurodegeneration and symptom onset, paving the way for a future of efficacious therapeutic interventions.

Chapter 4. DIMERIC ALPHA-SHEET PEPTIDES ARE MORE POTENT THAN THEIR MONOMER FORMS

4.1 INTRODUCTION

Using dimeric in place of monomeric peptides is an enticing way to increase the valency of a small molecule without drastically changing its chemical and biochemical properties. Disulfide bond formation through cysteine residues is an easy method to achieve peptide dimerization that is relatively resistant to degradation. We have designed a host of α-sheet templated peptides with a wide range of sequences and cysteine residues placed at different points throughout the hairpin structure to facilitate peptide dimer formation. We used these peptides to compare their ability to inhibit aggregation via ThT fluorescence and inhibit toxicity in cell culture.

4.2 METHODS

4.2.1 *Peptide Synthesis*

The α-sheet and other control peptides were produced using standard solid phase peptide synthesis with a Liberty Blue (CEM) microwave peptide synthesizer on Rink amide resin with Fmoc chemistry and oxyma activation. The resin-bound peptides were cleaved and side chains deprotected with (trifluoroacetic acid) TFA/DODT/TIPS/H2O (92.5:2.5:2.5:2.5) and precipitated with cold ether. Crude peptides were purified by Reverse phase-HPLC to ~98% purity (Phenomenex 5 μm C12 100 Å semiprep column). Purified peptides were confirmed by mass spectrometry (MS) on a Bruker Esquire Ion Trap electrospray mass spectrometer, and peptide stocks were lyophilized for storage at −20 °C. Pure monomeric peptides were dissolved and dimerized using 10% isopropyl alcohol (IPA) and 0.1 M ammonium carbonate buffer (pH 9.8)

with mixing on a stir plate for 24 h at room temperature and re-purified to separate monomer and dimer forms.

4.2.2 *Thioflavin-T (ThT) aggregation assay*

Aβ(1-42) hereafter referred to as Aβ, was obtained from the ERI Amyloid Laboratory, LLC (Oxford, CT). Aβ was aliquoted using hexafluoroisopropanol (HFIP, Sigma-Aldrich, St. Louis, MO, USA) for use when needed. Aβ was sonicated at 1 mg/ml in HFIP in a bath sonicator for 5 min, followed by 25 min on ice, twice. The resulting solution was then blown under a gentle stream of N_2 gas and concentrated using a SpeedVac concentrator (Savant ISS110, Thermo Fisher Scientific) for 30 min on low setting, thus creating a monomerized Aβ film that was stored at -20 °C and could be thawed and prepared as necessary. Aβ stocks were prepared by removing a film aliquot from -20 °C, and letting it equilibrate to RT (5 min). The film was dissolved to 0.75 mg/mL in filtered 6mM NaOH (pH 11.6, Sigma-Aldrich), flicked to ensure the film was in solution, and sonicated for 5 min. This solution was transferred using a glass pipette to a 0.22 μm Costar Spin-X cellulose acetate centrifuge filter (Sigma- Aldrich), and centrifuged at 7,000 rpm for 2 min. This solution was then transferred using a glass pipette to an Eppendorf LoBind microcentrifuge tube (Sigma-Aldrich) and concentration was measured using a NanoDrop 2000 Spectrometer (Thermo Fisher Scientific) at 280 nm using an extinction coefficient of 1490 M^{-1} cm^{-1}. The resulting stock solution rested at 25 °C for four hours, after which it was either used immediately or stored at 4 °C until needed (no longer than 1 week). Stock Aβ was diluted using phosphate buffered saline (PBS) buffer (10 mM phosphate, 130 mM NaCl, and 2.7 mM KCl; Sigma-Aldrich) to the relevant working concentration for each experiment, as described previously (1, 2, 3). Briefly, a portion of the stock Aβ was added first to a separate LoBind tube. Concentrated stock ThT (Thermo Fisher

Scientific) was prepared monthly, by dissolving ThT powder to 5 mg/ml in H_2O; concentration was measured of 1:10 dilutions of the stock using a NanoDrop 2000 Spectrometer at 412 nm using an extinction coefficient of 36,000 M^{-1} cm^{-1}. In another separate tube, the concentrated stock ThT in H2O was first added, with the calculated volume corresponding to a final concentration of 24 μM ThT for aggregation studies. PBS buffer was added to this tube and mixed by pipette. A portion of this solution was then added gently – along the side of the tube – to the Aβ-containing LoBind tube and mixed once by pipette. In the case of inhibition studies, the ThT-PBS solution was first added to a tube containing concentrated inhibitor peptide and this final solution was used to dilute Aβ and 60 μL of the resulting solution was added to a single well in a black 384-well plate and read on a multimode plate reader (PerkinElmer, Waltham, MA). Relevant parameters include: λ_{ex} 438 nm, λ_{em} 495 nm, measurement height 7.5 mm, 8 flashes, with readings taken after 120h incubation.

4.2.3 *MTT Cell Viability Assay*

Cell viability was determined using a 3-(4,5-dimethylthiazol-2-yl)-2,5-diphenyltetrazolium bromide (MTT) assay. The SH-SY5Y cells (American Type Culture Collection, Manassas, VA, USA), neuroblastoma from human, were cultured in 1:1 DMEM:F12 (Invitrogen, Waltham, MA, USA) supplemented with 10% FBS (Invitrogen), 100 units/ml penicillin (Invitrogen), and 100 μg/ml streptomycin (Invitrogen). Primary murine cardiac cells were provided by the Regnier lab and plated immediately after isolation. The cells were seeded in 96-well plate at 4×10^4 cells per well for SH-SY5Y and 2×10^5 for primary cardiomyocytes and cultured in CO_2 water-jacketed incubator (37 ºC, 5% CO_2; Forma Scientific) for 24 hours. The cell culture medium was removed and replaced with 100 μL preincubated Aβ in medium, either with

or without designed peptides. 75 μM Aβ was incubated at 25 ºC for the desired duration and diluted to 30 μM with cell culture media before application. The cells were cultured with experimental solution for 24 h at 37 ºC before addition of 25 μL MTT (5 mg/mL in PBS; Sigma-Aldrich) and incubated for 4 h at 37 ºC. 100 μL lysis buffer (20% SDS, 50% DMF, 1% glacial acetic acid, and 0.2% HCl) was added to each well and incubated overnight at 25 ºC covered in foil. The optical density was read at 570 nm with a multimode plate reader (PerkinElmer). The cell passage numbers for the experiments were 6 to 8.

4.3 RESULTS

We have previously reported inhibition of aggregation and toxicity in the AD system using synthetic Aβ with α-sheet peptides in excess 4:1 (by concentration)[50]. Here, we show the increased capacity for inhibition using dimeric α-sheet peptides at sub-stoichiometric ratios with two designs, AP500 and AP510, highlighted in this discussion. Aβ was held constant at 75 μM for inhibition experiments. AP500 inhibited Aβ aggregation by 75% even when Aβ was in excess 50:1 (by concentration, Error! Reference source not found.), and the IC50 for AP510 occurred at a ratio of Aβ:AP510 between 100:1 and 250:1 (**Figure 4.2**). Sub-stoichiometric inhibition of aggregation at such high levels is unprecedented, implicating the essential role that α-sheet must play in the aggregation mechanism.

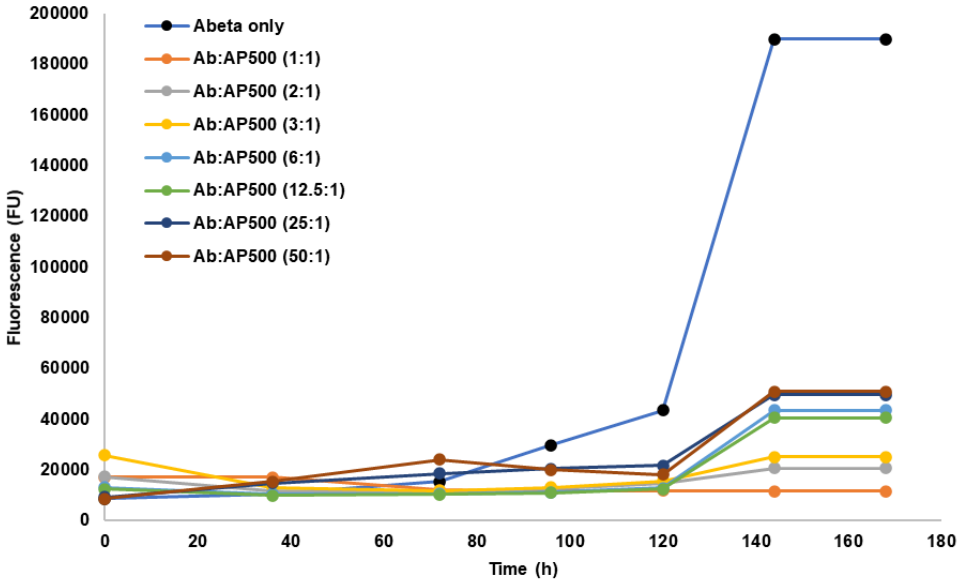

Figure 4.1. Inhibition of aggregation by AP500 where Aβ was in excess.

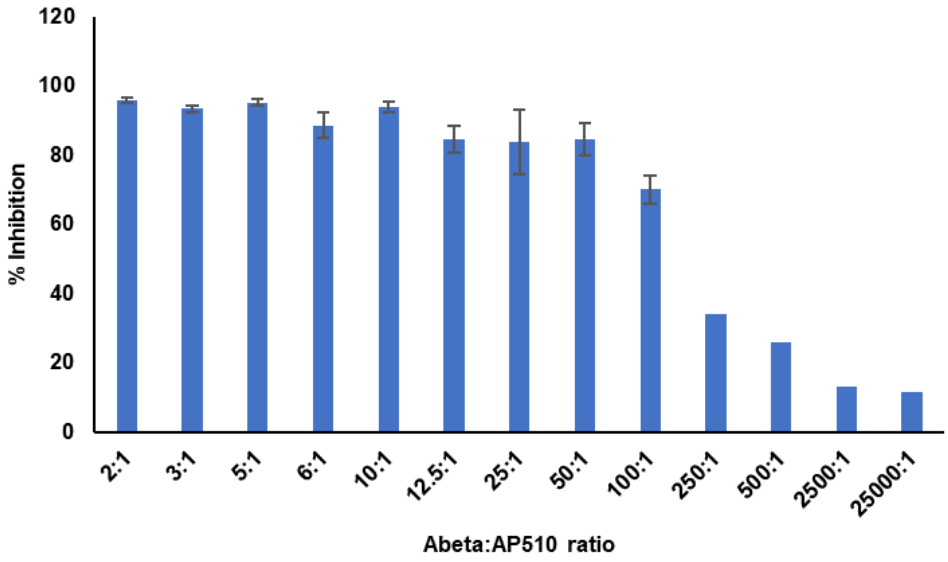

Figure 4.2. Inhibition of aggregation by AP510 where Aβ was in excess.

With the encouraging preliminary results indicating such extreme inhibitory capacity of dimeric α-sheet peptides, we next turned to characterize their effect on cell toxicity in neuroblastoma SH-SY5Y cells, as well as in primary murine cardiomyocytes (CMs). We were

particularly interested in whether Aβ oligomers would be similarly toxic in CMs as in neuroblastoma cells, as recently it has been shown that Aβ oligomers and fibrils were found in the myocardium of AD patients[154]. CMs from these patients showed altered cell shortening and calcium transients and the patients presented with anticipated diastolic dysfunction. This is particularly interesting as it proposes that AD and heart failure (HF) may exist as correlated and systemic diseases that each have effects on the other, rather than isolated in their progression and pathogenesis. Pre-incubated α-sheet Aβ oligomers reduced CM cell viability to 51% of the media-only control, whereas addition of dimeric AP510 (2:1 Aβ:AP510 by concentration) rescued cell viability back to 91%, roughly on par with the vehicle only control (**Figure 4.3**). From these data we determine that the α-sheet mechanism of toxicity is also a pathway by which Aβ oligomers can disrupt cardiac function, rather than it proceeding through some other, non-structure related mechanism.

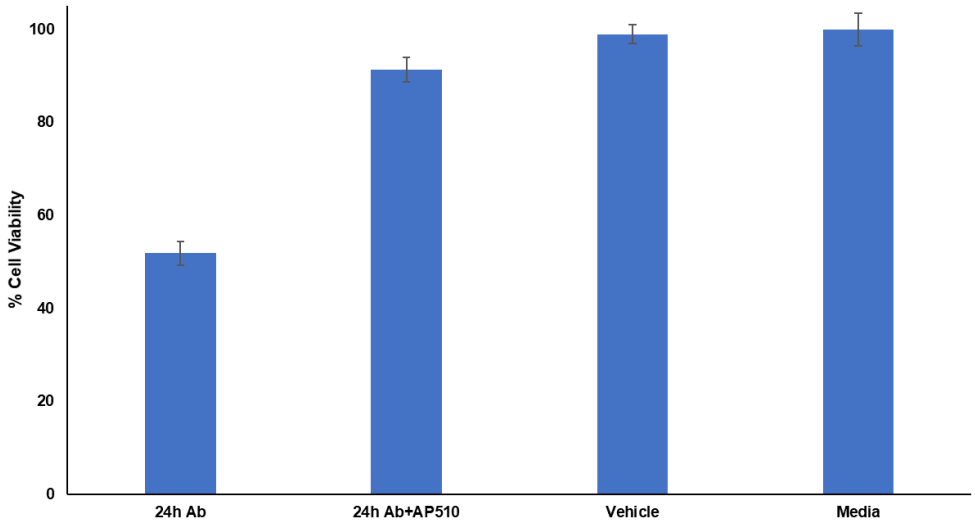

Figure 4.3. Inhibition of toxicity by AP510 in primary CMs isolated from mice.

Previous data reported inhibition of Aβ toxicity with α-sheet peptides in excess 4:1 (peptide:Aβ). **Figure 4.4** shows the improved capacity of dimeric α-sheet peptides to inhibit toxicity when Aβ was in excess 2:1 (Aβ:peptide). The improved capacity of dimeric α-sheet peptides over their monomeric counterparts – at sub-stoichiometric ratios – is a very exciting avenue to pursue potential routes of further α-sheet peptide intervention strategies in amyloid systems.

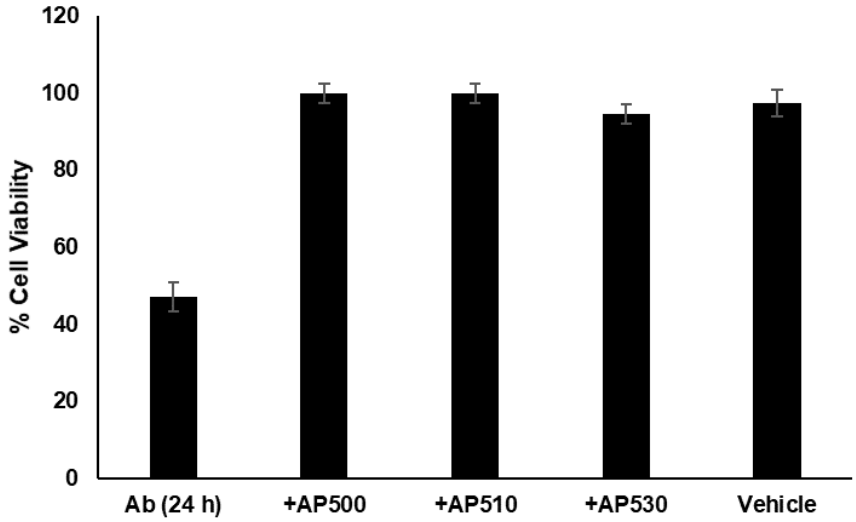

Figure 4.4. Inhibition of toxicity by α-sheet dimers. Aβ in excess 2:1 (by concentration).

4.4 CONCLUSIONS

Preliminary data indicate that dimeric α-sheet peptides are far more potent than their monomeric counterparts. Their effects include inhibition of both aggregation and toxicity *in vitro* and may provide an avenue by which to increase the effective dose of a future therapeutic without dramatically changing the chemical or biochemical properties of the stable, soluble α-sheet peptides. Studies are continuing with a wide range of α-sheet peptide sequences with dimer

linkages formed at a variety of positions throughout the hairpin structure. These studies will help to inform the effect on efficiency due to sequence alterations and steric environment through placement of the disulfide bond. Dimeric α-sheet peptides present an exciting pathway for a future of biomarker detection agents and potential therapeutics in amyloid diseases.

Chapter 5. CONCLUSIONS AND SUGGESTIONS FOR FUTURE STUDIES

5.1 KEY FINDINGS

This project made four major contributions to the field of Alzheimer's disease (AD) research, diagnosis, and treatment. First, it was determined that Aβ forms the primary toxic oligomers in the lag phase of aggregation, prior to high molecular weight (HMW) β-sheet oligomer or plaque formation. Amyloid has been a major focus of AD research for many decades, and largely touted as the primary actor in disease pathogenesis[1-4,11-31]. Unfortunately, the primary focus in this research has been directed at the amyloid plaques that coat neurons and are the pathological hallmarks of disease, despite growing evidence that cognitive impairment is not correlated with Aβ plaques but rather with the formation of early-stage low molecular weight (LMW) oligomers[12-25]. Though most approaches aimed at early detection and interventions have moved to targeting soluble oligomers formed prior to plaque deposition, many of these techniques are still focused on the relatively late, β-sheet-rich, HMW protofibrils[117-128]. This is likely because these oligomers are much easier to characterize and isolate and are present at stages when symptoms or clinical manifestations begin to appear. In this project, however, we utilized a rigorous set of protocols and techniques to characterize the pathogenesis of specific Aβ aggregates over time[50]. By focusing on structural characterizations using strict biophysics and biochemistry, we were able to correlate toxicity with a specific set of Aβ oligomers that formed in the lag phase of aggregation, prior to β-sheet formation. Early-stage, LMW soluble oligomers were the primary toxic components, whereas the late-stage, HMW soluble oligomer protofibrils and fibril plaques were largely non-toxic. This was a major finding and advancement for AD research, indicating the need for a

refocusing of AD diagnostic and intervention strategies to the earliest possible stages of aggregation that primary toxicity is associated with.

The second major contribution that this project made was that it established α-sheet as a unique secondary structure associated with the toxic state of Aβ oligomers[50]. The first aspect of this was to synthesize and characterize stable α-sheet peptides. As α-sheet is a unique, non-standard secondary structure, there are no existing criteria built into systems or analyses that favor α-sheet structure determination. Stable α-sheet peptides were synthesized and characterized using a variety of techniques, including circular dichroism (CD), microfluidic modulation spectroscopy in the IR region (MMS-IR), and nuclear magnetic resonance spectroscopy (NMR). CD and NMR had previously been reported for α-sheet peptides, but there was not enough data from NMR to calculate a structure[64-65]. Thus, we designed a peptide with an intramolecular disulfide bond to stabilize the α-sheet structure across the strands of the hairpin, and were able to definitively characterize the peptide structure as it was predicted and as discrete from α-helix and β-sheet. Additionally, FTIR had been reported for dry films of α-sheet peptides[64-65], however, utilizing MMS-IR allowed us to characterize the α-sheet structure in solution. After characterizing the α-sheet structure with this range of techniques, we were then able to isolate and identify α-sheet formation in Aβ oligomers spectroscopically using CD and MMS-IR. Additionally, by using a wide range of established and novel biophysical and biochemical techniques, we showed that α-sheet peptides specifically bound and sequestered Aβ oligomers in the early, toxic stages of aggregation (where α-sheet was most prevalent), and inhibited aggregation and toxicity *in vitro*, *ex vivo*, and *in vivo* utilizing transgenic (Tg) mice and *C. elegans* studies. The implications of this

work in the field of AD diagnosis and treatment cannot be overstated, as effective, early-stage diagnosis and treatment is necessary for efficacious intervention.

Our third contribution to the field of AD research is a novel technique for detecting toxic α-sheet oligomers in biological samples. The soluble oligomer binding assay (SOBA) is a novel, ELISA-like assay with key innovations that has the potential to diagnose AD decades before plaques or symptoms present in patients. Current biomarkers diagnose AD at the later stages of disease after the primary neurotoxicity has already taken place[117-128]. Plaque deposition, tau phosphorylation, and neurodegeneration all occur downstream of Aβ oligomerization. Utilizing our expertise in structural characterizations allowed us to identify the α-sheet structure as the earliest possible biomarker in AD pathogenesis. Building on this, SOBA was designed as a standalone diagnostic with prognostic capacity to predict progression to AD. SOBA diagnosed mild cognitive impairment associated with AD (MCI) and AD patients with unprecedented accuracy, as well as sensitivity and specificity that far exceeds other approaches. Additionally, in a small patient cohort, it predicted progression to AD before any other current biomarker diagnostic or clinical evaluation could. SOBA is an exciting new tool that we believe will revolutionize the field of AD diagnosis and pave the way for a future of efficacious AD interventions and therapeutics.

The final major discovery from this research program is the effectiveness of α-sheet interventions regardless of peptide sequence, as well as the applicability of the α-sheet hypothesis across amyloid systems. The α-sheet hypothesis has been proposed as a conserved structure associated with the toxic oligomers of amyloid systems, regardless of starting structure or sequence. Thus, it was essential to show the efficacy of α-sheet interventions (mainly inhibiting

aggregation and toxicity) regardless of peptide sequence. α-sheet peptides can be templated with any sequence by designing each strand of the hairpin with alternating L- and D-amino acids. We have designed a large library of α-sheet peptides with a wide range of sequences and have characterized them all for conserved structure and effectiveness at inhibiting aggregation and toxicity *in vitro*. Additionally, designing multi-valent α-sheet dimers improved the efficiency of these designs by several orders of magnitude. Furthermore, we have shown that using α-sheet peptides as a capture agent in SOBA was able to identify Parkinson's disease (PD) patients with high accuracy compared with control or AD patients, indicating the applicability of the α-sheet approach as a conserved motif in different amyloid systems.

5.2 Future Directions

5.2.1 *α-sheet and the connection between Alzheimer's and Heart Failure*

The connection between AD and heart failure (HF) has been proposed in recent years, as evidenced by the presence of oligomeric Aβ in the hearts of patients with AD[154]. This presents a case for AD and HF as systemic, connected diseases rather than discrete ones. There are two major ways that the work outlined in this dissertation can be applied to further the understanding of this connection. First, through the use of transgenic (Tg) AD mice or by collecting post-mortem samples from AD patients, heart tissue could be tested for the presence of α-sheet structure by SOBA (through homogenization of tissue) as well as FITC-labeling of α-sheet peptides and 'staining' myocardial tissue for pathological inclusions containing α-sheet-rich Aβ. Additionally, it would be interesting to test plasma from HF patients to screen for α-sheet Aβ species circulating in patients that have no symptoms of AD but may have initiated neurotoxicity through the

oligomerization of Aβ caused by factors of HF. This set of studies would help to inform the connection between HF and AD and whether the two affect one another through the same mechanism that we have characterized in AD. If the two systems of pathology proceed through an α-sheet-mediated mechanism, then the basis and scope of our hypothesis reaches even further than originally anticipated, extending into a theory of systemic α-sheet diseases that are interconnected.

5.2.2 *Characterization of the biodistribution and tolerability of α-sheet*

We have characterized the essential role that α-sheet plays in the pathogenesis of AD through a variety of techniques outlined above. These data have been isolated primarily to their operation either *in vitro* or *ex vivo*, with a limited set of data involving brief *in vivo* studies where mice were sacrificed soon after injection with α-sheet peptide. The logical next step in the development of α-sheet peptides as therapeutic agents is to characterize their biodistribution and tolerability *in vivo*. We know that α-sheet peptides are very soluble, up to 20 mg/mL in water and saline, however, we do not know much about their characteristics *in vivo*. Specifically, different concentrations of α-sheet peptide injections should be characterized in wild type (WT) and Tg mice for their tolerability. Furthermore, the biodistribution of injected α-sheet peptide should be characterized to understand the kinetics of α-sheet dispersal throughout the body, whether it accumulates in the brain and other organs, or if it is quickly filtered in the body by the liver or kidneys. Studies in this regard will help to inform the future for α-sheet therapeutics, and whether α-sheet peptides alone can be used to target amyloid oligomers in the brain or if a secondary molecule is necessary to cross the blood brain barrier (BBB). Furthermore, injection of α-sheet

peptide should not elicit any major inflammation or immune response, however, this should be characterized and proven to show the tolerability and potential clinical application of α-sheet peptides.

5.2.3 *Treatment of Tg mice with α-sheet*

Injection of α-sheet peptide directly into the brains of Tg mice – who were soon after sacrificed – resulted in a specific reduction of the presence of A11-detectable, toxic oligomers. To build on this, once the biodistribution, kinetics, and tolerability of α-sheet peptides have been established, studies should be conducted to test the treatment of Tg AD mice with α-sheet peptides. This would involve the demonstration of α-sheet peptide injection that accumulates in the brain and specifically binds to Aβ oligomers in the early stages of disease. Mice should undergo a plasma draw before the start of treatment and tested using SOBA to characterize α-sheet content. Next, mice should receive a varying set of α-sheet concentrations injected for treatment, a range of treatment frequencies, and a range of treatment durations, with plasma draws and SOBA analysis occurring at each stage throughout the process to monitor the reduction in or persistence of α-sheet-containing Aβ oligomers as treatment progresses. This process would mirror a theoretical future clinical trial where the measure of improvement would be a reduction in α-sheet-containing Aβ oligomers circulating in the blood. Additionally, mice should be continuously monitored for behavioral symptoms throughout the treatment cycle and sacrificed at the end with gross pathology characterized to assess the extent of plaque formation and any neurodegeneration that may have occurred.

5.2.4 *Diagnostic for amyloid diseases*

Primary work with SOBA has shown that the platform is applicable for detecting a range of oligomers formed in at least two amyloid systems, AD and Parkinson's disease (PD). There was minimal work involved in expanding SOBA to a new detection system, which was achieved by changing the detection antibody from Aβ-specific to α-synuclein specific (the main protein associated with pathogenesis in PD). The ease of applicability of SOBA to a new system indicates that this diagnostic could be applied as a ubiquitous platform for detecting α-sheet oligomers associated with a wide range of amyloid diseases simply by exchanging detection antibodies used in the assay. SOBA as a diagnostic platform could be an extremely useful tool with widespread clinical applications.

5.3 FINAL THOUGHTS

Alzheimer's disease research is necessarily an interdisciplinary field that requires collaborations between representatives from a wide range of academic disciplines. Engineers, biophysicists, biochemists, and clinicians must all come together to communicate and collaborate if any meaningful progression toward a treatment for AD is to arise from the fundamental science that academic researchers are conducting every day. The divide in approaches must be bridged through meaningful communication and collaboration between academic labs as well as clinicians. Furthermore, scientists should not withdraw from the public discussion which surrounds the decisions made by lawmakers regarding the practice of Science. All professions, from journalists and political scientists, to ethicists and elected officials, have equal value in contributing to the dialogue surrounding the future of medicine, and the future of AD treatment. In the current climate of the Information Age, dissemination of discoveries has never been more facile: we should

welcome the discussion and collaboration made possible in this age and use our resources to propel our society toward a brighter future.

BIBLIOGRAPHY

[1] Alzheimer's Association. (2019). *Alzheimer's disease facts and figures.* [Ebook]. Chicago. Retrieved from https://www.alz.org/alzheimers-dementia/facts-figures

[2] Masters, CL et al. Alzheimer's disease. Nat. Rev. Disease Primers 2015;1:15056.

[3] Chiti F & Dobson CM. Protein misfolding, functional amyloid, and human disease. Annu. Rev. Biochem. 2006;75:333–66.

[4] Braak, H & Braak, E. Neuropathological stageing of Alzheimer-related changes. Acta Neuro. 1991;82:239-59.

[5] Giuffrida ML, et al. The monomer state of β-amyloid: Where the Alzheimer's disease protein meets physiology. Rev Neurosci. 2010;21:83–93.

[6] Whitson JS, Selkoe DJ, Cotman CW. Amyloid β protein enhances the survival of hippocampal neurons *in vitro*. Science 1989;243:1488–90.

[7] Morley JE, et al. A physiological role for amyloid-β protein: Enhancement of learning and memory. J Alzheimers Dis 2010;19:441–9.

[8] Bishop GM, Robinson SR. Physiological roles of amyloid-β and implications for its removal in Alzheimer's disease. Drugs Aging 2004;21:621–30.

[9] Hiltunen M, van Groen T, Jolkkonen J. Functional roles of amyloid-beta protein precursor and amyloid-beta peptides: Evidence from experimental studies. J Alzheimers Dis 2009;18:401–12.

[10] Koudinov AR, Berezov TT. Alzheimer's amyloid-β (A β) is an essential synaptic protein, not neurotoxic junk. Acta Neurobiol Exp 2004;64:71–9.

[11] Z. Jaunmuktane, et al. Evidence for human transmission of amyloid-β pathology and cerebral amyloid angiopathy. Nature 2015;525;247–50.

[12] Selkoe DJ. Alzheimer's disease: Genes, proteins, and therapy. Physiol Rev 2001;81:741–66.

[13] Mullan M, et al. A pathogenic mutation for probable Alzheimer's disease in the APP gene at the N-terminus of beta-amyloid. Nat Genet 1992;1:345–7.

[14] Masters CL, et al. Amyloid plaque core protein in Alzheimer disease and Down syndrome. Proc Natl Acad Sci 1985;82:4245–9.

[15] Glenner GG, Wong CW, Quaranta V, Eanes ED. The amyloid deposits in Alzheimer's disease: Their nature and pathogenesis. Appl Pathol 1984;2:357–69.

[16] McLean CA, et al. Soluble pool of Abeta amyloid as a determinant of severity of neurodegeneration in Alzheimer's disease. Ann Neurol 1999;46:860–6.

[17] Haass C, Selkoe DJ. Soluble protein oligomers in neurodegeneration: Lessons from the Alzheimer's amyloid β-peptide. Nat Rev Mol Cell Biol 2007;8:101–12.

[18] Lambert MP, et al. Vaccination with soluble Abeta oligomers generates toxicity-neutralizing antibodies. J Neurochem 2001;79:595–605.

[19] Wang J, Dickson DW, Trojanowski JQ, Lee VM. The levels of soluble versus insoluble brain Abeta distinguish Alzheimer's disease from normal and pathologic aging. Exp Neurol 1999;158:328–37.

[20] Yang T, Li S, Xu H, Walsh DM, Selkoe DJ. Large soluble oligomers of amyloid β-protein from Alzheimer brain are far less neuroactive than the smaller oligomers to which they dissociate. J Neurosci 2017;37:152–63.

[21] Lambert MP, et al. Diffusible, nonfibrillar ligands derived from Abeta1-42 are potent central nervous system neurotoxins. Proc Natl Acad Sci USA 1998;95:6448–53.
[22] Ahmed M, et al. Structural conversion of neurotoxic amyloid-$\beta_{(1-42)}$ oligomers to fibrils. Nat Struct Mol Biol 2010;17:561–7.
[23] Hardy, JA, Higgins, GA. (1992) Alzheimer's disease: the amyloid cascade hypothesis. Science 1992;256:184-5.
[24] Hsia Y, et al. Plaque-independent disruption of neural circuits in Alzheimer's disease mouse models. Proc. Natl. Acad. Sci. U. S. A., 1999;96:3228–33.
[25] Tomiyama T, et al. A new amyloid beta variant favoring oligomerization in Alzheimer's-type dementia. Ann. Neurol. 2008;63:377-87.
[26] Miller Y, Ma B, and Nussinov R. Polymorphism in Alzheimer Abeta amyloid organization reflects conformation selection in a rugged energy landscape. Chem. Rev., 2010;110:4820–38.
[27] Ono K, Condron MM, Teplow DB. Structure-neurotoxicity relationships of amyloid beta-protein oligomers. Proc. Natl. Acad. Sci. U. S. A., 2009;106:14745-50.
[28] Lesne S, Koh MT, Kotilinek L, Kayed R, Glabe CG, Yang A, Gallagher M and Ashe KH. A specific amyloid-beta protein assembly in the brain impairs memory. Nature, 2006;440:352–7.
[29] M. Townsend, G. M. Shankar, T. Mehta, D. M. Walsh and D. J. Selkoe DJ. Effects of secreted oligomers of amyloid beta-protein on hippocampal synaptic plasticity: a potent role for trimers. J Physiol, 2006;572:477–92.
[30] Shankar GM, et al. Amyloid-beta protein dimers isolated directly from Alzheimer's brains impair synaptic plasticity and memory. Nat Med 2008;14:837–42.
[31] Quist, A. et al. Amyloid ion channels: a common structural link for protein-misfolding disease. Proc. Natl. Acad. Sci. USA 2005;102:10427–32.
[32] Walsh DM, et al. Naturally secreted oligomers of amyloid beta protein potently inhibit hippocampal long-term potentiation in vivo. Nature 2002;416:535–9.
[33] Wang HW, et al. Soluble oligomers of beta amyloid (1-42) inhibit long-term potentiation but not long-term depression in rat dentate gyrus. Brain Res 2002;924:133–40.
[34] Ehrnhoefer DE, et al. EGCG redirects amyloidogenic polypeptides into unstructured, off-pathway oligomers. Nat. Struct. Mol. Biol 2008;15:558–66.
[35] Ladiwala RA, Dordick JS, and Tessier PM. Aromatic small molecules remodel toxic soluble oligomers of amyloid beta through three independent pathways. J. Biol. Chem 2011;286:3209–18.
[36] Glabe CG. Structural classification of toxic amyloid oligomers. J Biol Chem 2008;283:29639–43.
[37] Roychaudhuri R, Yang M, Hoshi MM, and Teplow DB. Amyloid beta-protein assembly and Alzheimer disease. J Biol Chem 2009;284:4749–53.
[38] Pujol-Pina R, et al. SDS-PAGE analysis of Aβ oligomers is disserving research into Alzheimer's disease: appealing for ESI-IM-MS. Sci Rep 2015;5:14809.
[39] Kinoshita A, Fukumoto H, Shah T, Whelan CM, Irizarry MC & Hyman BT. Demonstration by FRET of BACE interaction with the amyloid precursor protein at the cell surface and in early endosomes. J Cell Sci 2003;116:3339-46.

[40] De Strooper B. Proteases and proteolysis in Alzheimer disease: a multifactorial view on the disease process. Physiol. Rev. 2010;90:465-94.
[41] Kumar S. et al. Extracellular phosphorylation of the amyloid beta-peptide promotes formation of toxic aggregates during the pathogenesis of Alzheimer's disease. EMBO J. 2011;30:2255-65.
[42] Jarrett JT, Berger EP, and Lansbury PT. The carboxy terminus of the beta amyloid protein is critical for the seeding of amyloid formation: implications for the pathogenesis of Alzheimer's disease. Biochemistry 1993;32:4693–7.
[43] Portelius E, et al. Distinct cerebrospinal fluid amyloid beta peptide signatures in sporadic and PSEN1 A431E-associated familial Alzheimer's disease. Mol. Neurodegener 2010;5:2.
[44] Lee J, Culyba EK, Powers ET, and Kelly JW. Amyloid-beta forms fibrils by nucleated conformational conversion of oligomers. Nat. Chem. Biol. 2011;7:602–9.
[45] Bernstein SL, et al. Amyloid-beta protein oligomerization and the importance of tetramers and dodecamers in the aetiology of Alzheimer's disease. Nat. Chem 2009;1:326–31.
[46] Economou NJ, et al. Amyloid beta-protein assembly and Alzheimer's disease: dodecamers of Aβ42, but not of Aβ40, seed fibril formation. J. Am. Chem. Soc 2016;138:1772–5.
[47] Cohen SIA, et al. Proliferation of amyloid-β42 aggregates occurs through a secondary nucleation mechanism. Proc. Natl. Acad. Sci. USA 2013;110:9758–63.
[48] Bitan G, Fradinger EA, Spring SM, and Teplow DB. Neurotoxic protein oligomers–what you see is not always what you get. Amyloid 2005;12:88–95.
[49] Hepler RW, et al. Solution state characterization of amyloid beta-derived diffusible ligands. Biochemistry 2006;45:15157–67.
[50] Shea D. et al. α-sheet secondary structure in amyloid β-peptide drives aggregation and toxicity in Alzheimer's disease. PNAS 2019;118:8895-900.
[51] Klein WL, Krafft GA, and Finch CE. Targeting small Aβ oligomers: the solution to an Alzheimer's disease conundrum? Trends in Neurosci. 2001;24:219-224.
[52] Kuo YM, et al. Water-soluble Aβ (N-40, N-42) oligomers in normal and Alzheimer disease brains. J of Bio. Chem. 1996;271:4077-4081.
[53] Ding H, Wong PT, Lee EL, Gafni A, and Steel DG. Determination of the oligomer size of amyloidogenic protein beta-amyloid(1-40) by single-molecule spectroscopy. Biophys. J 2009;97:912–21.
[54] Ryan TM, et al. Small angle x-ray scattering analysis of Cu^{2+}-induced oligomers of the Alzheimer's amyloid β peptide. Metallomics, 2015;7:536–43.
[55] Miller Y, Ma B, Tsai CJ, and Nussinov R. Hollow core of Alzheimer's Aβ42 amyloid observed by cryoEM is relevant at physiological pH. Proc. Natl. Acad. Sci. USA 2010;107:14128–33.
[56] Hyung SJ, et al. Insights into antiamyloidogenic properties of the green tea extract (-)-epigallocatechin-3-gallate toward metal-associated amyloid-β species. Proc. Natl. Acad. Sci. USA 2013;110:3743–8.
[57] Derrick JS, et al. A redox-active, compact molecule for cross-linking amyloidogenic peptides into nontoxic, off-pathway aggregates: in vitro and in vivo efficacy and molecular mechanisms. Am. Chem. Soc 2015;137:14785–97.

[58] Kayed R, et al. Common structure of soluble amyloid oligomers implies common mechanism of pathogenesis. Science 2003;5618:486-9.
[59] Glabe CG, and Kayed R. Common structure and toxic function of amyloid oligomers implies a common mechanism of pathogenesis. Neurology 2006;66:74-8.
[60] Kayed R, et al. Conformation dependent monoclonal antibodies distinguish different replicating strains or conformers of prefibrillar Aβ oligomers. Mol. Neurodeg. 2010;5:57.
[61] Armen R, Alonso D, and Daggett V. Anatomy of an amyloidgenic intermediate: Conversion of β-sheet to α-pleated sheet structure in transthyretin at acidic pH. Structure 2004;12:1847-63.
[62] Armen R, DeMarco M, Alonso D, and Daggett V. Pauling and Corey's α-pleated sheet structure may define the prefibrillar amyloidogenic intermediate in amyloid disease. PNAS 2004;101: 11622-7.
[63] Daggett V. α-sheet: The toxic conformer in amyloid diseases? Acc. Of Chem. Res. 2006;39:594-602.
[64] Hopping G, et al. Designed α-sheet peptides inhibit amyloid formation by targeting toxic oligomers. eLife 2014;3:e01681.
[65] Kellock J, Hopping G, Caughey B, and Daggett V. Peptides composed of alternating L- and D-amino acids inhibit amyloidogenesis in three distinct amyloid systems independent of sequence J. of Mol. Bio. 2016;428:2317-28.
[66] Maris N, Shea D, Bleem A, Bryers J, Daggett V. Chemical and physical variability in structural isomers of an L/D α-sheet peptide designed to inhibit amyloidogenesis. Biochemistry 2018;57: 507-10.
[67] Bleem A, Francisco R, Bryers JD, Daggett V. Designed alpha-sheet peptides suppress amyloid formation in Staphylococcus aureus biofilm. *Nature Biofilms and Microbiomes* 2017;3:16.
[68] Bi TM, Daggett V. The role of alpha-sheet in amyloid oligomer aggregation and toxicity. Yale J. of Bio. And Med. 2018;91:247-255.
[69] Sciacca MFM, et al. Two-step mechanism of membrane disruption by Aβ through membrane fragmentation and pore formation. Biophys. J 2012;103:702-10.
[70] Chimon S, et al. Evidence of fibril-like β-sheet structures in a neurotoxic amyloid intermediate of Alzheimer's β-amyloid. Nat. Struct. Mol. Biol 2007;14:1157-64.
[71] Pham JD, Chim N, Goulding CW, and Nowick JS. Structures of oligomers of a peptide from β-amyloid. J. Am. Chem. Soc 2013;135:12460-7.
[72] Petkova AT, Yau WM, and Tycko R. Experimental constraints on quaternary structure Alzheimer's beta-amyloid fibrils. Biochem 2006;45:498-512.
[73] Paravastu AK, Leapman RD, Yau WM, and Tycko R. Molecular structural basis for polymorphism in Alzheimer's beta-amyloid fibrils. 2008, 105, 18349-18354.
[74] McDonald JM, et al. The presence of sodium dodecyl sulphate-stable Abeta dimers is strongly associated with Alzheimer-type dementia. Brain 2010;133:1328-41.
[75] O'Nuallain B, et al. Amyloid beta-protein dimers rapidly form stable synaptotoxic protofibrils. J. Neurosci. 2010;30:14411–9.
[76] Noguchi A, et al. Isolation and characterization of patient-derived, toxic, high mass amyloid beta-protein (Abeta) assembly from Alzheimer disease brains. J. Biol. Chem. 2009;284:32895–905.

[77] Matsumura S, et al. Two distinct amyloid β-protein (Aβ) assembly pathways leading to oligomers and fibrils identified by combined fluorescence correlation spectroscopy, morphology and toxicity analyses. J. Biol. Chem. 2011;286:11555-62.
[78] Hatanpaa K, et al. Loss of proteins regulating synaptic plasticity in normal aging of the human brain and in Alzheimer disease. J. of Neuropath. Exp. Neur. 1999;58:637-43.
[79] M. Talantova, et al. Aβ induces astrocytic glutamate release, extrasynaptic NMDA receptor activation, and synaptic loss. Proc. Natl. Acad. Sci. USA 2013;110:E2518–27.
[80] Um JW, et al. Alzheimer amyloid-β oligomer bound to postsynaptic prion protein activates Fyn to impair neurons. Nat. Neurosci 2012;15:1227–35.
[81] Lai Ay, and McLaurin J. Mechanisms of amyloid-beta peptide uptake by neurons: the role of lipid rafts and lipid raft-associated proteins. Int. J. Alzheimer's Dis 2010;2011:548380.
[82] Kawarabayashi T, et al. Dimeric amyloid β protein rapidly accumulates in lipid rafts followed by apolipoprotein E and phosphorylated tau accumulation in the Tg2576 mouse model of Alzheimer's disease. J. Neurosci 2004;24:3801–9.
[83] Hong S, et al. Soluble Aβ oligomers are rapidly sequestered from brain ISF in vivo and bind GM1 ganglioside on cellular membranes. Neuron 2014;82:308–19.
[84] Cerf E, et al. Antiparallel beta-sheet: a signature structure of the oligomeric amyloid beta-peptide. Biochem. J., 2009;421:415-23.
[85] Fonte V, et al. A glycine zipper motif mediates the formation of toxic β-amyloid oligomers *in vitro* and *in vivo*. Mol. Neurodeg. 2011;6:61.
[86] Hung LW, et al. Amyloid-β peptide neurotoxicity is modulated by the rate of peptide aggregation: Aβ dimers and trimers correlate with neurotoxicity. J. of Neuro. 2008;28:11950-58.
[87] Doyle DA, et al. The structure of the potassium channel: molecular basis of K+ conduction and selectivity. Science 1998;280:69-77.
[88] Umeda T, et al. Intraneuronal amyloid β oligomers cause cell death via endoplasmic reticulum stress, endosomal/lysosomal leakage, and mitochondrial dysfunction in vivo. Neurosci. Res 2011;89:1031–42.
[89] Resende R, Ferreiro E, Pereira C, and Resende de Oliveira C. Neurotoxic effect of oligomeric and fibrillar species of amyloid-beta peptide 1-42: involvement of endoplasmic reticulum calcium release in oligomer-induced cell death. Neuroscience 2008;155:725–37.
[90] Cho DH, et al. S-nitrosylation of Drp1 mediates beta-amyloid-related mitochondrial fission and neuronal injury. Science 2009;324:102–5.
[91] Wogulis M, et al. Nucleation-dependent polymerization is an essential component of amyloid-mediated neuronal cell death. J. Neurosci. 2005;25:1071-80.
[92] Cummings J, et al. Alzheimer's disease drug development pipeline: 2019. Alz. & Dem: Trans. Res. & Clin. Int. 2019;5:272-93.
[93] Sevigny J, et al. The antibody aducanumab reduces Aβ plaques in Alzheimer's disease. Nature 2016;537:50-56.
[94] Haeberlein SH, et al. Clinical development of Aducanumab, an anti-Aβ human monoclonal antibody being investigated for the treatment of early Alzheimer's disease. J Prev Alz Disease 2017;4:255-63.
[95] Imbimbo BP, et al. Solanezumab for the treatment of mild-to-moderate Alzheimer's disease. 2012;8:135-149.

[96] Samadi H, Sultzer D. Solanezumab for Alzheimer's disease. Drug Eval. 2011;11:787-98.
[97] Meilandt W, et al. Characterization of the selective *in vivo* and *in vitro* binding properties of Crenezumab: insights into Crenezumab's unique mechanism of action. Neurology 2018;90:174.
[98] Cummings JL, et al. A phase 2 randomized trial of crenezumab in mild to moderate Alzheimer disease. Neurology. 2018;90:e1889-97.
[99] Adolfsson O, et al. An effector-reduced anti-β amyloid (Aβ) antibody with unique Aβ binding properties promotes neuroprotection and glial engulfment of Aβ. J. of Neuro. 2012;32:9677-89.
[100] Sakamoto K, et al. BACE1 inhibitor Lanabecestat (AZD3293) in a phase 1 study of healthy Japanese subjects: pharmacokinetics and effects on plasma and cerebrospinal fluid Ab peptides. J. of Clin. Pharmacology 2017;57:1460-1471.
[101] Breydo L, et al. (2016) Structural differences between amyloid beta oligomers. Biochem Biophys Res Commun 477:700–705.
[102] Huang THJ, et al. (2000) Structural studies of soluble oligomers of the Alzheimer beta- amyloid peptide. J Mol Biol 297:73–87.
[103] Torii H (2008) Amide I infrared spectral features characteristic of some untypical conformations appearing in the structures suggested for amyloids. J Phys Chem B 112: 8737–8743.
[104] Zandomeneghi G, Krebs MR, McCammon MG, Fändrich M (2004) FTIR reveals structural differences between native β-sheet proteins and amyloid fibrils. Protein Sci 13: 3314–3321.
[105] Hilaire MR, Ding B, Mukherjee D, Chen J, Gai F (2018) Possible existence of α-sheets in the amyloid fibrils formed by a TTR105-115 mutant. J Am Chem Soc 140:629–635.
[106] Quadros A, et al. (2003) Increased TNFalpha production and Cox-2 activity in orga- notypic brain slice cultures from APPsw transgenic mice. Neurosci Lett 353:66–68.
[107] Kuo YM, et al. (2000) Elevated A β and apolipoprotein E in A betaPP transgenic mice and its relationship to amyloid accumulation in Alzheimer's disease. Mol Med 6:430–439.
[108] Luo Q, et al. (2018) A self-destructive nanosweeper that captures and clears amyloid β-peptides. Nat Commun 9:1802–1806.
[109] Link CD, et al. (2003) Gene expression analysis in a transgenic Caenorhabditis elegans Alzheimer's disease model. Neurobiol Aging 24:397–413.
[110] Perni M, et al. (2017) Delivery of native proteins into C. elegans using a transduction protocol based on lipid vesicles. Sci Rep 7:15045.
[111] Drake J, Link CD, Butterfield DA (2003) Oxidative stress precedes fibrillar deposition of Alzheimer's disease amyloid beta-peptide (1-42) in a transgenic Caenorhabditis elegans model. Neurobiol Aging 24:415–420.
[112] Hassan WM, Dostal V, Huemann BN, Yerg JE, Link CD (2015) Identifying Aβ-specific pathogenic mechanisms using a nematode model of Alzheimer's disease. Neurobiol Aging 36:857–866.

[113] Jack Jr CR, et al. (2013) Tracking pathophysiological processes in Alzheimer's disease: an updated hypothetical model of dynamic biomarkers. Neurology 12:207-216.
[114] Leuzy A, Heurling K, Ashton NJ, Scholl M, Zimmer ER (2018) In vivo detection of Alzheimer's disease. Yale J of Biology and Med 91:291-300.
[115] Busche MA & Hyman BT. Synergy between amyloid-b and tau in Alzheimer's disease. Nat Neurosci 2020.
[116] Price JL, Morris JC. Tangles and plaques in nondemented aging and "preclinical" Alzheimer's disease. Ann. Neurol. 1999;45:358-368.
[117] Herukka SK, et al. Recommendations for cerebrospinal fluid Alzheimer's disease biomarkers in the diagnostic evaluation of mild cognitive impairment. Alz & Dem 2017;13:285-95.
[118] Olsson B. et al. CSF and blood biomarkers for the diagnosis of Alzheimer's disease: a systematic review and meta-analysis. Lancet Neurol 2016;15:673-84.
[119] Diniz BS, Pinto Junior JA, Forlenza OV. Do CSF total tau, phosphorylated tau, and beta-amyloid 42 help to predict progression of mild cognitive impairment to Alzheimer's disease? A systematic review and meta-analysis of the literature. World J Biol Psychiatry 2008;9:172-82.
[120] Ferreira L, Ferreira Santos-Galduroz R, Ferri CP, Fernandes Galduroz JC. Rate of cognitive decline in relation to sex after 60 years-of-age: a systematic review. Geratr Gerontol Int 2014;14:23-31.
[121] Ferreira D, et al. Improving CSF biomarkers' performance for predicting progression from mild cognitive impairment to Alzheimer's disease by considering different confounding factors: a meta-analysis. Front Aging Neurosci 2014;6:287.
[122] Van Rossum IA, Vos S, Handels R, Visser PJ. Biomarkers as predictors for conversion from mild cognitive impairment to Alzheimer-type dementia: implications for trial design. J Alzheimers Dis 2010;20:881-91.
[123] Ritchie C, et al. Plasma and cerebrospinal fluid amyloid beta for the diagnosis of Alzheimer's disease dementia and other dementias in people with mild cognitive impairment (MCI). Cochrane Database Syst Rev 2014;6:CD008782.
[124] Noel-Storr AH, et al. Systematic review of the body of evidence for the use of biomarkers in the diagnosis of dementia. Alzheimer's Dement 2013;9:e96-e105.
[125] Hu Y, Su B, Zheng H, Kim JR. A peptide probe for detection of various beta-amyloid oligomers. Mol Biosyst 2012;8:2741-52.
[126] Sun L, et al. A hydrogel biosensor for high selective and sensitive detection of amyloid-beta oligomers. Int J of Nanomed 2018;13:843-56.
[127] Laske C, et al. Innovative diagnostic tools for early detection of Alzheimer's disease. Alz & Dement 2015;11:561-78.
[128] Swati S, et al. In vivo assessment of retinal biomarkers by hyperspectral imaging: early detection of Alzheimer's disease. ACS Chem Neuro 2019.
[129] Nabers A, et al. Amyloid-b Secondary structure distribution in cerebrospinal fluid and blood measured by an immune-infrared-sensor: A biomarker candidate for Alzheimer's disease. Analytical Chem 2016;88:2755-2762.

[130] Nabers A, et al. Amyloid blood biomarker detects Alzheimer's disease. EMBO Mol Med 2018;10:e8763.
[131] Nabers A, et al. Ab and tau structure-based biomarkers for a blood- and CSF-based two-step recruitment strategy to identify patients with dementia due to Alzheimer's disease. Alz & Dem 2019;11:257-263.
[132] Fiandaca MS, et al. Identification of preclinical Alzheimer's disease by a profile of pathogenic proteins in neutrally derived blood exosomes: A case-control study. Alz & Dem 2015;11:600-607.
[133] O'Bryant SE, et al. A blood-based screening tool for Alzheimer's disease that spans serum and plasma: findings from TARC and ADNI. PLOS ONE 2011;10:1371.
[134] Mapstone M, et al. Plasma phospholipids identify antecedent memory impairment in older adults. Nature Med 2014;20:415-418.
[135] Janelidze S, et al. Plasma p-tau181 in Alzheimer's disease: relationship to other biomarkers, differential diagnosis, neuropathology and longitudinal progression to Alzheimer's dementia. Nature Med 2020;26:379-386.
[136] Thijssen EH, et al. Diagnostic value of plasma phosphorylated tau181 in Alzheimer's disease and frontotemporal lobar degeneration. Nature Med 2020;26:387-397.
[137] Barthelemy NR, et al. Blood plasma phosphorylated-tau isoforms track CNS change in Alzheimer's disease. J of Exp Med 2020;217:e20200861.
[138] Youn YC, et al. Blood amyloid-b oligomerization associated with neurodegeneration of Alzheimer's disease. Alz Res & Ther 2019;11:40.
[139] Kim K, et al. Clinically accurate diagnosis of Alzheimer's disease via multiplexed sensing of core biomarkers in human plasma. Nature Comm 2020;11:119.
[140] Yoon SP, et al. Retinal microvascular and neurodegenerative changes in Alzheimer's disease and mild cognitive impairment compared with control participants. Ophthalmology Retina 2019;3:489-499.
[141] Preische O, et al. Serum neurofilament dynamics predicts neurodegeneration and clinical progression in presymptomatic Alzheimer's disease. 2019;25:277-283.
[142] Mattsson N, et al. Comparing 18F-AV-1451 with CSF t-tau and p-tau for diagnosis of Alzheimer disease. 2018;90:5.
[143] Galasko D, et al. Synaptic biomarkers in CSF aid in diagnosis, correlate with cognition and predict progression in MCI and Alzheimer's disease. 2019;5:871-882.
[144] Janelidze S, et al. CSF Ab42/Ab40 and Ab42/Ab38 ratios: better diagnostic markers of Alzheimer disease. Ann Clin & Trans Neur 2016;3:154-165.
[145] Lista S, et al. Diagnostic accuracy of CSF neurofilament light chain protein in the biomarker-guided classification system for Alzheimer's disease. Neurochem Int 2017;108:355-360.
[146] Waite, J. H. & Qin, X. Polyphosphoprotein from the Adhesive Pads of Mytilus edulis †. Biochemistry 40, 2887–2893 (2001).
[147] Neddens J et al. Phosphorylation of different tau sites during progression of Alzheimer's disease. Acta Neuro Comm 2018;6:52.

[148] Lee, H., Dellatore, S. M., Miller, W. M. & Messersmith, P. B. Mussel-Inspired Surface Chemistry for Multifunctional Coatings. Science 318, 426–430 (2007).
[149] Orishchin, N. et al. Rapid Deposition of Uniform Polydopamine Coatings on Nanoparticle Surfaces with Controllable Thickness. Langmuir 33, 6046–6053 (2017).
[150] Kang, S. M. et al. One-Step Modification of Superhydrophobic Surfaces by a Mussel-Inspired Polymer Coating. Angew. Chem. Int. Ed. 49, 9401–9404 (2010).
[151] Ding, Y. H., Floren, M. & Tan, W. Mussel-inspired polydopamine for bio-surface functionalization. Biosurface Biotribology 2, 121–136 (2016).
[152] Lee, Y. B. et al. Polydopamine-mediated immobilization of multiple bioactive molecules for the development of functional vascular graft materials. Biomaterials 33, 8343–8352 (2012).
[153] Xu, L. Q., Yang, W. J., Neoh, K.-G., Kang, E.-T. & Fu, G. D. Dopamine-Induced Reduction and Functionalization of Graphene Oxide Nanosheets. Macromolecules 43, 8336–8339 (2010).
[154] Troncone, L, et al. Ab amyloid pathology affects the hearts of patients with Alzheimer's disease. *J Am Coll Cardiol* 2016;68:2395-2407.

APPENDIX A

Summary of NOE satisfaction by different AP407 Models.

	NOE Satisfaction (%)				NOE Violations	
Category	Short Range	Med. Range	Long Range	All	n	Mean Distance
All Models	100	100	100	10	0	0 Å
Cluster 1[a]	98.6	70.6	66.7	97.1	13	1.0 Å
Cluster 2[b]	96.3	35.3	66.7	93.6	29	1.5 Å
Cluster 3[c]	94.7	29.4	50	91.6	38	1.9 Å
Clust. 1+2	99.3	88.2	83.3	98.7	6	1.5 Å
Clust. 1+3	99.8	82.4	83.3	98.9	5	0.6 Å

a. The cluster containing 60% of all structures
b. The cluster containing 20% of all structures
c. The cluster containing 20% of all structures

Notes:

455 Total NOEs
432 short range
17 medium range
6 long range

Analysis of the unique satisfaction for each of the three clusters.

a. Of the 455 NOEs, 402 are satisfied by each of the three clusters and 53 have cluster dependent satisfaction.
b. Of the 455 NOEs, 26 are satisfied by 2/3 clusters.
c. Of the 455 NOEs, 27 are satisfied by only 1/3 clusters.
    i. Cluster 1 uniquely satisfied 18 restraints
    ii. Cluster 2 uniquely satisfied 3 restraints
    iii. Cluster 3 uniquely satisfied 6 restraints.
    iv. Clusters 2 and 3 are needed to satisfy only 9 NOEs (or 2% of the total number of restraints)

APPENDIX B

Review papers with CSF diagnostic marker references:

Review Reference	Year	CSF marker(s)	All Markers	Number of studies included	Comments
Olsson et al. (118)	2016	Aβ1-42, Tau, P-tau	NFL, NSE, VLP-1, HFABP, Aβ1-40, Aβ1-38, sAPPa, sAPPb, Albumin ratio, YKL-40/MCP-1, GFAP	131, 151, 89	CSF signature of elevated tau and p-tau and reduced Aβ1-42 consistently observed in MCI patients who progress to AD
Ferreira et al. (120)	2014	Aβ1-42, Tau, P-tau		12	Aβ1-42/p-tau ratio had the highest capability to predict conversion to AD
Ritchie et al. (123)	2014	Aβ1-42		14	CSF Aβ1-42 levels not recommended in an MCI population as a test for AD
Ritchie et al. (117)	2017	Tau, P-tau, Ab1-42		18	CSF max sensitivity/specificity was achieved for p-tau/Ab42 with 96%/95% respectively
Ferreira et al. (121)	2014	Aβ1-42, Tau, P-tau		7 reviews and 26 primary studies	Best performance for the prediction of conversion to AD was achieved with combinations of two or all three CSF markers
Noel-Storr et al. (124)	2013	Aβ1-42	FDG-PET, PIB-PET, MRI	37	Few large studies and high variability in biomarker assessment
van Rossum et al. (122)	2010	Aβ1-42, Tau, P-tau		7, 11, 8	Combination of Aβ1-42 and tau was the best predictor of conversion to AD
Diniz et al. (119)	2008	Aβ1-42, Tau, P-tau		4, 5, 3	MCI patients with high tau, high p-tau, and low Aβ1-42 at baseline are more likely to convert to AD

Plasma and CSF diagnostic techniques:

Reference	Year(s)	Approach	Sensitivity (Max)	Specificity (Max)	AUC
PLASMA					
Nabers et al. (129-131)	2016 ; 2018 ; 2019	Aβ soluble β-sheet structure formation (IR)	75	88	0.83
Fiandaca et al. (132)	2015	Neurally derived blood exosome protein analysis	96	na	0.999 max (0.991 0.988 0.987 0.731 for p-tau181, p-S396tau, Ab42, and t-tau)
O'Bryant et al. (133)	2011	Multianalyte profiling with 11 protein expression levels, combined with biological (glucose/cholesterol) and demographic (age, apoE) status) variables	75	91	0.88
Mapstone et al. (134)	2014	Mass Spectrometry Lipidomics	80	80	0.85 (MCI/AD to Normal CO)
Janelidze et al. (135)	2020	Blood p-tau181	93 (late stage)	81 (late stage)	0.96
Thijssen et al. (136)	2020	Blood p-tau181	89	85	0.93
Barthelemy et al. (137)	2020	Blood p-tau217 & p-tau181			ptau-217 - 0.99 / 0.92 (two cohorts) ptau-181 - 0.98 / 0.75 (two cohorts)
Youn et al. (138)	2019	Multimer Detection System-Oligomeric Amyloid-β (MDS-OAβ)	78	86	0.844
Kim et al (139)	2020	Carbon nanotube sensor array to measure biomarker concentrations	90	90	0.94
Yoon et al (140)	2019	Imaging with AngioPlex to measure retinal microvasculature			
Preische et al. (141)	2019	Serum neurofilament light chain (NfL) levels measured in familial AD (FAD) casees	89	82	0.89
CSF					
Mattsson et al. (142)	2018	18F-AV-1451 PET imaging and CSF t-tau and p-tau			0.836-0.939
Galasko et al. (143)	2019	CSF levels of tau and Aβ42 measured	82	79	0.88 max for Ab42/tau
Janelidze et al. (144)	2016	CSF levels of Aβ42, Aβ40, Aβ38, and their ratios	97	95	0.975 42/40 vs 0.964 42/38
Lista et al. (145)	2017	CSF levels of neurofilament light chain (NfL)			77
O'Bryant et al. (133)	2011	Multianalyte profiling with 11 protein expression levels, combined with biological (glucose/cholesterol) and demographic (age, apoE) status) variables			0.92

APPENDIX C

Note: COc = pre-symptomatic CO converter, COo = CO converter to non-AD MCI, and MCIc is the paired converter from corresponding COc (same patient).

Patient	LPAge	PrimaryDx	Gender	APOE	Abeta42 (pg/ml)	tau (pg/ml)	ptau (pg/ml)	CDRS16 Score	MMS Score	ptau/tau	ptau/tau/ab42	tau/ab42	ptau/ab42	SOBA
1	73	AD	F	4,4	48.89	270.6	215.64	1	20	0.7969	0.01630	5.53487	4.41072	42932.5
2	73	AD	M	3,3	86.79	166.21	85.73	1	21	0.5158	0.00594	1.91508	0.98779	54644.5
3	81	AD	M	4,4	94.12	36.49	31.24	1	24	0.8561	0.00910	0.38770	0.33192	44059.5
4	67	AD	M	3,3	191.8	106.26	71.39	2	17	0.6718	0.00350	0.55401	0.37221	42348
5	75	AD	M	3,4	185.18	81.83	62.75	1	18	0.7668	0.00414	0.44189	0.33886	32781.5
6	56	AD	M	4,4	284.77	69.08	47.92	1	26	0.6937	0.00244	0.24258	0.16828	61405.25
7	72	AD	M	3,3	151.92	65.39	41.51	1	24	0.6348	0.00418	0.43042	0.27324	52702
8	71	AD	M	4,4	NA	NA	NA	1	26	NA	NA	NA	NA	117374
9	83	AD	M	3,4	169.32	65.39	46.93	2	20	0.7177	0.00424	0.38619	0.27717	67576.33
10	57	AD	M	3,4	278	45.64	27.06	0.5	30	0.5929	0.00213	0.16417	0.09734	50079.33
11	76	AD	F	3,3	154.49	68.06	67.07	0.5	27	0.9855	0.00638	0.44055	0.43414	51343.33
12	77	AD	M	3,4	152.31	64.56	42.01	0.5	26	0.6507	0.00427	0.42387	0.27582	63517
13	80	AD	F	3,4	151.55	66.82	35.04	1	19	0.5244	0.00346	0.44091	0.23121	57720.67
14	78	AD	F	3,4	167.29	58.25	57.68	1	21	0.9902	0.00592	0.34820	0.34479	49402.5
15	69	AD	M	3,4	125.94	46.26	26.08	1	23	0.5638	0.00448	0.36732	0.20708	76580.33
16	68	AD	F	3,4	241.17	40.69	34.13	0.5	28	0.8388	0.00348	0.16872	0.14152	61055
17	77	AD	M	2,4	151.29	98.63	75.44	0.5	20	0.7649	0.00506	0.65193	0.49864	57195.5
18	68	CO	F	3,3	246.82	34.08	24	0	30	0.7042	0.00285	0.13808	0.09724	13080.5
19	66	CO	M	3,4	253.34	49.92	38.39	0	30	0.7690	0.00304	0.19705	0.15154	11524
20	69	CO	M	3,3	455.11	68.5	42.76	0	28	0.6242	0.00137	0.15051	0.09396	15166
21	75	CO	M	3,4	350.87	78.82	58.21	0	30	0.7385	0.00210	0.22464	0.16590	13706
22	79	CO	M	3,3	245.77	38.25	22	0	29	0.5752	0.00234	0.15563	0.08951	14200.5
23	67	CO	F	3,3	275.3	32.99	19.45	0	30	0.5896	0.00214	0.11983	0.07065	26851
24	67	CO	M	2,3	432.81	49.93	37.86	0	29	0.7583	0.00175	0.11536	0.08747	13755
25	75	CO	F	3,3	661.86	61.84	38.59	0	30	0.6240	0.00094	0.09343	0.05831	17419.33
26	73	CO	M	3,3	239.45	49.11	32.7	0	28	0.6659	0.00278	0.20510	0.13656	15029
27	81	CO	F	3,3	289.1	39.43	25.41	0	29	0.6444	0.00223	0.13639	0.08789	16529.33
28	69	CO	F	4,4	193.49	78.6	42.62	0	28	0.5422	0.00280	0.40622	0.22027	13418.33
29	75	CO	M	3,3	350.57	40.69	25.06	0	29	0.6159	0.00176	0.11607	0.07148	11185
30	NA	CO	NA	NA	NA	NA	NA	NA	NA	NA	NA	NA	NA	13346
31	17	CO	NA	NA	NA	NA	NA	NA	NA	NA	NA	NA	NA	12748
32	77	Coc	M	3,3	266.82	42.9	22	0	27	0.5128	0.00192	0.16078	0.08245	49833.67
33	74	COc	F	4,4	69.45	42.9	26.26	0	30	0.6121	0.00881	0.61771	0.37811	83517
34	84	COc	M	3,4	155.02	42.9	24.24	0	30	0.5650	0.00364	0.27674	0.15637	55158
35	76	COc	F	4,4	151.66	61.48	38.07	0.5	30	0.6192	0.00408	0.40538	0.25102	57071
36	81	COc	F	3,4	207.38	58.59	33.48	0.5	30	0.5714	0.00276	0.28252	0.16144	52699.33
37	82	COc	M	3,3	376.6	61.29	28.12	0	30	0.4588	0.00122	0.16275	0.07467	38381.33
38	74	COc	F	3,4	159.01	47.12	33.69	0	30	0.7150	0.00450	0.29633	0.21187	56104
39	87	COc	M	3,3	172.4	40.82	29.36	0	27	0.7193	0.00417	0.23677	0.17030	51546.67
40	82	Coo	M	2,3	130.07	38.25	19.45	0	29	0.5085	0.00391	0.29407	0.14953	17727
41	68	COo	M	3,3	188.72	11.71	16.74	0	30	1.4295	0.00757	0.06205	0.08870	18244
42	76	COo	F	3,4	177.48	55.54	30.82	0.5	28	0.5549	0.00313	0.31294	0.17365	18275
43	82	MCI	F	3,4	472.03	337.32	270.51	0.5	27	0.8019	0.00170	0.71462	0.57308	43038.5
44	69	MCI	F	3,4	114.56	51.5	44.19	0.5	27	0.8581	0.00749	0.44955	0.38574	44360
45	67	MCI	M	4,4	77.86	44.66	51.85	0.5	27	1.1610	0.01491	0.57359	0.66594	41074
46	55	MCI	M	4,4	149.46	44.66	35.4	0.5	25	0.7927	0.00530	0.29881	0.23685	69810.25
47	70	MCI	M	4,4	122.5	88.41	96.34	1	22	1.0897	0.00890	0.72171	0.78645	38118.67
48	82	MCI	M	3,3	528.19	123.68	118.01	0.5	25	0.9542	0.00181	0.23416	0.22342	55509.67
49	79	MCI	M	3,4	138.2	56.26	43.69	0.5	24	0.7766	0.00562	0.40709	0.31614	36171.33
50	81	MCI	M	2,4	189.32	138.19	142.89	0.5	28	1.0340	0.00546	0.72993	0.75475	57793.33
51	80	MCI	F	3,4	304.64	227.37	192.86	0.5	28	0.8482	0.00278	0.74636	0.63308	53689.67
52	80	MCI	M	3,3	323.01	127.72	191.74	0.5	28	1.5013	0.00465	0.39541	0.59360	65545.33
53	65	MCI	M	4,4	34.83	87.32	99.34	0.5	27	1.1377	0.03266	2.50703	2.85214	115468
54	67	MCI	F	4,4	202.51	79.06	107.52	0.5	24	1.3600	0.00672	0.39040	0.53094	42056
55	84	MCI	M	3,3	746.68	91.41	72.06	0.5	30	0.7883	0.00106	0.12242	0.09651	54028
56	84	MCI	F	3,3	247.45	72.45	56.83	1	24	0.7844	0.00317	0.29279	0.22966	107648.7
57	65	MCI	M	3,4	228.43	126.65	138.64	0.5	25	1.0947	0.00479	0.55444	0.60693	45598.67
58	76	MCI	M	3,4	217.21	148.79	185.85	0.5	24	1.2491	0.00575	0.68501	0.85562	59020.67
59	78	MCI	F	3,3	95.73	57.61	49.23	0.5	30	0.8545	0.00893	0.60180	0.51426	57422
60	67	MCI	F	3,4	297.7	160.28	162.69	0.5	29	1.0150	0.00341	0.53839	0.54649	58006.33
61	67	MCI	M	3,3	NA	NA	NA	0.5	29	NA	NA	NA	NA	53388.5
62	80	MCIc	M	3,3	527.09	70.72	66.48	0.5	26	0.9400	0.00178	0.13417	0.12613	48154
63	77	MCIc	F	4,4	142.36	88.77	106.92	0	25	1.2045	0.00846	0.62356	0.75105	56017.33
64	87	MCIc	M	3,4	167.98	45.64	28.58	0.5	27	0.6262	0.00373	0.27170	0.17014	48026.33
65	77	MCIc	F	4,4	198.38	80.99	64.6	0.5	30	0.7976	0.00402	0.40826	0.32564	71320.5
66	80	MCIc	F	3,4	187.22	80.99	50.6	0.5	28	0.6248	0.00334	0.43259	0.27027	52251.67
67	86	MCIc	M	3,3	433.37	73.41	31.25	0	27	0.4257	0.00098	0.16939	0.07211	37560
68	79	MCIc	F	3,4	146.74	48.8	28.85	0.5	25	0.5912	0.00403	0.33256	0.19661	47692
69	88	MCIc	M	3,3	161.59	156.75	158.55	0.5	30	1.0115	0.00626	0.97005	0.98119	62414.67
70	87	Other	M	2,3	230.74	46.26	24	1	29	0.5188	0.00225	0.20049	0.10401	13654
71	73	Other	M	3,3	316.66	40.69	23.44	0.5	30	0.5761	0.00182	0.12850	0.07402	15792.5
72	77	Other	F	3,4	363.85	63.39	39.06	0.5	26	0.6162	0.00169	0.17422	0.10735	17906.5

VITA

Dylan C. Shea graduated *cum laude* from the University of Delaware in May 2016 with a Bachelor of Engineering in Chemical Engineering. During his undergraduate studies, he developed low-temperature catalysts under the direction of Raul Lobo. After a brief internship with DuPont in his final year of school, Dylan decided to attend the University of Washington for a PhD in Molecular Engineering. In a major shift in interest, Dylan decided to focus his graduate studies in the realm of bioengineering, with a particular interest in neurodegenerative diseases that stemmed from the loss of his dear Aunt Donna to Creutzfeldt-Jakob Disease. In his doctoral studies, Dylan focused on Alzheimer's disease research under the direction of Valerie Daggett, whose lab stands alone in their approach to amyloid diseases as interrelated through the novel protein structure, α-sheet. Dylan was initially drawn to Dr. Daggett's lab as she was one of very few researchers in the country that worked in some capacity with prion diseases like CJD. Dylan identified and characterized the α-sheet structure that was associated with the toxic state of Alzheimer's proteins and made significant progress toward the application of this hypothesis to a few amyloid diseases. Dylan developed a novel technology designed to diagnose Alzheimer's disease in the earliest possible stages of disease pathogenesis and showed that this same approach could diagnose other amyloid diseases as well. Dylan has been named as a co-inventor on a patent for this technology.